S-nitrosoglutathione (GSNO) inhibits hydrogen peroxide production by α-ketoglutarate dehydrogenase and pyruvate dehydrogenase: investigating the effects of sex and high fat diets on mitochondrial nitrogen signaling and redox balance.

Kevin Wang

School of Human Nutrition

McGill University

Montreal

April 2023

A thesis submitted to McGill University in partial fulfillment of the requirements of the degree of Master of Science in Human Nutrition

ABSTRACT

The oxidation and reduction (redox) of select protein cysteine thiols is an important interface that elicits changes in cell metabolism in response to fluctuations in nutrition status. Our group has previously shown that protein S-glutathionylation (PSSG), a protein redox modification, is a key regulatory mechanism for numerous mitochondrial flavin-dependent dehydrogenases in the coupling of nutrient oxidation with the genesis of H_2O_2, a nonradical reactive oxygen species (ROS) secondary messenger involved in cell signaling pathways. Two such enzymes include α-ketoglutarate dehydrogenase (KGDH) and pyruvate dehydrogenase (PDH), both important sources of H_2O_2 that serve as entry points for metabolites into the Krebs cycle. Metabolic enzymes can also be subjected to protein S-nitrosylation (PSNO), a redox modification involving the addition and removal of nitric oxide (NO) from proteinaceous thiols.

The primary goal of this study was to determine whether H_2O_2 production by KGDH and PDH is regulated by protein S-nitrosylation. This included elucidating whether sex-differences or high-fat diets affect the PSNO status of KGDH and PDH. Our investigation was conducted in two different systems: an isolated liver mitochondrial system and a purified enzyme system. Using S-nitrosoglutathione (GSNO) in conjunction with well-established assays for measuring H_2O_2 production and enzyme activities, we discovered that S-nitrosylation does indeed impact KGDH and PDH. Moreover, we reveal for the first time sex-dimorphic differences in their redox modification in both a control and high-fat diet context. Combined, our findings demonstrate a novel mechanism for mediating mitochondria-to-cell signaling.

RÉSUMÉ

L'oxydation et la réduction (redox) de thiols de cystéine de certaines protéines constituent une modification importante qui provoque des changements métaboliques en réponse des

fluctuations de l'état nutritionnel. Notre équipe a précédemment démontré que la S-glutathionylation des protéines (PSSG), une modification redox des protéines, est un mécanisme pertinent chez nombreux déshydrogénases flavin-dépendantes mitochondriales qui effectuent le couplage de l'oxydation des nutriments avec la genèse de H_2O_2, une espèce réactive d'oxygène non radical (ROS) qui sert de second messager dans la signalisation cellulaire. Parmi ces enzymes comprennent la déshydrogénase de l'α-cétoglutarate (KGDH) et la déshydrogénase du pyruvate (PDH) qui représentent d'importantes enzymes génératrices d'oxygène réactif, en plus d'être des points d'entrée pour les métabolites dans le cycle de Krebs. Ces enzymes métaboliques peuvent également être soumises à la S-nitrosylation des protéines (PSNO), une modification redox impliquant l'ajout et l'élimination d'oxyde nitrique (NO) généré par les synthases d'oxyde nitrique (NOS) à partir de thiols protéiques.

L'objectif principal de l'étude est de déterminer si l'H_2O_2 peut être régulé par la S-nitrosylation dans les enzymes KGDH et PDH. En outre, l'étude élucidera l'impact du sexe biologique et d'un régime riche en graisses sur ce phénomène. Notre enquête sera menée dans deux systèmes différents : un système mitochondrial hépatique isolé et un système d'enzyme purifié. En utilisant la S-nitrosoglutathione (GSNO) comme catalyseur de S-nitrosylation en conjonction avec des tests bien établis pour mesurer la production de H_2O_2 et les activités enzymatiques, nous avons découvert que la S-nitrosylation affecte KGDH et PDH. De plus, nous révélons des différences sexe-dimorphiques dans leur modification redox dans de contextes de régime contrôlé et riche en graisses. Ensemble, nos résultats démontrent un nouveau mécanisme de médiation de la signalisation mitochondriale-à-cellule.

ACKNOWLEDGEMENTS

First and foremost, I want to acknowledge my supervisor, Prof. Ryan Mailloux. His assistance, experience, and mentorship have been invaluable throughout my M.Sc. Thesis project. Next, I want to thank my two supervisory committee members, Prof. Jacqueline Bede, and Prof. Stan Kubow. Their feedback was crucial in improving my understanding of my project and the timely completion of my thesis. I would also like to thank Mrs. Diane Langan and Ms. Karen Hope Stone. Their expertise in mouse care was extremely helpful in my ability to obtain experimental results.

Finally, I would like to acknowledge my fellow student lab members from the Mailloux group, Olivia Koufos, Amanda Moore, Cathryn Grayson, and Jonathan Hirschenson. Their aid and input contributed greatly to the successful completion of my M.Sc. Thesis project.

CONTRIBUTION OF AUTHORS

All sample preparation, mice surgeries, and mitochondrial and enzymatic assays were performed by Kevin Wang, with support from Olivia Koufos, Cathryn Grayson, and Dr. Ryan Mailloux. All calculations, data analysis, and interpretation of results were completed by Kevin Wang in consultation with Dr. Ryan Mailloux. All chapters of this thesis were written by Kevin Wang under the supervision of Dr. Ryan Mailloux.

TABLE OF CONTENTS

LIST OF FIGURES

LIST OF TABLES

LIST OF EQUATIONS

ABBREVIATIONS

ACAT	Acetyl-CoA acetyltransferase
ACN	Aconitase
AD	Alzheimer's disease
ADH	Alcohol dehydrogenase
ADMA	asymmetric dimethylarginine
ADP	Adenosine diphosphate
AF	Auranofin
ALS	Amyotrophic lateral sclerosis
ANOVA	Analysis of Variance
ANT	Adenine nucleotide translocase
ATP	Adenosine triphosphate
AUR	Amplex UltraRed
BCKDH	Branched chain ketoacid dehydrogenase
BSA	Bovine serum albumin
CDNB	1-Choro-2,4-dinitrobenzene
cGMP	Cyclic GMP
CM	Control Match diet
CO_3^{2-}	Carbonic acid
CoASH	Coenzyme A
CPI-613	Devimistat
CPT2	Carnitine palmitoyl transferase-2
CS	Citrate synthase
CypD	Cyclophilin D
Cys_P	Peroxidatic cysteine
Cys_R	Resolving cysteine
Cyt *c*	Cytochrome *c*
Cyt c_1	Cytochrome c_1
DHA	Dihydrolipoic acid
DHODH	Dihydroorotate dehydrogenase
DMSO	Dimethyl sulfoxide
DYNLL1	Dynein light chain LC8-Type 1
Δp	Proton motive force

ECH	Enoyl-CoA hydratase
EGTA	Ethylene glycol – bis (β-aminoethyl ether) – N, N, N′, N’-tetraacetic acid
ETC	Electron transport chain
ETFDH/ETFQO	Electron-transfer flavoprotein:ubiquinone oxidoreductase
FAD/$FADH_2$	Flavin adenine dinucleotide
FCCP	Carbonyl cyanide-*p*-trifluoromethoxyphenylhydrazone
Fe^{2+}	Ferrous ion
Fe^{3+}	Ferric ion
Fe-S	Iron-sulfur
FMN	Flavin mononucleotide
G3PDH	Glycerol-3-phosphate dehydrogenase
GAPDH	Glyceraldehyde 3-phosphate dehydrogenase
Gpx	Glutathione peroxidase
GR	Glutathione reductase
Grx	Glutaredoxin
GSH	Reduced glutathione
GSNO	S-nitrosoglutathione
GSNOR	GSNO reductase
GSSG	Oxidized glutathione/glutathione disulfide
GTP	Guanosine triphosphate
H^+	Proton
H_2O_2	Hydrogen peroxide
HD	Huntington’s disease
HEPES	4-(2-hydroxyethyl)-1-piperazineethanesulfonic acid
HFD	High-fat diet
HNO^-	Nitroxyl anion
HRP	Horseradish peroxidase
IκB	Inhibitory subunit of the NF-κB
IDH	Isocitrate dehydrogenase
IMM	Inner mitochondrial membrane
IMS	Intermembrane space
IPC	Ischemic preconditioning
I/R	Ischemia/reperfusion
Irβ	Insulin receptor β-subunit
IRS1	Insulin receptor substrate 1
Keap1	Kelch-like ECH-associated protein 1
KGDH	α-ketoglutarate dehydrogenase
KMV	3-methyl-2-oxopentanoic acid
LA	Lipoic acid
LMW	Low-molecular weight

L-NMMA	N^G-monomethyl-L-arginine
•LOO^-	Lipid peroxyl radicals
MDH	Malate dehydrogenase
MESH	D-mannitol, EGTA, sucrose, HEPES
MPC	Mitochondrial pyruvate carrier
mPTP	Mitochondrial permeability transition pore
NAD^+/NADH	Nicotinamide adenine dinucleotide
$NADP^+$/NADPH	Nicotinamide adenine dinucleotide phosphate
NAFLD	Non-alcoholic fatty liver disease
NF-κB	Nuclear factor κB
NNT	Nucleotide transhydrogenase
NO	Nitric oxide
•NO	Nitric oxide radical
NO^+	Nitrosonium
NO_2^-	Nitrite
NOS	Nitric oxide synthase
Nrf2	Nuclear factor-E2-related factor 2
O_2	Molecular oxygen
$O_2^{\bullet-}$	Superoxide radical
OADH	2-oxoadipate dehydrogenase
•OH	Hydroxyl radical
$ONOO^-$	Peroxynitrite
OXPHOS	Oxidative phosphorylation
PC	Pyruvate carboxylase
PD	Parkinson's disease
PDH	Pyruvate dehydrogenase
P_i	Inorganic phosphate
PINK1	PTEN induced putative kinase 1
PKB	Protein kinase B/Akt
PKG	cGMP-dependent protein kinase
PRODH	Proline dehydrogenase
Prx	Peroxiredoxin
PSNO	Protein S-nitrosylation/protein S-nitrosothiols
PSSG/PGLU	Protein S-glutathionylation
RET	Reverse electron transfer
RNS	Reactive nitrogen species
ROS	Reactive oxygen species
SCAD	Short-chain acyl-CoA dehydrogenase
SCS	Succinyl-CoA synthase
SDH	Succinate dehydrogenase

SEM	Standard Error of the Mean
SeOH	Selenenic acid
SeSG	Selenenyl-glutathione mixed disulfide
SNO	S-nitrosothiol
SOD	Superoxide dismutase
SOH	Sulfenic acid
SO_2H	Sulfinic acid
T2D	Type-2 diabetes
TPP	Thiamine pyrophosphate
TR	Thioredoxin reductase
Trx	Thioredoxin
UCP	Uncoupling protein
UQ	Ubiquinone
UQH_2	Ubiquinol
VDAC	Voltage-dependent anion channel
VLCAD	Very long chain acyl-CoA dehydrogenase

1 - INTRODUCTION

A central component to sustaining cellular life is the maintenance of a consistent, steady state system, or homeostasis. Like the pH of a cellular environment, oxidation-reduction (redox) status must also be kept in check. Redox reactions are involved in nearly all fundamental biological processes including aerobic respiration, which supplies energy in the form of adenosine triphosphate (ATP) to mammalian cells. The production of ATP by aerobic organisms mostly occurs in mitochondria, double membrane organelles that conserve energy released from nutrient oxidation pathways in the form of a protonmotive force (Δp). Establishing the Δp occurs by the transfer of electrons from nutrient-oxidizing dehydrogenases and flavoproteins, through the respiratory complexes of the electron transport chain (ETC), to molecular oxygen (O_2). The Δp established from this transfer is tapped by complex V (ATP synthase) to phosphorylate adenosine diphosphate (ADP) with inorganic phosphate (Pi), generating ATP. This process is called oxidative phosphorylation (OXPHOS) (*5*). Many nutrient oxidizing pathways, such as glycolysis, fatty acid oxidation, and amino acid metabolism, converge on the central metabolic pathway, the Krebs cycle, to generate the reduced forms of electron carriers, nicotinamide adenine dinucleotide (NADH) and flavin adenine dinucleotide ($FADH_2$), which are required to produce ATP by OXPHOS. Electron transfer reactions in mitochondria are far from perfect, and electrons can prematurely "spin-off" and react with O_2 to generate reactive oxygen species (ROS). The term "ROS" is a broad one used to describe all oxygen-centered radicals generated by biological systems. In mitochondria, the proximal ROS formed by redox reactions are superoxide ($O_2^{\bullet-}$) and hydrogen peroxide (H_2O_2), with the availability of the latter dominating over the former (*24*). Mitochondria contain 16 sources of ROS, 12 of which are associated with OXPHOS (*17*). However, while both are cytotoxic at high concentrations, H_2O_2, and to a lesser extent $O_2^{\bullet-}$, can be

beneficial when produced in a controlled manner. It is now appreciated that H_2O_2 is a mitochondria-to-cell secondary messenger required for the modulation of various physiological functions (*23*). Additionally, defects in maintaining this H_2O_2 budget has been linked to many pathologies via the induction of oxidative distress, but also due to its function in triggering various cell signaling pathways. For example, higher rates of H_2O_2 genesis by mitochondria have been related to alterations in cell redox buffering and the induction of oncogenesis and metastasis in cancer cells (*1*). Later in the literature review, I will detail OXPHOS and nutrient metabolism, as well as the systems used to control H_2O_2 genesis. These systems include redox sensitive and ubiquitous post-translational modifications like protein S-nitrosylation (PSNO), which I have discovered to be integral for the control of cellular H_2O_2. Coupled with this, I will also present PSNO in the context of other redox modifications, namely, protein S-glutathionylation (PGLU), which is now known to serve as a vital feedback loop to desensitize H_2O_2 signals and prevent oxidative distress after reduced glutathione (GSH) pool oxidation.

RATIONALE

Nitric oxide (NO)-mediated redox signaling has been extensively studied for decades. Metabolic pathways, maintenance of cellular redox homeostasis and myocardial contractility are a few examples of cellular and physiological activities mediated by NO-signaling (*84*, *85*). Nonetheless, there is still much to discover with respect to the modulation of mitochondrial bioenergetics and redox reactions by nitro-group addition. To be begin, only a few studies to our knowledge have documented that α-ketoglutarate dehydrogenase (KGDH) and pyruvate dehydrogenase (PDH) can be targeted for S-nitrosylation, specifically on the E2 subunit. These findings showed S-nitrosylation inhibits their activities, which can be prevented with lipoic supplementation (*127*). Furthermore, this inhibition has implications towards modulating immune

cell activity through control of macrophage activation and the availability of Krebs Cycle metabolites. However, the impact of this modification on KGDH- and PDH-driven H_2O_2 generation has not been considered. This is surprising given our group's discovery that another redox modification, protein S-glutathionylation, establishes regulatory feedback loops for the inhibition of KGDH and PDH-mediated H_2O_2 production. Protein S-glutathionylation-mediated regulation of H_2O_2 production by KGDH and PDH contains notable differences between male and female mitochondria. Additionally, we have also observed diet effects in relation to H_2O_2 production, namely that high-fat diet (HFD) feeding leads to augmented H_2O_2 production by KGDH and PDH in male, but not female, mitochondria. Therefore, research into KGDH and PDH regulation by protein S-nitrosylation should also encompass both sexes challenged with high fat diets to determine if inherent sex dimorphisms play a significant role. Additionally, an in-depth understanding of KGDH and PDH regulation by protein S-nitrosylation could prove very applicable towards developing novel approaches in the treatment of different diseases. Protein S-glutathionylation, as well as protein S-nitrosylation, is known for conferring protection of key enzymes against oxidative damage and reducing ROS production, which has been linked to diet-induced obesity, insulin resistance, and the pathogenesis of non-alcoholic fatty liver disease (NAFLD) (*175*). Thus, research focused on the S-nitrosylation of KGDH and PDH under high-fat diet conditions in liver mitochondria would be useful in determining if protein S-nitrosylation shares similar therapeutic properties to protein S-glutathionylation. These combined factors provide the rationale behind this thesis project as there is an urgent need for new novel research on the protein S-nitrosylation of KGDH and PDH and its physiological relevance in the pathogenesis of human diseases.

OBJECTIVES

The primary objective of this thesis project was to elucidate the role of protein S-nitrosylation in the modulation of KGDH and PDH, two key α-ketoacid dehydrogenases, using GSNO as the nitro-addition catalyst. Specific objectives that are to be addressed in this study are listed as followed:

1. Examine the effect of GSNO titrations on H_2O_2 production by KGDH and PDH in liver mitochondria from C57BL6N mice or purified from porcine heart.
2. Determine if a sex dimorphic effect exists for GSNO-mediated H_2O_2 production by KGDH and PDH in liver mitochondria from male and female C57BL6N mice.
3. Assess the effect of prolonged exposure to a HFD on the GSNO-mediated regulation of H_2O_2 genesis by KGDH and PDH and determine if sex dimorphisms persist after diet exposure.

HYPOTHESES

I predict that the metabolic enzymes KGDH and PDH are targets for GSNO-mediated inhibition of H_2O_2 production. I postulate that this will occur on the vicinal cysteine thiols of the lipoic acid moiety within the E2 subunit, resulting in a decrease in H_2O_2 production. I hypothesize that KGDH and PDH in female mice liver mitochondria will be less affected by GSNO due to fundamental differences in the redox buffering capacity of the mitochondrial matrix in comparison to male mitochondria. Feeding mice a high-fat diet will lead to an increase in H_2O_2 production in liver mitochondria, which will subsequently be suppressed by GSNO.

2 - LITERATURE REVIEW

2.1 - Nutrient Metabolism

2.1.1 - Glycolysis

Glycolysis in mammalian cells is a 10-step process that involves the oxidation of glucose in the cytoplasm into two molecules of pyruvate (*2*). Glycolysis can be subdivided into two phases: the preparatory phase, and the payoff phase. The preparatory phase breaks down the 6-carbon glucose molecule at the cost of two ATP molecules into two 3-carbon glyceraldehyde-3-phosphate (G3P) molecules. It begins with the phosphorylation of glucose at its C6 position by hexokinase in the presence of Mg^{2+} to yield glucose-6-phosphate. This first step in the preparatory phase requires ATP input and commits the glucose to glycolysis (*3*). Next, phosphohexose isomerase rearranges glucose-6-phosphate to fructose-6-phosphate in the presence of Mg^{2+}. ATP is expended to phosphorylate fructose-6-phosphate into fructose 1,6-bisphosphate via phosphofructokinase-1. The 6-carbon backbone is then split into two 3-carbon compounds, G3P, and dihydroxyacetone phosphate, by aldolase. The final step in the preparatory phase is catalyzed by triphosphate isomerase, which converts dihydroxyacetone phosphate into the second G3P molecule (*3*).

The payoff phase oxidizes G3P into pyruvate to yield one NADH, via NAD+ reduction, and two ATP molecules, through substrate-level phosphorylation, per G3P molecule (*3*). First, each G3P is phosphorylated by the glyceraldehyde-3-phosphate dehydrogenase (GAPDH) complex to yield 1,3-bisphosphoglycerate. The oxidation of G3P at this step is also paired with the reduction of NAD+ to NADH. Phosphoglycerate kinase catalyzes a nucleophilic attack on the terminal phosphate group of 1,3-bisphosphoglycerate by ADP which results ATP synthesis and 3-phosphoglycerate. This glucose derivative is then rearranged by phosphoglycerate mutase and dehydrated by enolase to form phosphoenolpyruvate. Finally, pyruvate kinase facilitates the transfer of a phosphate group from phosphoenolpyruvate to ADP to yield ATP, generating pyruvate (*3*). The newly synthesized pyruvate have two main fates which depend on cellular

conditions (*3*). First, pyruvate is used to generate lactate under anaerobic conditions. When O_2 is limiting, such as in exercising muscle tissue, pyruvate is reduced to lactate using NADH generated by glycolysis, which is catalyzed by lactate dehydrogenase. The regeneration of NAD+ preserves its availability for glycolysis (*3*). Lactate generated by the vigorous activity of more glycolytic muscle fibers can be used to fuel gluconeogenesis in the liver or can be to support OXPHOS in neighboring oxidative muscle fibers. However, under aerobic conditions where O_2 availability is not a limiting factor, cytoplasmic pyruvate is instead translocated to the mitochondria by mitochondrial pyruvate carriers (MPCs) where it can be used in more efficient, but O_2-dependent, ATP-producing processes (*4*). Overall, glycolysis net yields 2 ATP and 2 NADH from the breakdown of one glucose molecule. The net reaction for glycolysis is summarized in Equation 1 and depicted in Figure 1 below.

Equation 1: Summary of glycolysis net reaction:

$$Glucose\ (6C) + 2\ NAD^+ + 2\ ADP + 2\ P_i = 2\ Pyruvate\ (3C) + 2\ NADH + 2\ H^+ + 2\ ATP$$ (*3*)

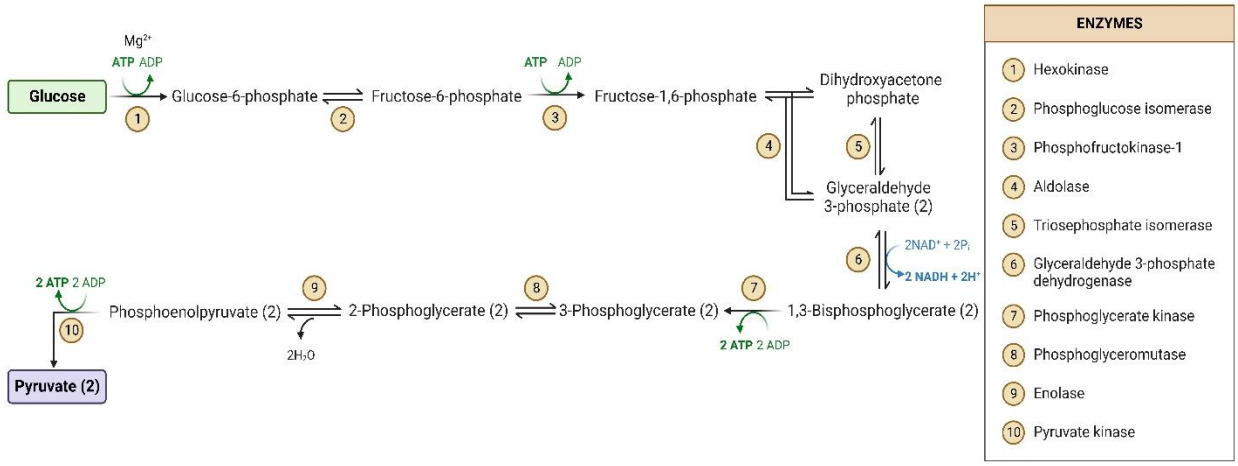

Figure 1: Glucose is oxidized to pyruvate by glycolysis. One glucose molecule can be oxidized into two pyruvates in the cytoplasm, net yielding two ATP and 2 NADH. Steps 1-5 represent the preparatory phase of glycolysis and steps 6-10 represent the payoff phase of glycolysis. The enzymes that mediate each step of glycolysis are listed in the legend on the right. Created with BioRender.com (*177*).

2.1.2 - Krebs Cycle

The Krebs cycle (Tricarboxylic Acid Cycle or Citric Acid Cycle) is the central metabolic pathway in energy metabolism and is comprised of 8 enzymes that work in tandem to degrade, convert, and oxidize fuels for the genesis of the electron carriers, NADH and $FADH_2$, to produce ATP (*5*). The 8 enzymes are in the matrix of mitochondria and consist of Fe-S clusters containing isomerases/hydratases, flavoproteins, dehydrogenases, and synthases. The catabolism of different nutrients, such as monosaccharides (e.g., glucose), amino acids, fatty acids, ketone bodies, and lactate, for ATP production depends on their conversion by disparate metabolic pathways into common intermediates that can enter the Krebs cycle. These intermediates include acetyl-CoA, α-ketoglutarate, fumarate, and oxaloacetate, Krebs cycle metabolites that are used for further catabolism. Acetyl-CoA serves as a point of convergence for the degradation of monosaccharides, ketone bodies, and fatty acids while α-ketoglutarate is a vital entry point for amino acids. In the case of pyruvate, it must first be transported into mitochondria after glycolysis for further oxidation. This is achieved by MPC, which translocates pyruvate across the inner mitochondrial membrane (IMM) into the matrix using energy derived from the Δp (*4*).

Once inside the matrix, pyruvate is metabolized by pyruvate carboxylase (PC) or PDH. The former carboxylates pyruvate in the presence of biotin and carbonic acid (CO_3^{2-}) forming oxaloacetate, a reaction that is dependent on ATP (*5*). PDH catalyzes the oxidative decarboxylation of pyruvate, converting it to acetyl-CoA in the presence of NAD^+ and Coenzyme A (CoASH). This reaction also yields NADH and the energy released from the oxidative decarboxylation for its production and the genesis of acetyl-CoA is coupled to the evolution of CO_2 (*7*). The synthesis of both oxaloacetate and acetyl-CoA serves as a crucial stepping-stone for the entry of pyruvate generated by monosaccharide metabolism into the Krebs cycle.

Oxaloacetate enters the Krebs cycle via a condensation reaction with acetyl-CoA mediated by citrate synthase (CS) to generate citrate, a 6-carbon compound (*5*). This reaction is energetically favourable in nature and drives the Krebs cycle forward. The next steps in the cycle involve the isomerization of citrate to isocitrate by aconitase (ACN), followed by its oxidation by isocitrate dehydrogenase (IDH) to yield α-ketoglutarate and CO_2. The oxidation of isocitrate is catalyzed by IDH1 and the decarboxylation of isocitrate is coupled to the reduction of NAD^+ to NADH. Mitochondria also contain an isocitrate dehydrogenase isoform called IDH2 which couples the oxidative decarboxylation of isocitrate to the reduction of nicotinamide adenine dinucleotide phosphate ($NADP^+$ to NADPH) instead. Next, α-ketoglutarate undergoes oxidative decarboxylation to produce succinyl-CoA, which is mediated by KGDH (*5*).

KGDH is an α-ketoacid dehydrogenase complex that contains 3 subunits: E1, E2, and E3 (*6*). The E1 subunit functions as an α-ketoglutarate decarboxylase that mediates the decarboxylation of α-ketoglutarate, followed by its transfer to thiamine pyrophosphate (TPP) to yield succinyl-TPP. The E2 subunit is a dihydrolipoamide:succinyl-CoA transferase responsible for generating succinyl-CoA. It contains a lipoic acid (LA) with two oxidized vicinal cysteine thiols at its catalytic site that mediate the synthesis of succinyl-CoA from E1-bound succinyl-TPP and CoASH. This process reduces the two lipoic acid vicinal thiols, leaving behind a dihydrolipoic acid (DHA) group in its place, and rendering the E2 subunit catalytically inactive. The E3 subunit of KGDH possesses dihydrolipoyl dehydrogenase activity and regenerates the catalytically active E2 lipoic arm by transferring the electrons from the DHA to an FAD group. The reduced $FADH_2$ group then transfers its electrons to NAD^+, generating NADH and completing one catalytic cycle of KGDH (*6*).

It is noteworthy that KGDH is part of the family of flavoproteins called α-keto acid dehydrogenases, which all have the same basic E1, E2, and E3 subunit composition. For example, PDH is also an α-keto acid dehydrogenase comprised of E1, E2, and E3 subunits. PDH E1 is a pyruvate decarboxylase and PDH E2 is a dihydrolipoamide:acetyl-CoA transferase (*7*). Similarly, other α-keto acid dehydrogenases like branched chain ketoacid dehydrogenase (BCKDH) and 2-oxoadipate dehydrogenase (OADH) also consist of E1 and E2 subunits that are specific for these flavoenzymes (*8*). However, the E3 subunit for all α-keto acid dehydrogenases is interchangeable. Furthermore, different α-keto acid dehydrogenases harbor different combinations in the ratios of their E1:E2:E3 subunits when fully formed into functional multimer complexes. Mammalian PDH is ~ 9.5 MDa and has an E1:E2:E3 subunits ratio of 40:40:20 whereas KGDH contains 12 E1, 24 E2, and 12 E3 subunits, equating to a ratio of 25:50:25, and is ~ 3.2 MDa (*9,10*). KGDH and PDH are also modulated by different mechanisms. For example, PDH activity, unlike KGDH, is tightly regulated by a kinase/phosphatase system involving pyruvate dehydrogenase kinase (PDK) and pyruvate dehydrogenase phosphatase (PDP) (*7*).

Once formed by KGDH, succinyl-CoA is hydrolyzed to succinate via succinyl-CoA synthase (SCS), generating ATP or GTP as a by-product. The selection between ATP or GTP is dependent on the active SCS isoform (*11*). Succinate is then oxidized by succinate dehydrogenase (SDH), producing fumarate and $FADH_2$ via the reduction of FAD. Notably, SDH is also referred to as complex II and is thus part of the respiratory chain since it transfers electrons directly from succinate, through FAD, to the ubiquinone (UQ) pool in the ETC (*12*). Fumarate is then hydrated by fumarase to produce malate, which in turn get oxidized by malate dehydrogenase (MDH) to regenerate oxaloacetate and produce another NADH molecule. The regeneration of oxaloacetate signifies one complete turn of the Krebs cycle. One completed turn of the Krebs cycle produces 3

NADH, 1 $FADH_2$, and 1 ATP or GTP per unit of pyruvate contributed by glycolysis (*5*). The Krebs cycle is displayed below in Figure 2.

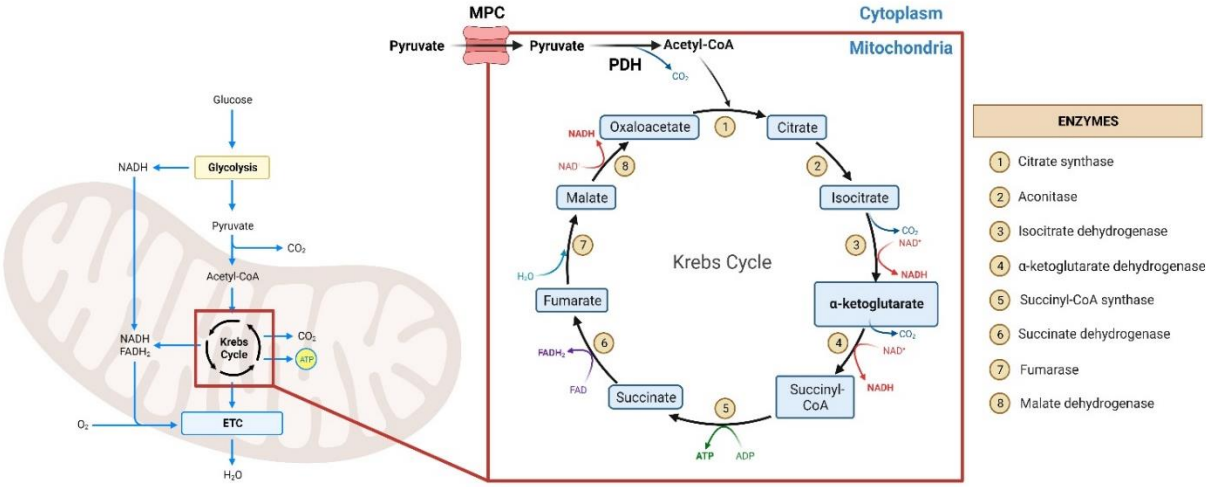

Figure 2: Pyruvate from glycolysis is further oxidized in the mitochondria by the Krebs cycle. Under aerobic conditions, cytoplasmic pyruvate is transported into the mitochondria by mitochondrial pyruvate carriers (MPCs) to undergo further oxidation by the Krebs cycle. Prior its entry into the Krebs cycle, pyruvate is decarboxylated to acetyl-CoA by PDH. The net yield from one turn of the Krebs cycle is 3 NADH, 1 $FADH_2$ and 1 ATP per pyruvate. The enzymes that mediate each step of the Krebs cycle are listed in the legend on the right. Created with BioRender.com (*178*)

2.1.3 - Electron Transport Chain and ATP Synthesis

NADH and $FADH_2$ produced by the Krebs cycle and PDH are oxidized by the ETC to establish a Δp for ATP production. The ETC is comprised of multi-subunit enzymes commonly referred to as complexes I-IV that are embedded in the IMM. Notably, only complexes I, III and IV are transmembrane proteins whereas complex II is inserted into the IMM but does not span the membrane. Electron transfer through the complexes is thermodynamically driven by redox centers in the individual multi-subunit enzymes, which contain donor and acceptor redox pairs arranged in order of increasing electron affinity. For example, the redox potential for the $NADH/NAD^+$ pair

is -320 mV at complex I whereas the corresponding electron conducting Fe-S clusters in the complex are around -250 mV (*13*). This makes electron transfer reactions thermodynamically favorable. Overall, the redox difference between NAD at complex I and O_2 at complex V is + 1,140 mV (O_2/H_2O pair is approximately +820 mV) meaning the thermodynamic change in kJ/mol for electron movement in the ETC is large enough to catalyze proton translocation across the IMM by complexes I, III and IV (*13*). This creates a transmembrane difference in protons, or Δp, a stored form of Gibbs free energy which is tapped by complex V to make ATP. It is important to note that although complex II is part of the chain, the change in Gibbs free energy for electron transfer through SDH is ~ 0 kJ/mol, thereby negating its capacity to partake in proton transfer reactions.

Complex I (NADH:ubiquinone oxidoreductase) is the entry point for electrons from NADH into the ETC. It is composed of 46 subunits and is ~ 1 MDa in size, but only 13 of these subunits are required for its activity (*14*). The other subunits are required to stabilize the complex, and aid in its assembly. Complex I is subdivided into three main modules based on the function of each individual part. The N-module contacts the matrix and oxidizes NADH, the Q module is comprised of subunits that form the UQ binding site, and the P-module is required to pump protons (*14*). Of note, the P-module is formed from hydrophobic subunits that are encoded by the mitochondrial genome (*7*,*14*). NADH oxidation by the N-module results in electron transfer to flavin mononucleotide (FMN), reducing it to $FMNH_2$. Electrons are then transferred through several Fe-S clusters in the N-module to ubiquinone (UQ) in the Q-module binding site, reducing it to ubiquinol (UQH_2) (*14*). Notably, electron transfer to the Q-module and the release of UQH_2 represent a highly favorable thermodynamic reaction, and this energy is coupled to the movement of the P-module and the pumping of protons (*14*).

Electrons also enter the ETC at complex II (SDH) via electron donors following succinate oxidation (*15*). Complex II is a succinate:ubiquinone oxidoreductase that combines the oxidation of succinate to fumarate with the reduction of FAD+ to $FADH_2$ (*15*). Complex II is composed of four subunits: SDHA-D subunits. Succinate is oxidized at the SDHA subunit, which contacts the matrix, and the electrons are passed through several Fe-S clusters to the UQ-binding site embedded within the IMM (*15*). One key characteristic that differentiates complex II from the rest of the ETC complexes is the similarity in potential between redox pairs succinate/fumarate and UQ/UQH_2, making the electron transfer reactions between these pairs not energetically favourable. This renders complex II incapable of pumping protons directly into the IMS when succinate oxidation is paired with the reduction of UQ (*5*). In addition to SDH, other dehydrogenases that contribute to the ETC by feeding their electrons into the UQ/UQH_2 pool include dihydroorotate dehydrogenase (DHODH), glycerol-3-phosphate dehydrogenase (G3PDH), proline dehydrogenase (PRODH), and the electron-transfer flavoprotein:ubiquinone oxidoreductase (ETFQO) system (*17*).

Electrons from UQH_2 are then passed to cytochrome c_1 (cyt c_1) by complex III, a ubiquinone:cytochrome *c* oxidoreductase (*5*). Complex III spans the IMM and contains two UQ-binding sites, Q_P and Q_N, and the Fe-S-containing Rieske protein, which facilitates the interaction between complex III and cyt c_1 (*18*). The Q_P site is associated with the B_L B-type heme group and faces the IMS while the Q_N site is localized to the mitochondrial matrix side of the IMM in conjunction with the B_H B-type heme group. UQH_2 initially binds with the Q_P site, triggering two separate electron transfer reactions. One electron is given to cyt c_1 through the Rieske protein, which consequently pumps protons into the IMS, while the second electron is cycled between the complex III subunits to regenerate UQH_2 (*18*). The source of protons used for this regenerative

cycle is in the mitochondrial matrix. Therefore, electron transfer reactions through complex III contribute to the proton gradient via direct pumping of protons into the IMS or through the scavenging of matrix protons to regenerate UQH_2, which is subsequently exported to the IMS (*5*).

Electrons from cyt c_1 are then donated to cytochrome *c* (cyt *c*), followed by molecular oxygen (O_2), the final electron acceptor in the ETC, via cytochrome *c* oxidase in complex IV. Complex IV is comprised of 13 subunits, but its catalytic core consists of the mitochondria-encoded subunits MTCO1, MTCO2, and MTCO3. MTCO1 and MTCO2 contain two heme A moieties, *a* and a_3, and two copper-sulfur centers, Cu_A and Cu_B, while MTCO3 serves as the structural core of the enzyme (*19*). The electrons from cyt c_1 are first transferred through the copper-sulfur centers, then to the heme groups, where they will finally react with O_2 bound to a_3. The reduction of O_2 results in the synthesis of two H_2O, thereby contributing to the Δp through the scavenging of four matrix protons per unit of O_2 (*5*). Overall, the ETC is capable of pumping out 4 protons at complex I, 2 protons at complex III, and 4 protons at complex IV. Therefore, NADH, which delivers electrons at the complex I level, can translocate approximately 10 matrix protons into the IMS. Electrons that enter the ETC at the complex II level, such as during succinate oxidation, will instead translocate 6 matrix protons since complex I is bypassed (*20*).

The pumping of matrix protons into the IMS and establishment of the transmembrane electrochemical gradient of proteins is an integral aspect of the ETC. This transmembrane electrochemical gradient is referred to as a proton motive force (Δp) and is the driving force in the production of ATP by complex V and ATP Synthase within the mitochondria (*5*). Complex V/ATP Synthase is composed of the hydrophobic F_O and the hydrophilic F_1 subunits (*16*). Complex V generates ATP by pairing the re-entry of IMS protons into the mitochondrial matrix with the phosphorylation of ADP to ATP. The re-entry of IMS protons is mediated by the F_0 subcomplex.

As the F_0 subunit binds IMS protons, its structure undergoes a rotational change in conformation. This rotation turns the F_1 subcomplex, generating the mechanical force for the catalysis of ATP synthesis (*16*). The net yield from one complete rotation of complex V is approximately 3 ATP molecules (*5*). Oxidative phosphorylation by the ETC is shown in Figure 3.

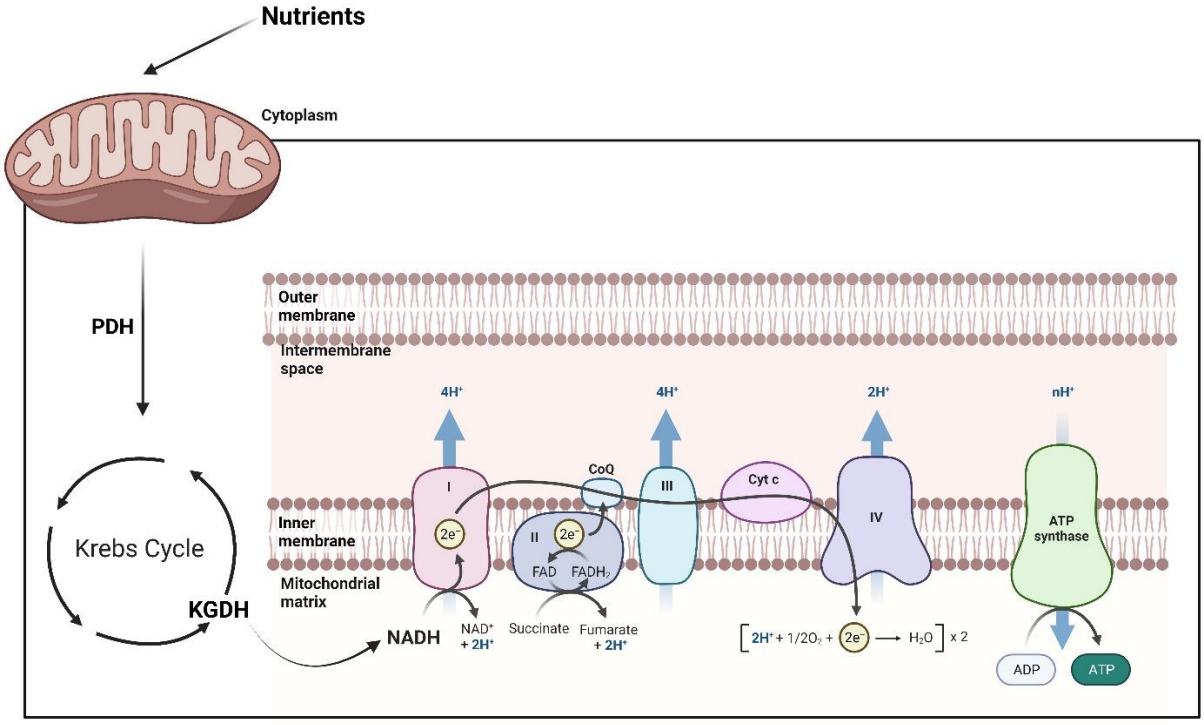

Figure 3: Electron carriers generated by nutrient metabolism contribute to the Electron Transport Chain (ETC) to generate ATP by oxidative phosphorylation. Nutrient oxidation produces electron carriers, such as NADH and $FADH_2$, that facilitate electron-transfer reactions through ETC complexes I–IV. These reactions catalyze the translocation of mitochondrial matrix protons into the IMS, generating an electrochemical proton concentration gradient along the IMM known as the proton motive force (Δp). ATP synthase/complex V utilizes the Δp to couple the re-entry of protons to the synthesis of ATP. Created with BioRender.com (*179*).

Additionally, protons can re-enter the matrix from the IMS in ways that do not involve ATP synthase. The solute anion carrier superfamily describes a class of enzymatic transporters that can couple the Δp to the import of charged compounds across the IMM and into the matrix (*21*). For example, IMS protons can enter the matrix through uncoupling proteins (UCPs), such as UCP1, which catalyzes thermogenesis in brown fat adipose tissue (*22*). Finally, nicotinamide

nucleotide transhydrogenase (NNT) makes use of the Δp to catalyze the transfer of a proton from NADH to NADP+, reducing it to NADPH (*23*). In these cases, the proton motive force generated by the ETC is uncoupled from ATP production by ATP Synthase, hence, why it is referred to as uncoupled respiration.

2.2 - Reactive Oxygen Species (ROS)

The electron transfer reactions in the ETC are not completely efficient. Electrons can leak out, or "spin-off", prematurely from the ETC before reaching complex IV, react with O_2, and produce reactive oxygen species (ROS) (*24*). The term "ROS" is used to describe all oxyradicals and nonradicals that are found naturally. Proximal ROS produced in the mitochondria are $O_2^{\bullet-}$ and H_2O_2, which are present in cellular concentrations ranging from $10^{-10} – 10^{-12}$ M and $10^{-7} – 10^{-9}$ M, respectively (*25*). $O_2^{\bullet-}$ is formed when electrons leak from the ETC as a single unit while H_2O_2 is made when electrons leak as pairs (*17*). Both of these ROS can catalyze further oxidation of neighboring target molecules to generate stronger oxidizing agents, such as hydroxyl radicals (•OH), peroxynitrite ions ($ONOO^-$; a reactive nitrogen species; RNS) and lipid peroxyl radicals ($\bullet LOO^-$) (*17, 26*). Hydroxyl radicals are especially dangerous as their highly reactive nature allows them to directly inactivate crucial enzymes through the oxidation of catalytic residues, alter lipid membrane fluidity by initiating a cascade of lipid peroxidation, and enhance DNA mutations via breaks in their double-stranded structure (*27, 28*). Hydroxyl radicals can be produced from $O_2^{\bullet-}$ and H_2O_2 through the Haber-Weiss reaction, which uses Fenton chemistry and iron ions as intermediaries in a two-step mechanism to generate biological •OH (*29*). Ferric iron (Fe^{3+}) is first reduced by $O_2^{\bullet-}$, yielding Fe^{2+} and O_2. The ferrous iron (Fe^{2+}) then reacts with H_2O_2 to produce •OH, OH^-, and regenerate Fe^{3+}. Therefore, the net reaction for •OH production is an input of $O_2^{\bullet-}$ and H_2O_2 and an output of O_2, •OH, and OH^-, mediated by iron. The Haber-Weiss and Fenton reactions are summarized below in Equation 2 (*29*).

Equation 2: •OH Production by Haber-Weiss Reaction

$Fe^{3+} + O_2^{\bullet-} \rightarrow Fe^{2+} + O_2$ (1)

$Fe^{2+} + H_2O_2 \rightarrow Fe^{3+} + OH^- + \bullet OH$ (Fenton reaction) (2)

$O_2^{\bullet-} + H_2O_2 \rightarrow O_2 + OH^- + \bullet OH$ (Haber-Weiss reaction) (3)

In addition, $O_2^{\bullet-}$ itself is known to disable Krebs cycle enzymes and ETC complexes through the rapid disassembly of their Fe-S clusters ($k \approx 10^7$ M^{-1} s^{-1}) (*30*). To counteract this, cells contain an abundant amount of superoxide dismutases (SOD), an antioxidant enzyme that neutralizes $O_2^{\bullet-}$ to H_2O_2 at an even faster kinetic rate ($k \approx 2 \times 10^9$ M^{-1} s^{-1}) (*24*). Thus, H_2O_2 is the predominant ROS found in the cell. While H_2O_2 is considered a strong oxidizing agent, it is certainly more manageable in comparison to other oxyradical species, partly due to its higher activation energy threshold, which limits the number of targets H_2O_2 is capable of oxidizing, and mainly poses a serious threat to cells when it accumulates to higher concentrations. Indeed, H_2O_2 at lower concentrations is known to modulate normal cellular functions through redox signaling pathways, a phenomenon known as "oxidative eustress" (*23*).

1.2.1 - Mitochondrial H_2O_2 Production and KGDH and PDH as Significant Sources

There has been a concerted effort towards studying sites of H_2O_2 production and several mitochondrial sources have been identified and well characterized. The α-ketoacid dehydrogenase complexes, which include OADH, BCKDH, PDH, and KGDH, are linked with the $NADH/NAD^+$ isopotential group in the mitochondria and each possess an FAD within their dihydrolipoamide dehydrogenase subunit where electron leaks can occur (*17*). Additionally, complex I contains two sites of H_2O_2 production: its flavin-containing NAD-binding site and its quinone binding site. The dehydrogenase complexes linked with the UQ/UQH_2 isopotential group, such as complex II,

DHODH, G3PDH, PRODH, ETFQO, and complex III, also have known sites for producing $O_2^{\bullet-}$ and H_2O_2 (*17*).

Complexes I and III were initially seen as the primary sources of ROS in the mitochondria, but there has been significant evidence pointing at other sites being major producers. Early work by Starkov et al. in 2004 revealed that KGDH was not only capable of producing $H_2O_2/O_2^{\bullet-}$ in rat brain mitochondria, but it was actually a primary source of H_2O_2 under normal conditions, as evidenced by the significant decrease in H_2O_2 observed in mitochondria from knock-out mice deficient in dihydrolipoyl dehydrogenase activity compared to their wild-type littermates (*31*). Tretter and Adam-Vizi performed a similar separate study in 2004 using synaptic mitochondria in isolated nerve terminals (synaptosomes) which also showed that KGDH could produce H_2O_2 at significant rates (*32*). Moreover, this same study demonstrated that NADH alone was sufficient in stimulating H_2O_2 production by KGDH through a reverse reaction referred to as reverse electron transfer (RET), suggesting that ROS from KGDH is generated at its E3 subunit. In 2013, Fisher-Wellman et al. demonstrated PDH displayed high rates of H_2O_2 production in skeletal muscle mitochondria (*33*). Quinlan et al. supported these findings in 2014 when they found that the rates of H_2O_2 production by KGDH and PDH in muscle mitochondria were nearly 8X and 4X than that observed in complex I, respectively (*34*). The Mailloux group had similar results in cardiac and liver mitochondria, again, confirming that KGDH and PDH were significant sources of H_2O_2, and that KGDH had a higher rate production than PDH (*35*). A later study by Slade et al. established a hierarchy of H_2O_2 producers in liver mitochondria, identifying complex III, KGDH, and PDH as the three largest contributors, with complex I producing essentially negligible amounts of H_2O_2 in comparison (*36*). Collectively, these findings strongly suggest that previous studies may have miscredited a significant portion of mitochondrial ROS production to complex I, rather than

through the α-ketoacid dehydrogenase complexes. H_2O_2 production by KGDH and PDH can occur via contributions to the NADH pool, which may lead to electron leaks at the NAD-binding site in complex I (*17*). Alternatively, KGDH and PDH can produce H_2O_2 by side reactions during the oxidation of $FADH_2$, which occurs between their E2 and E3 subunits when they are consuming their respective substrates, α-ketoglutarate, and pyruvate (*34*). Typically, $FADH_2$ is oxidized by NAD+ at E3 to keep the enzymes active, but it can also be oxidized by O_2 to generate a $O_2^{\bullet-}$ and FADH• pair. These radicals can couple to generate a singlet flavin-oxygen adduct, which can then be converted to H_2O_2 and FAD^+. If $O_2^{\bullet-}$ and FADH• diffuse from each other, each radical can separately generate H_2O_2 (*176*). Additionally, FADH• can produce more $O_2^{\bullet-}$ if it reacts with O_2, as well as reduce the lipoyl moieties to lipoate thiyl radicals within the E2 subunit. This is especially relevant when NAD+ availability is compromised, or when the NAD+ pool is overly reduced in favour of NADH. This effectively compromises the enzyme permanently and can potentially cascade into a chain-reaction of consecutive oxidation events, causing widespread oxidative damage throughout the mitochondria (*34*). A schematic graphic of $H_2O_2/O_2^{\bullet-}$ genesis by KGDH and PDH is shown below in Figure 4.

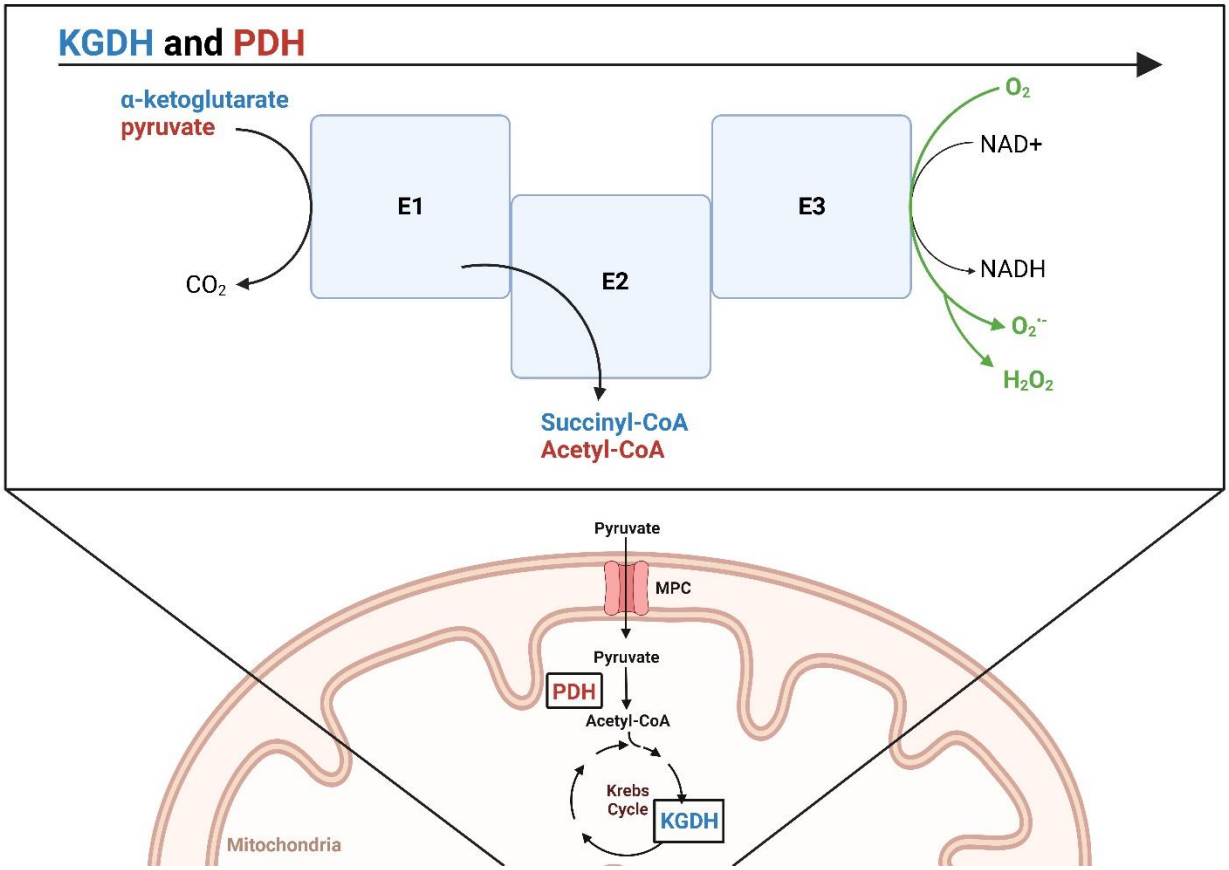

Figure 4: H_2O_2/ $O_2^{\bullet-}$ is produced at the E3 subunits of KGDH and PDH. KGDH and PDH can produce H_2O_2 or $O_2^{\bullet-}$ at their E3 subunits when electrons leak out and react with O_2. KGDH (Blue) and PDH (Red) catalyze the oxidative decarboxylation of α-ketoglutarate to succinyl-CoA, and pyruvate to acetyl-CoA, respectively. Both enzymes reduce NAD+ to NADH at their E3 subunits. Created with BioRender.com (*180*).

1.2.2 - Mitochondrial Antioxidant Defenses

Mitochondria have several antioxidant systems to defend against oxidative damage. As previously mentioned, superoxide dismutase (SOD) rapidly dismutases $O_2^{\bullet-}$ into H_2O_2. Cells contain two isoforms of SOD: SOD1 (Cu/Zn-dependent cytosolic and IMS isoform) and SOD2 (Mn-dependent mitochondrial isoform) (*37*). H_2O_2 induces oxidative distress at higher concentrations, which can compromise cellular function, and must therefore be quenched prior to its accumulation. This can occur through catalase, an enzyme commonly found in peroxisomes as well as liver and cardiac mitochondria (*38*). Mitochondrial catalase converts H_2O_2 into water and oxygen in an NADPH-independent manner only when it has reached the high nM to low µM range

(*38*). However, there is some evidence showing that catalase may indeed play a regulatory role in maintaining steady-state H_2O_2 concentrations as well. For example, a study done by Dogar et al. analyzed mitochondrial H_2O_2 production using the NNT-deficient C57BL6J mouse strain, revealing that ROS levels were comparable to non-NNT-deficient mice due to an upregulation of catalase which compensated for the absence of NNT (*39*).

Mitochondria also contain two NADPH-dependent antioxidant systems that quench H_2O_2: the glutathione peroxidase (Gpx) system and the thioredoxin (Trx) system (*39*). The Gpx system relies on glutathione (GSH), a tripeptide composed of glycine, cysteine, and glutamate (*40*). In the presence of H_2O_2, glutathione peroxidase oxidizes two units of GSH into a glutathione disulfide molecule (GSSG) while quenching the H_2O_2 to water. This conversion is catalyzed by a selenocysteine residue within the active site of Gpx that becomes oxidized when quenching H_2O_2 (*41*). The reaction is initiated by the oxidation of selenocysteine to a selenenic acid (SeOH), which is resolved in two stages: 1) the SeOH attacks GSH forming a selenenyl-glutathione mixed disulfide (SeSG) and 2) the second GSH resolves the SeSG forming GSSG and reactivating the Gpx enzyme. The GSH units can be regenerated from GSSG by glutathione reductase (GR), which will reduce GSSG back into two GSH molecules through the oxidation of NADPH into NADP+ (*41*). Therefore, the GSH antioxidant system is dependent on the availability of NADPH to continuously quench H_2O_2 within the mitochondria.

The thioredoxin (Trx) system is also an NADPH-dependent antioxidant system that works with peroxiredoxins (Prx) to remove H_2O_2 in the mitochondria (*39*). The Trx/Prx system is like that of GSH and Gpx except that it is reliant on intra- and inter-disulfide exchange reactions mediated by two different catalytic cysteines in Prx, a peroxidatic cysteine (Cys_P) and a resolving cysteine (Cys_R) (*42*). First, Cys_P is oxidized to sulfenic acid (SOH). Although most cysteine thiols

react slowly with H_2O_2, the peroxidatic cysteine is surrounded by positively charged amino acids which lower the pKa of its thiol, promoting its deprotonation and forming a thiolate anion that catalyzes the nucleophilic attack of H_2O_2 (*42*). Prx is a homodimer in which its two subunits are arranged in a head-to-tail manner (*43*). Thus, the SOH group on Cys_P of one Prx can react with Cys_R of a second Prx directly across from it to generate a disulfide bridge between the two Prx. The Prx-SS-Prx disulfide moiety is resolved by Trx, which exchanges the Prx disulfide bridge on to itself, reducing the cysteine residues on Prx to regenerate their reduced thiols. The disulfide bridge on Trx is subsequently reduced by thioredoxin reductase (TrxR) to regenerate the cysteine thiols on Trx, allowing it to undergo another cycle of thiol disulfide exchange reactions with oxidized Prx, which in turn, allows for the removal of more H_2O_2 (*44*). The reductase activity of TrxR is also dependent on the oxidation of NADPH, making both the Gpx and Trx systems NADPH-dependent antioxidant systems. The different antioxidant systems are shown below in Figure 5.

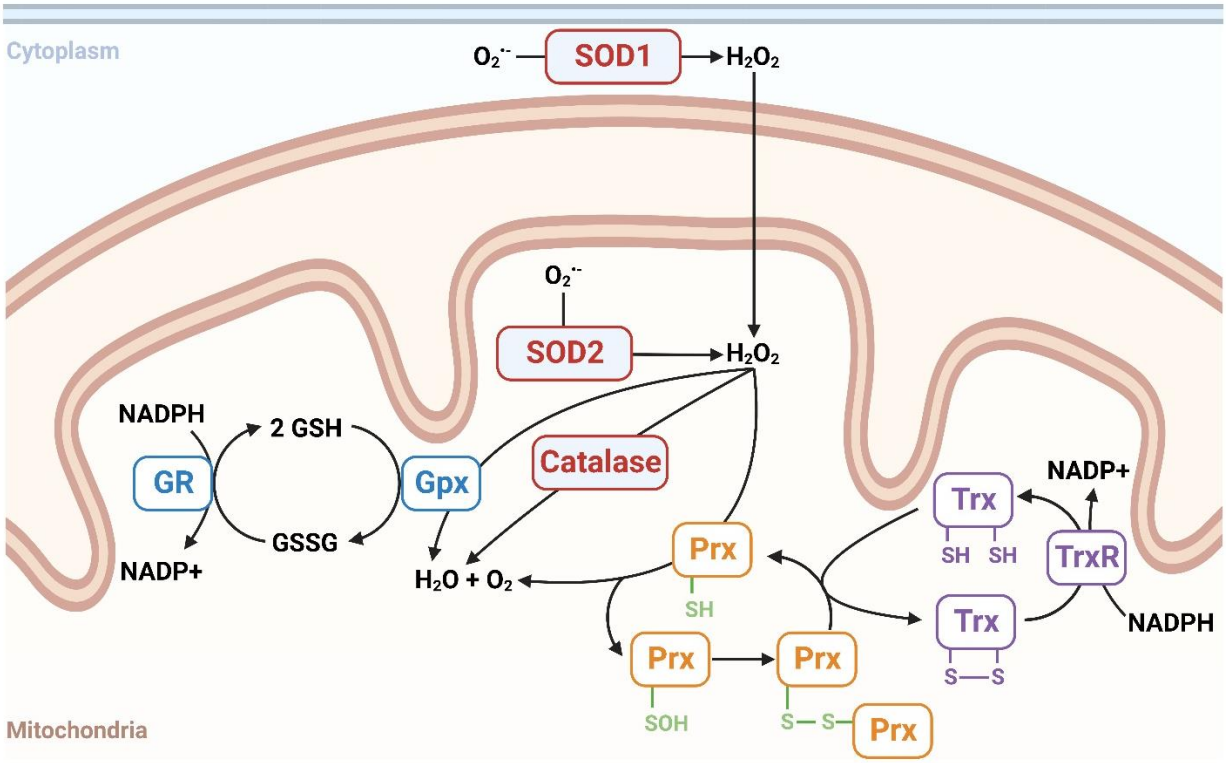

Figure 5: Mitochondrial antioxidant systems quench H_2O_2 and $O_2^{\bullet-}$. The NADPH-independent antioxidant systems (red) include SOD1/SOD2 and catalase. SOD1 and SOD2 rapidly dismutate $O_2^{\bullet-}$ to H_2O_2 in the cytoplasm and mitochondria, respectively. Catalase quenches H_2O_2 to water in the mitochondria. The NADPH-dependent antioxidant systems include the Prx/Trx system (orange/purple) and the Gpx system (blue). The Prx/Trx system quenches H_2O_2 through a disulfide bridge exchange mechanism. The Gpx system employs GSH to remove H_2O_2. Created with BioRender.com (*180*).

2.3 - Oxidative Eustress and Distress

While one might assume that oxidative stress should be avoided altogether for fear of irreparable oxidative damage, the relationship between oxidative stress and health is far less one-dimensional. In fact, ROS is required, albeit at lower concentrations, to induce physiologically relevant redox signaling pathways. Therefore, the definition of oxidative stress has since been expanded to encompass the benefits associated with low ROS concentrations. “Oxidative distress” describes the damaging effects from high amounts of ROS in the cell while the positive effects observed at lower concentrations is termed “oxidative eustress” (*23*). H_2O_2 is an oxidant species

that also serves as a secondary messenger. When H_2O_2 is present at its physiological concentration (~1-10 nM), it can reportedly regulate redox signaling pathways through reversible cysteine oxidation, methionine oxidation, and short-lived lipid oxidation, which can, in turn, lead to cell proliferation, cell migration, and angiogenesis (*23*). For example, H_2O_2 can react with peroxiredoxin-2 (Prx2) to produce oxidizing equivalents that consequently target and modify cysteine residues on the STAT3 transcription factor, a key regulator for immune function, cell migration, programmed cell death, and a myriad of other cellular functions (*45,46*). This mechanism of H_2O_2 signaling between Prx2 and STAT3 is referred to as a redox relay model, where the redox signal is mediated through thiol peroxidase oxidation rather than directly on the target protein (*47*). Alternatively, redox signals are also regulated through H_2O_2-mediated inactivation of peroxiredoxins and other targets by hyperoxidizing specific cysteinyl residues to sulfinic acid (SO_2H). The resulting effect is a localized accumulation of H_2O_2, which then leads H_2O_2 signal transduction through the oxidation of specific protein targets. This form of H_2O_2-mediated redox signaling is known as the floodgate model (*48*). Sulfiredoxins subsequently regenerate peroxiredoxin activity by reducing the hyperoxidized cysteinyl residues (*49*). Therefore, while the concentration H_2O_2 remains in its physiological range, it can serve as an important secondary messenger for redox-sensitive signaling pathways in the cell. A critical aspect of this signaling mechanism is maintaining that range of H_2O_2 concentration before the cellular environment begins to experience oxidative distress. As such, cells possess redox switches, or "master regulators", that can modulate the enzymatic activities in specific redox signaling pathways and of entire systems through redox sensing as a whole.

The mammalian Nrf2/Keap1 complexes have been well studied as an adaptive response system to redox signaling (*23*). Nrf2 (nuclear factor-E2-related factor 2) is an important

transcription factor for antioxidant and detoxification enzymes while Keap1 (Kelch-like ECH-associated protein 1) regulates Nrf2 activity. Under normal, non-stressed cellular conditions, Keap1 ubiquitinates Nrf2, marking it for degradation and suppressing its transcriptional capabilities. However, under oxidative distress, specific cysteinyl residues on Keap1 may be targeted for oxidation, preventing it from ubiquitinating Nrf2. Thus, Nrf2 is no longer degraded, leading to its accumulation in the nucleus and the induced expression of its targeted genes (*23*). Similar to the Nrf2/Keap1 system, nuclear factor κB (NF-κB) can also be regulated by oxidant-mediated signals. NF-κB is a transcription factor complex that activates the expression of inflammatory, immune, and acute phase response genes. Upon oxidation by H_2O_2, the inhibitory subunit of the NF-κB (IκB) is released, activating the complex (*23*) . Interestingly, Nrf2 and NF-κB also undergo another layer of regulation that permits fine-tuning of their activities. For example, NF-κB activity is upregulated by nuclear thioredoxin reductase 1 (TrxR1) but inhibited by increased nuclear H_2O_2. Nrf2 is similarly regulated by TrxR1, and this method of regulatory fine-tuning results in oscillations in their transcription factor activities. It has been proposed that these oscillations serve as a method for cells to stall in their decision-making before committing to a specific action (*50*).

2.4 - Regulation of ROS Production

The mitochondrial levels of $O_2^{\bullet-}/H_2O_2$ are regulated by controlling the method in which they are degraded or produced. Degradation of ROS occurs through different antioxidant systems, which was previously discussed. The regulation of its production is another important aspect of modulating its availability in the cell and this is mediated through proton leaks and redox signals.

1.4.1 - Proton Leaks

Proton leaks describe the re-entry of IMS protons into the mitochondrial matrix through alternative systems besides Complex V/ATP Synthase. The uncoupling of ATP synthesis by

proton return to the matrix can lower the overall strength of the Δp, which can actually result in a more efficient ETC via reduced protonic back pressure and lead to a decrease in H_2O_2 production (*51*). This has been demonstrated in studies with protonophores, such as FCCP, while other groups revealed that small increases in the Δp lead to upregulated H_2O_2 production (*51*). Proton leakage occurs primarily through adenine nucleotide translocase (ANT) and the uncoupling proteins (UCP1-5) (*52*). ANT catalyzes the exchange of free ATP with free ADP across the IMM and is responsible for proton leaks as well (*53*).

The uncoupling proteins on the other hand are responsible for managing inducible proton leaks in the mitochondria, though there still remains some controversy as to whether their role in proton leakage is also linked with mitochondrial $O_2^{\bullet-}/H_2O_2$ production. Five isoforms of UCPs exist within mammalian cells, UCP1-5. UCP1 is located in the mitochondria of brown fat adipocytes and is responsible for nonshivering thermogenesis, a process in which the Δp is paired with the generation of heat rather than ATP (*54*). UCP2 and UCP3 share approximately 60% homology with UCP1. However, while UCP1 is exclusively expressed in brown fat, the other isoforms are found in other tissues. UCP2 is found more ubiquitously throughout the body, such as in the kidney, pancreas, macrophages, and spleen, and is overexpressed in many cancers. UCP3 is almost exclusively located in skeletal muscle tissue, but also expressed at lower levels in cardiac and brown fat tissue (*55*). Finally, UCP4 and UCP5 are primarily expressed in the central nervous system and the brain (*56*). The role of UCPs in modulating ROS production is still under much debate. For example, several groups have demonstrated that the activation of UCP1 and subsequent increase in proton leakage was associated with an increase in mitochondrial H_2O_2 production (*22, 52, 57, 58*). This is in contrast to UCP2 and UCP3, where some studies have shown the opposite in that the activation of UCP2/3 resulted in a decrease in H_2O_2 production (*59,60*). A recent

systematic review on the UCP proteins confirms that there is some agreement with this observation within the scientific community, but notes that it is still not definitive as to whether the mechanism for this inhibition of H_2O_2 production is related to upregulated proton leakage, or a different physiological function, such as the transport of Ca^{2+}, lipid hydroperoxides, or C4 metabolites (e.g., oxaloacetate, aspartate) (*61*).

1.4.2 - Redox Signals

Redox signals offer another form of control over $O_2^{\bullet-}/H_2O_2$ production in the mitochondria through the post-translational redox modification of protein cysteine thiol groups. Sulfenylation, a process that describes the oxidation of target cysteine thiols by H_2O_2 directly, has been extensively researched. This reaction first requires the ionization of the cysteine sulfur group into a thiolate anion before it can perform a nucleophilic attack on H_2O_2, resulting in the oxidation of the protein cysteine thiol into sulfenic acid (*52*). While it has been proposed that direct sulfenylation of enzymatic ROS producers by H_2O_2 may serve as a form of negative feedback control, the opposite has been argued in that sulfenylation does not in fact meet the necessary requirements for protein regulation by covalent modification (*22, 52*). In fact, early work by Nulton-Persson and Szweda demonstrated that in cardiac mitochondria challenged with H_2O_2, NADH-linked ADP-dependent respiration decreased due to the reversible inhibition of KGDH (*62*). However, this was not due to direct modifications of KGDH by H_2O_2, but rather through a separate redox-sensitive mechanism known as protein S-glutathionylation (*63*).

2.5 - Protein S-glutathionylation

Protein S-glutathionylation is a reversible post-translational redox modification involving the addition of a reduced glutathione (GSH) moiety to a reactive protein cysteine thiol (*64*). These modifications can occur either as a spontaneous reaction or be enzymatically driven. Spontaneous protein glutathionylation reactions are dependent on the ratio of reduced glutathione to oxidized

glutathione (2GSH:GSSG). The ratio is kept high at around 50-100 (*52*). As the cell experiences an increase in H_2O_2 concentration, the ratio will decrease, denoting the oxidation of the glutathione pool. When the GSH:GSSG ratio approaches approximately 1, non-enzymatic spontaneous protein S-glutathionylation can be induced (*25*). There are three mechanisms in which spontaneous protein S-glutathionylation can occur (*25*):

1. A protein cysteine thiol is ionized to a thiolate anion and performs a nucleophilic attack on glutathione.
2. The thiolate anion is oxidized to sulfenic acid by H_2O_2 and performs a nucleophilic attack on GSSG.
3. The cysteine thiol is transformed into a protein thiyl radical, then forms a protein thiyl radical-glutathionyl intermediate.

Of note, a GSH:GSSG ratio of ~ 1 is indicative of oxidative distress (*65*). Thus, it is not expected for proteins to be spontaneously and non-enzymatically S-glutathionylated in normal, homeostatic cells. One exception to this is the transcription factor, *c*-Jun, which can reportedly undergo reversible S-glutathionylation by GSSG at a specific cysteine residue in its DNA binding site when the GSH:GSSG ratio is as high as 13 (*66*). In addition, some mitochondrial proteins, such as complex II, UCP2, and UCP3, have been observed to be basally S-glutathionylated in normal conditions, perhaps suggesting that these are amenable to spontaneous modification in a less oxidized environment (*67*, *68*).

Nonetheless, most S-glutathionylation modifications are enzyme-driven. The glutaredoxin (Grx) family are the main catalysts for enzyme-mediated protein S-glutathionylation in the cell. Glutaredoxins are small, heat-stable, thiol oxidoreductases that govern the addition or removal of a glutathione moiety from the target protein. Glutaredoxin-1 (Grx1) was the first glutaredoxin

discovered to mediate glutathionylation modifications via its protein deglutathionylation activity (*25*). Grx1 contains a thioredoxin fold with three α-helices and four β-sheets (*69*). Situated in the first loop region within the first α-helix at its N-terminus, Grx1 contains a *CXXC* motif that is required for its (de)glutathionylase activity, while at its C-terminus, Grx1 possesses a glutathione binding domain (*69, 70*). Grx1-mediated deglutathionylation of a modified protein cysteine thiol group is accomplished through a three-step mechanism. First, the catalytic cysteine on Grx1 removes the glutathionyl moiety from a target protein through a thiol disulfide exchange reaction. Next, a glutathione molecule that is bound to the GSH-binding domain in the C-terminus of Grx1 is ionized, allowing it to attack the newly acquired glutathione moiety at the catalytic cysteine. This yields GSSG, which subsequently gets released from Grx1, thereby reactivating the enzyme. Finally, GSSG is reduced into two units of GSH by glutathione reductase (GR) in a NADPH-dependent manner, thus completing the deglutathionylation cycle (*25*). Grx1 is found in the cytoplasm and intermembrane space of the mitochondria in heart, kidney, skeletal muscle, and liver cells. It is known to play an integral regulatory role in a broad array of cellular functions, such as cell division, apoptosis, energy metabolism, and crosstalk between cell signaling pathways (*71*).

Glutaredoxin-2 (Grx2) is a Grx1 homologue that is primarily located within the mitochondrial matrix and like Grx1, it can catalyze glutathionylation and deglutathionylation events on target proteins. Moreover, Grx2 is known to mediate these modifications of target proteins, such as complex I, in response to changes in the redox status of the glutathione pool (*72*). When the glutathione pool is more oxidized, Grx2 will catalyze protein S-glutathionylation of its targets while a more reduced glutathione pool will lead to protein deglutathionylation. Grx1 shares a similar catalytic mechanism and while the relationship between Grx1 activity and the redox state

of the GSH pool was previously unclear, recent evidence has revealed that Grx1 does indeed share a similar sensitivity to intracellular GSH as Grx2 (*73, 74*). A unique trait of Grx2 is that it can reduce the oxidized form thioredoxin-2 (Trx2) to reactivate its enzymatic activity. This is an important compensatory mechanism in the mitochondria that can keep the Trx2 antioxidant system active in conditions where thioredoxin reductase-2 (TrxR2) may be deactivated from oxidative distress (*75*).

Similar to Grx1, Grx2 is highly expressed heart, kidney, skeletal muscle, and liver tissues. Notably, Grx2 also possesses three splice variants: Grx2a, Grx2b, and Grx2c. Grx2a is the splice variant isoform expressed in the aforementioned tissues while Grx2b and Grx2c are exclusively found in testes. Moreover, these two isoforms localize to the cytoplasm and nuclear lumen as opposed to strictly the mitochondrial matrix (*76*). Far fewer targets of Grx2 have been identified in comparison to Grx1, but the significance of its regulation on those protein targets is well-established. Mitochondrial enzymes, such as complex I, UCP3, PDH, and KGDH, are known to be modified by Grx2 and many groups have demonstrated that Grx2-mediated protein S-glutathionylation and deglutathionylation of its targets acts as a critical form of regulation on energy metabolism and mitochondrial bioenergetics (*25*). For example, Nulton-Persson et al. demonstrated this in 2003 when they examined changes in respiratory and KGDH enzyme activity in rat heart mitochondria in response to H_2O_2 treatment (*63*). They saw that reduced GSH levels decreased in response to H_2O_2 treatment prior to KGDH inactivation but then recovered simultaneously with enzyme activity. Moreover, they identified glutaredoxin as the primary facilitator for KGDH glutathionylation and deglutathionylation (*63*). The mechanism for its modification was later found to occur through the specific S-glutathionylation of the catalytic vicinal thiols in the lipoic acid moieties of the E2 subunit (*77*). Protein S-glutathionylation is also

known to regulate H_2O_2 production; in fact, the Grx2-mediated S-glutathionylation of both KGDH and PDH has shown to suppress their H_2O_2 production by approximately 90% (*78*).

Furthermore, H_2O_2 production by KGDH and PDH appear to be differentially regulated by glutathionylation between the sexes and Mallay et al. were one of the first groups to report on the presence of these site-specific sex dimorphisms. They demonstrated that H_2O_2 generated by KGDH and PDH in male liver mitochondria occurred at 5- and 3-times higher rates than in females, respectively (*79*). Additionally, increased glutathionylation of KGDH and PDH inhibited H_2O_2 production in males while having no effect in females (*79*). It is well established that sex dimorphisms exist between male and female liver mitochondria in general, such as higher mitochondrial protein content, higher antioxidant levels, and less overall H_2O_2 production in females, all of which point to their more efficient mitochondrial machinery and greater redox buffering capacity (*80*). However, this was the first study that clearly illustrates these differences at the enzymatic level, providing a much closer look at how H_2O_2 production by KGDH and PDH are regulated between the sexes. In addition to KGDH and PDH, recent evidence has revealed that DHODH is also targeted for glutathionylation. Koufos et al. not only demonstrated that glutathionylation inhibited H_2O_2 production and dihydroorotate oxidation by DHODH, but that there was also sex dimorphic effect in that DHODH from female mitochondria were more resistant to being inhibited (*81*). Interestingly, the loss of Grx2 expression in muscle has also been linked with ameliorated fuel consumption, increased total energy expenditure, and decreased body weight and fat mass, suggesting a possible connection between redox signaling in the mitochondria and the treatment of diet-induced obesity and related diseases (*82*). The relationship between H_2O_2 production by mitochondrial dehydrogenases and their modification by Grx2-mediated reversible protein S-glutathionylation in response to changes in cellular redox status raises the question as to

whether these enzymes are similarly regulated by other reversible redox-sensitive modifications, such as protein S-nitrosylation, which describes a nitro-addition to a target cysteine residue (*83*).

2.6 - Protein S-Nitrosylation

2.6.1 - NO-related Redox Signaling

Nitric oxide (NO) is a gaseous compound that was discovered to be of physiological relevance in vascular relaxation by Furchgott et al. and Salvador Moncado nearly 30 years ago (*84, 85*). NO signaling can be split into two subcategories: classical and non-classical signaling. Classical signaling typically refers to the production of cyclic GMP (cGMP) from GTP and the activation of the cGMP-dependent protein kinase (PKG) pathway, which leads to a lowering in cytosolic K^+ and Ca^{2+} levels and the vasodilation of smooth muscle blood vessels (*86*). On the other hand, non-classical NO signaling governs a much wider range of functions in different tissues. One mechanism for non-classical NO signaling is *S*-nitrosylation, a reversible, covalent post-translational redox modification involving the addition of NO to a reactive cysteine thiol (*83*). Enzymatic activity can be regulated by the selective S-nitrosylation of catalytic cysteine thiols. These S-nitrosylated proteins are referred to as protein S-nitrosothiols (PSNOs) (*87*). Additionally, NO can elicit indirect redox signals as secondary messengers in the form of ROS or RNS, which can also target cysteine thiol groups (*87*). Therefore, the physiological effects that arise from NO signaling are mediated through the nitro-addition to key cysteine residues.

NO signaling is dependent on the local concentration of NO, which is influenced by spatial regulation and the compartmentalization of the NO source. Due to its short half-life (0.09-2 seconds) and the rapidity of its production (<0.1 seconds), NO effects are generally observed in confined regions near the source its production where its local concentration can be raised to a sufficient level to elicit a cell response (*88*). One source of NO is nitric oxide synthase (NOS), which exists as three isoforms in mammalian cells: NOS1 (nNOS; neuronal NOS), NOS2 (iNOS;

inducible NOS), and NOS3 (eNOS; endothelial NOS) (*89*). NOS1 and NOS3 are expressed constitutively within the cell cytosol and are responsible for generating homeostatic basal NO levels across various tissues (*90*). On the other hand, NOS2 is inducibly expressed in response to inflammatory signals and works in tandem with phagosomes and peroxisomes to remove dangerous pathogens (*91*). NOS is a dimer composed of two identical monomers in a tetrahedral format connected by a zinc ion at two C-X-X-X-X-C motifs (*90*). This motif allows NOS to bind to its substrate, L-arginine, and cofactor, tetrahydrobiopterin (BH_4), driving its dimerization and enzymatic activity. Each NOS monomer contains two domains: a carboxyl-terminal reductase domain and an amino-terminal oxygenase domain. Both domains are connected via a linker region, which, in the case of NOS1 and NOS3, can bind calmodulin, rendering them sensitive to Ca^{2+} (*90*). The reductase domain contains redox-active cofactors, such as NADPH, FAD, and FMN, which coordinate electron transfer reactions. The oxygenase domain is the site of dimerization for NOS and coordinates with a zinc ion, BH_4, heme, and L-arginine (*90*). In cases of substrate or cofactor deficiency, NOS becomes uncoupled and will subsequently generate $O_2^{\cdot-}$ instead of NO at its heme center (*89*). Interestingly, there have been some studies that have suggested the presence of another NOS isoform in the mitochondrial matrix and inner membrane, termed mitochondrial NOS (mtNOS). mtNOS is reportedly an nNOS homologue and is implicated in the regulation of oxygen consumption and mitochondrial biogenesis (*89*). However, mtNOS is controversial and its actual existence is still under much debate.

Another important source of biological NO is S-nitrosoglutathione (GSNO). GSNO is an abundant low-molecular weight (LMW) S-nitrosothiol (SNOs) in the cell and is an endogenously synthesized in the mitochondria via the transfer of NO from the heme iron of cytochrome c to glutathione (GSH) (*92*). GSNO can translocate to other compartments to increase its proximity to

its targets and effectively donate its NO moiety to catalytic cysteine thiols of key mitochondrial and cellular proteins, including KGDH (*93*).

2.6.2 - Regulation of Protein S-Nitrosylation

While NO, which is often endogenously present in its radical form (•NO), is an oxidant, it can only react with targets that possess unpaired electrons or transition metals (*94*). Therefore, PSNOs are commonly generated through an intermediate possessing a higher oxidation state, increasing its reactivity with the protein cysteine thiol groups. Fernando et al. proposed four different reactions schemes for S-nitrosylation, which are listed below in Figure 6 (*89*).

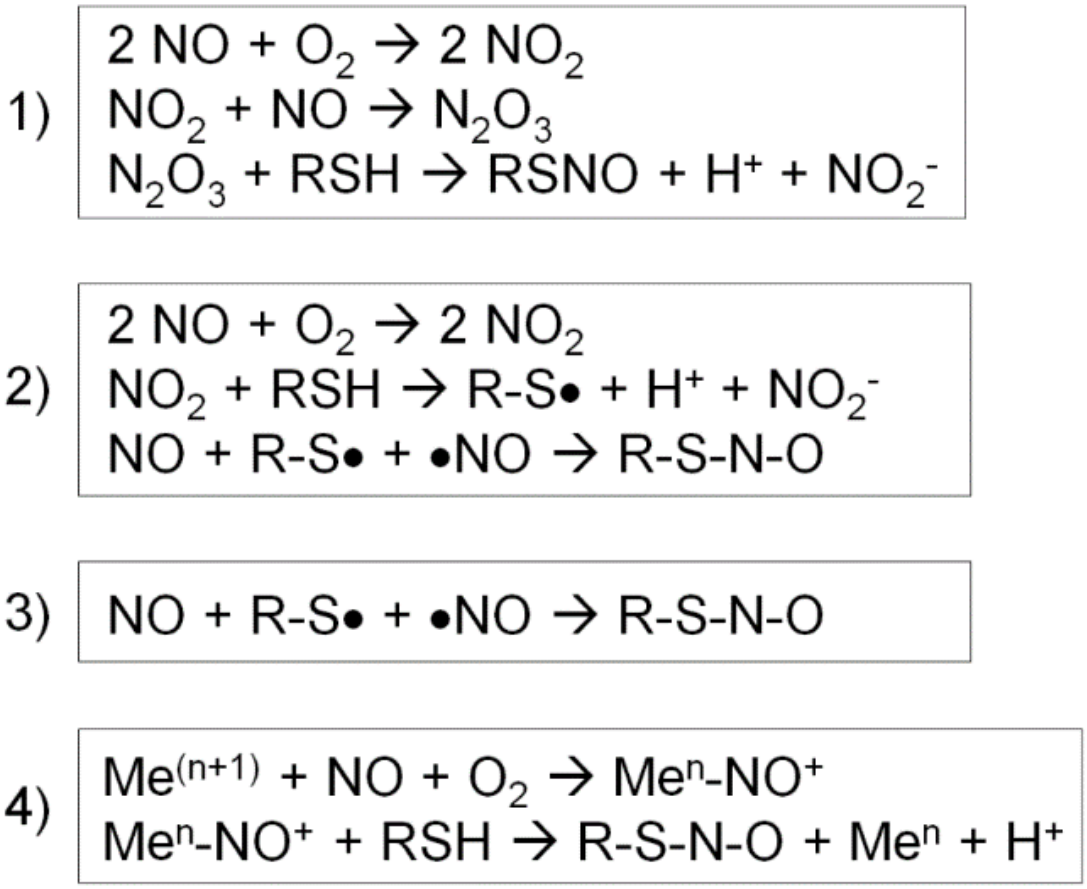

Figure 6: Four types of protein S-nitrosylation reactions. Reactions 1) through 4) represent four potential mechanisms in which a thiol-containing target (RSH, R-S•) may become S-nitrosylated (RSNO) (*89*).

In reaction 1) of Figure 6, NO reacts with molecular oxygen to produce a set of nitrogen oxide intermediates with increasing oxidation states. NO_2 will then undergo auto-oxidation with another NO molecule to generate N_2O_3, which can then react with a thiol-containing target (RSH), such as a protein cysteine residue, to produce a nitrosothiol (RSNO) and nitrite (NO_2^-) as a by-product. In reaction 2) of Figure 6, the NO_2 formed via NO and O_2 reacts with the thiol group, generating a thiol radical (R-S•) and nitrite. The thiol radical can then react with NO and NO• to make a nitrosothiol. Reaction 3) of Figure 6 is similar to reaction 2) but describes S-nitrosylation with a thiol radical as the starting reactant. Finally, reaction 4) in Figure 6 illustrates a metal-catalyzed S-nitrosylation reaction. A metalloenzyme containing a transition metal, such as Cu^{2+} or Fe^{3+}, oxidizes NO to produce a nitrosonium (NO^+)-metal intermediate. NO^+ can then react with a thiol group in close proximity to the metalloenzyme to create a nitrosothiol. Metal-catalyzed RSNO formation is seen in the auto-nitrosylation of hemoglobin and the synthesis of endogenous GSNO by cytochrome *c* (*95*).

S-nitrosylation of protein cysteine thiols occurs with a high degree of specificity and the targeting of select residues for modification is influenced by several factors. First, the proximity of the target cysteine thiol to an NO source greatly affects the likelihood in which the protein will get S-nitrosylated. Enzymes that exist near NO sources, such as NOS itself and its interacting enzymes, will have a higher affinity for S-nitrosylation. In fact, many groups have observed the S-nitrosylation of NOS1 and NO3, suggesting a possible shut-off mechanism for these constitutively expressed enzymes (*96*). Second, the targeted cysteine occurs within the signature motif, I/L-X-C-X2-D/E (*97*). This motif, which confers NOS specificity, must be within a α-helix with a large surface area and the cysteine thiol must have a high nucleophilicity to react with the nitrosyl group (*98*). Thirdly, the target cysteine residue must be in a suitable environment. As mentioned before,

NO itself has a low reductive potential and can only initiate direct oxidation in select cases. Therefore, it is often preceded with the production of nitrogen oxide intermediates, NO_2 and N_2O_3, by NO and O_2, which go on to S-nitrosylate the thiol group due to their higher oxidative state (*99*). This mechanism is heavily promoted in hydrophobic regions where NO and O_2 are more stably recruited and this type of environment has shown to improve the reaction rate by 30-300-fold (*100*). However, the accessibility of the cysteine thiol can sometimes be hindered in such hydrophobic-centric regions. Thus, it also relies on the nature of its neighbouring amino acid residues for its reactivity with NO. For the cysteine residue to remain a target for modification, the thiol group must have a lower pKa to maintain its nucleophilicity. This is promoted when the cysteine is surrounded basic residues within 6 Å and fewer bulky residues, such as Phe and Leu, within 8 Å to decrease steric hinderance, or α-helices containing positive dipole moments (*101*).

Protein S-nitrosylation levels are also regulated by cellular redox status, denitrosylation activity, and endogenous NOS inhibitors. In the case of redox status, antioxidant levels can affect global levels of protein S-nitrosylation, with one group linking the depletion of the antioxidant, GSH, with increased S-nitrosylation of mitochondrial proteins (*102*). An increase in protein S-nitrosylation due to a decrease in antioxidants also implies the opposite, where an increase in antioxidants infers an inhibition of S-nitrosylation through an elevation in the reducing potential within the cell (*89*). Furthermore, cellular S-nitrosylation levels are mediated through denitrosylation, which can occur in both an enzymatic and non-enzymatic manner (*103*). Non-enzymatic denitrosylation involves the cleavage of the nitrosyl group from the protein cysteine thiol and can occur spontaneously in the presence of direct and indirect antioxidants, such as ascorbate or GSH, metal ions, ROS, and other nucleophiles (*103*). On the other hand, enzymatic denitrosylation is catalyzed primarily through two different denitrosylase systems within the cell:

the S-nitrosoglutathione (GSNO)/GSNO reductase (GSNOR) system and the thioredoxin (Trx)/thioredoxin reductase (TrxR) system (*103*).

The Trx/TrxR system consists of Trx1/2 (cytoplasmic/mitochondrial), TrxR, and NADPH, and targets a range of S-nitrosylated proteins for denitrosylation, such as caspase-3 and nuclear factor-κB (NF-κB) (*103*). The mechanism for PSNO denitrosylation is likely very similar to how Trx/TrxR resolves protein disulfide bonds or deglutathionylation and begins with the formation of a mixed disulfide between Trx and the target protein. Trx contains a C-X-X-C dithiol motif at its catalytic site, consisting of residues Cys32 and Cys35 (*103*). The mixed disulfide formation is catalyzed by the nucleophilic attack of Cys32 on the sulfur at the P-SNO bond, releasing the NO moiety as a nitroxyl anion (HNO^-). This mixed protein-Trx disulfide intermediate is resolved by the neighbouring active cysteine residue on Trx, Cys35, through a disulfide exchange reaction. A new disulfide bridge is created between Cys32 and Cys35 on Trx, now oxidized Trx, and the newly denitrosylated protein is freed. Trx disulfide is subsequently reduced by the NADPH-dependent TrxR to regenerate the reduced form of Trx (*103*). The GSNO/GSNO system differs from the Trx/TrxR system in that it has only one target for denitrosylation: GSNO. GSNOR, previously identified as alcohol dehydrogenase 5 (ADH5), regulates the level of cellular and mitochondrial protein S-nitrosylation by metabolizing GSNO in an NADH-dependent manner, generating glutathione disulfide (GSSG) and a glutathione-*N*-hydroxysulfenamide intermediate, which subsequently gets reduced to ammonia (*104*). Interestingly, there is evidence suggesting that GSNO can also be enzymatically metabolized by the Trx/TrxR system, though it is unclear as to the exact impact this plays in a physiological context (*105*, *106*).

Finally, cellular PSNO levels are also influenced by the presence of endogenous NOS inhibitors, which can be separated into two categories: L-arginine analogues (competitive

inhibitors) and allosteric inhibitors. Endogenously produced L-arginine analogues include methylarginines, such as asymmetric dimethylarginine (ADMA) and N^G-monomethyl-L-arginine (L-NMMA), which both compete with the L-arginine binding sites on all three NOS isoforms (*107*). Allosteric NOS inhibitors include dynein light chain LC8-Type 1 (DYNLL1), which can inhibit the dimerization of NOS1 by binding to its PDZ domain in the N-terminus (*108*).

2.6.3 - Transnitrosylation

The specificity and selectivity of S-nitrosylation for targeted cysteines can be increased through a series of consecutive S-nitrosylation reactions, or transnitrosylation. Transnitrosylation involves the transfer of a nitrosyl group from an S-nitrosylated protein (nitrosylase) cysteine or metal center to another cysteine. Successive transnitrosylation reactions can occur which allows for NO-signals to be transmitted further away from the source of NO (*109*). Metal-catalyzed transnitrosylation is seen at the metal centers of hemoglobin and cytochrome c, where NO at the heme iron-sulfur cluster is transferred either to a neighboring cysteine thiol within the same molecule in the case of hemoglobin, or to the thiol group on GSH in the case of cytochrome c, generating GSNO, a major endogenous NO donor (*92*). Transnitrosylation between Cys-Cys residues occurs when the nitrosyl nitrogen atom on the donor/nitrosylase undergoes nucleophilic attack by the thiolate anion on the NO-acceptor (*99*). Only a few S-nitrosylases have been identified to date, and those that have been confirmed are bound by the same set of conditions denoting S-nitrosylation specificity, such as the proximity between the S-nitrosylase and NO-acceptor, and the redox potentials of the interacting proteins (*109*). Besides GSNO, other known S-nitrosylases include glyceraldehyde-3-phosphate dehydrogenase (GAPDH), and the calcium-/zinc-binding proteins S100A8/A9 (*89*). GAPDH is primarily recognized for its role in the conversion of glyceraldehyde-3-phosphate into D-glycerate 1,3-bisphosphate during glycolysis, but also plays a crucial role in the transcriptional regulation of apoptosis (*110*). In response to

stress signals, NOS2 is activated, triggering the S-nitrosylation of S100A8/A9, which consequently S-nitrosylates GAPDH at its catalytic Cys150 residue (*111*). This results in its translocation to the nucleus with the E3 ubiquitin ligase, Siah1. While Siah1 initiates apoptosis and degradation of nuclear proteins, nuclear GAPDH can transnitrosylate a range of targets involved in DNA repair, apoptosis, and deacetylation, such as DNA-activating protein kinase, p53, and HDAC2 (*111*). GAPDH has also been observed to translocate to the mitochondria in response to stress where it catalyzes the transnitrosylation of mitochondrial proteins Hsp60, acetyl-CoA acetyltransferase (ACAT), and voltage-dependent anion channel 1 (VDAC1) (*112*).

2.6.4 - S-Nitrosylation of Mitochondrial Proteins

The regulation mitochondrial proteins is tightly controlled by a variety of factors, including reversible post-translational modifications like protein S-nitrosylation. While the presence of mtNOS remains controversial, mitochondrial NO generated from other sources, such as GSNO, targets specific protein cysteine thiols for nitrosylation with a preference for enzymes localized to the IMM, IMS, and within the mitochondrial matrix. These enzymes include all the ETC complexes, key enzymes in the Krebs cycle and β-oxidation, and regulators of apoptosis (*89*).

In an oxidizing environment, Complexes I-V activity can be regulated through protein S-nitrosylation, which in turn, modulates ROS production at these sites as well (*113*). For example, Complex I is reversibly S-nitrosylated at Cys39 in the ND3 subunit by GSNO, resulting in a decrease in mitochondrial respiration and a reduction in H_2O_2 production by Complex I (*114*). Complex V/ATP Synthase is also regulated by reversible protein S-nitrosylation at Cys294, leading to a decrease in ATP synthesis (*115*). In addition to all the ETC complexes, cytochrome c is targeted for S-nitrosylation during the biosynthesis of GSNO. This occurs through a

transnitrosylation reaction between the nitrosylated iron center within the heme group of cytochrome c and the cysteinyl moiety of GSH (*116*).

Succinate dehydrogenase (SDH), synonymous with Complex II, is a catabolic enzyme complex that directly links the Krebs cycle with the ETC (*15*). SDH, as well KGDH, are targeted for protein S-nitrosylation, ultimately leading to the inhibition of their activities and, potentially, a decrease in H_2O_2 production at these sites (*113*). Many studies agree that the S-nitrosylation, and subsequent inhibition, of KGDH, complex I-V, and other mitochondrial proteins serves as protection against oxidative or nitrosative damage by acting as a barrier for reactive cysteine thiols against oxidation by ROS or RNS, similar to protein S-glutathionylation, and through the scavenging of NO prior to its reaction with $O_2^{\bullet-}$ to generate peroxynitrite radicals (*117*). Chouchani et al. demonstrated this in heart and liver mitochondria, revealing an inhibition of KGDH activity in response to increased concentrations of GSNO, a protein S-nitrosylation catalyst (*118*). Intriguingly, an early study by Sun et al. done in ischemia/reperfusion (I/R) models revealed that ischemic preconditioning resulted in the protein S-nitrosylation-dependent recovery KGDH activity, which is typically inhibited following I/R attack. This was further enhanced by GSNO treatment, suggesting that S-nitrosylation exhibits its protection on KGDH through an upregulation of its activity in I/R models instead of inhibition (*119*).

Furthermore, Chouchani et al. were able to identify five enzymes involved in fatty acid β-oxidation that are targeted for protein S-nitrosylation: very long chain acyl-CoA dehydrogenase (VLCAD), short-chain acyl-CoA dehydrogenase (SCAD), enoyl-CoA hydratase (ECH), carnitine palmitoyl transferase 2 (CPT2), and electron-transfer flavoprotein:ubiquinone oxidoreductase (ETFDH) (*118*). VLCAD, SCAD, ECH, and CPT2 initiate the first steps in β-oxidation, which are the oxidation and subsequent hydration of unsaturated carbons on very-long-chain and short-chain

fatty acids, while ETFDH is responsible for supplying electrons that arise from the oxidation of fatty acids to the mitochondrial ubiquinone pool (*118*). VLCAD in particular catalyzes the rate-limiting step in fatty acid β-oxidation and the reversible, but selective S-nitrosylation of its Cys^{238} residue by GSNO is associated with an increase in the oxidation of palmitoyl-CoA. Given that Cys^{238} is located within a loop structure, it is proposed that its S-nitrosylation enhances its flexibility and increases overall protein movement, allowing for superior substrate affinity and a lower K_M for VLCAD (*120*).

While S-nitrosylation of ETC complexes and mitochondrial metabolic enzymes confers protection against oxidative damage by ROS, the S-nitrosylation of mitochondrial pro- and anti-apoptotic enzymes elicits protection against cell death. Critical mitochondrial enzymes targeted for S-nitrosylation in this context include the mitochondrial permeability transition pore (mPTP), the voltage-dependent anion channel (VDAC), caspases, and Bcl-2 (*89*). The mPTP is embedded within the mitochondrial inner membrane and controls its permeability to extra-mitochondrial molecules. Under normal conditions, cyclophilin D (CypD), an essential mPTP cofactor, is S-nitrosylated, preventing its association with mPTP and leaving the mPTP closed. However, under oxidative stress, higher concentrations of ROS and RNS can oxidize the mPTP, resulting in conformational changes that allows it open and become permeable to larger molecules, eventually leading to mitochondrial swelling, loss of ATP synthesis, necrosis, and mitochondrial death (*121*). VDAC is localized to the mitochondrial outer membrane and regulates the transport of mitochondrial metabolites, as well as the regulation of mitochondrial-mediated apoptosis (*89*). The S-nitrosylation of VDAC is reported as having a similar effect as mPTP S-nitrosylation, where lower levels of NO confer apoptotic protection through VDAC inhibition and higher levels of NO result in an upregulation of its activity, leading to similar physiological consequences (*122*).

Likewise, caspases and Bcl-2 are also both intimately involved in apoptotic signaling pathways and inhibited upon S-nitrosylation, culminating in the protection against cell death (*91*).

2.6.5 - Implications of S-nitrosylation in Health and Disease

Protein S-nitrosylation has been proven to play an important role in redox homeostasis and is an integral component of NO-related signaling cascades. In a physiological context, S-nitrosylation of target proteins acts as protection against oxidative and nitrosative damage by ROS, RNS, and other strong oxidants, and is strongly implicated in ischemic preconditioning (IPC), a protective mechanism in the heart that involves brief exposure of cardiomyocytes to ischemia and reperfusion (I/R), allowing the myocardial tissue to build up a resistance to prolonged ischemic injury in the future (*119*). These cardioprotective effects are mainly due to the increased accumulation of cardiac mitochondrial PSNOs, which can occur through the activation of pharmacological agents, such as the nitro-vasodilator nitroglycerin, and the upregulation of NO-producers and catalysts, such as iNOS or endogenous GSNO (*119*). Other proposed mechanisms of cardiac IR protection by S-nitrosylation include the inhibition of H_2O_2 production at Complex I by transported S-nitrosylation agents, the S-nitrosylation of cardiac proteins involved in estrogen receptor activation, and the statin-mediated S-nitrosylation and activation of the thioredoxin system, which protects against oxidative damage through the decrease in ROS (*113*).

Furthermore, the dysregulation of S-nitrosylation has been linked to a large range of diseases spanning across many different tissue types. Studies performed in cardiac cells have connected the development of arrhythmias characteristic of sudden cardiac arrest and idiopathic dilated cardiomyopathies to the aberrant S-nitrosylation of Ca^{2+} channel proteins and related proteins (*105*). This observed irregularity in S-nitrosylation is traceable to the incorrect

compartmentalization of eNOS and nNOS, both of whom are localized to different, but specific regions within cardiac tissue and elicit opposite effects on myocardial contractility (*104*).

Protein S-nitrosylation and NO production has also been implicated in insulin resistance in Type II diabetes (T2D). In diabetic mice models, protein kinase B (PKB/Akt), insulin receptor β-subunit (IRβ), and insulin receptor substrate 1 (IRS1) are all clearly S-nitrosylated to a higher degree when compared to wild-type mice (*104*). Specifically, the iNOS-dependent S-nitrosylation, which is upregulated in diabetic models, and the exogenous GSNO-mediated S-nitrosylation of IRβ led to an inhibition of its tyrosine kinase activity, thereby preventing the propagation of insulin/insulin receptor signaling (*123*). Further evidence for the involvement of S-nitrosylation in T2D was shown in iNOS expression models where iNOS knockout mice fed a high-fat diet, which led to diet-induced obesity, had a greater glucose tolerance and normal insulin sensitivity and insulin-stimulated glucose uptake when compared with wild-type mice fed the same high-fat diet, implying a positive relationship between iNOS expression and the development of insulin resistance and T2D (*124*).

Neurodegenerative diseases, such as Parkinson's disease (PD), Alzheimer's disease (AD), Huntington disease (HD), and amyotrophic lateral sclerosis (ALS) are the benchmark examples of disease pathogenesis arising from oxidative stress and dysfunctional redox-signaling pathways within the mitochondria. In this respect, excessive protein S-nitrosylation and the resulting accumulation of PSNOs has been observed in models for PD, AD, HD, and ALS (*125*). In fact, the selective protein S-nitrosylation of PTEN induced putative kinase 1 (PINK1) has recently been recognized as one of the earliest hallmarks for PD (*126*). This highlights the significance and physiological relevance of protein S-nitrosylation since a greater understanding for its targets and

mechanisms of regulation could prove useful in deciphering novel approaches in treating human diseases.

3 - MATERIALS AND METHODS

3.1 - Materials

Material:	Source:		Material:	Source:
1-Choro-2,4-dinitrobenzene (CDNB)	Sigma-Aldrich		Glutathione (reduced) (GSH)	Sigma-Aldrich
3-methyl-2-oxopentanoic acid (KMV)	Sigma-Aldrich		HEPES	Sigma-Aldrich
α-ketoglutarate	Sigma-Aldrich		Horseradish Peroxidase (HRP)	Sigma-Aldrich
Adenosine Diphosphate (ADP)	Sigma-Aldrich		Hydrogen Peroxide (H_2O_2)	Sigma-Aldrich
Amplex Ultra Red (AUR)	Invitrogen		KGDH (purified)	Sigma-Aldrich
Auranofin (AF)	Sigma-Aldrich		NAD+	Sigma-Aldrich
Bovine Serum Albumin – Defatted (BSA)	Sigma-Aldrich		PDH (purified)	Sigma-Aldrich
Bradford reagent	Sigma-Aldrich		Pyruvate	Sigma-Aldrich
Coenzyme A (CoASH)	Sigma-Aldrich		S-nitrosoglutathione (GSNO)	Sigma-Aldrich
CPI-613	Sigma-Aldrich		Sucrose	Sigma-Aldrich
Dimethyl Sulfoxide (DMSO)	Sigma-Aldrich		Superoxide Dismutase (SOD)	Sigma-Aldrich
D-mannitol	Sigma-Aldrich		Thiamine Pyrophosphate (TPP)	Sigma-Aldrich
Ethylene glycol – bis (β-aminoethyl ether) - N, N, N′, N'-tetraacetic acid (EGTA)	Sigma-Aldrich			

Of note, all original figures generated under the "LITERATURE REVIEW" section were created using BioRender.com

3.2 - Study Design

The purified enzyme assays looked to assess the effects of GSNO, an S-nitrosylation catalyst. Purified KGDH and PDH purchased from Sigma Aldrich were treated with increasing concentrations of GSNO. The rate and amount of $H_2O_2/O_2^{\cdot-}$ produced by purified enzyme samples

incubated with increasing GSNO concentration was measured and compared against a zero control. The activities of purified KGDH and PDH were also simultaneously assessed with H_2O_2 measurements.

The effects of GSNO on $H_2O_2/O_2^{\cdot-}$ by KGDH and PDH were then assessed in isolated liver mitochondria from both male and female mice. Isolated liver mitochondria was treated with increasing concentrations of GSNO, and the rate and amount of $H_2O_2/O_2^{\cdot-}$ measured was compared against a zero control. Isolated mitochondria were also treated with mitochondrial antioxidant system inhibitors, 1-Choro-2,4-dinitrobenzene (CDNB) and auranofin (AF), to eliminate possible side-interactions with the S-nitrosylation catalyst with the goal of improving the specificity of S-nitrosylation by GSNO to the enzymes of interest, KGDH and PDH.

3.3 - Methods

3.3.1 - Animal Care

Animals were cared for in accordance with the principles and guidelines of the Canadian Council on Animal Care and the Institute of Laboratory Animal Resources (National Research Council). All procedures using mice were approved by the Facilities Animal Care Committee (FACC) in the Faculty of Agricultural and Environmental Sciences at McGill University. Male and female C57BL6N mice were purchased at either 4-weeks or 9-weeks of age from Charles River Laboratories and housed at 25˚C in the Small Animal Care Unit (SARU) at the McGill MacDonald campus on a 12-h day/night light cycle (lights on at 07:00h). The mice were provided free access to water at all times, which was replaced on a weekly basis by the SARU staff. Mice purchased at 9-weeks of age were placed on a standard chow diet (2920X Irradiated Teklad Global Soy Protein-Free Extruded Rodent Diet) until experimentation. Mice purchased at 4-weeks of age were placed on either a high-fat diet (HFD; TD.06415 Teklad Custom Diet; 45/fat) or a control match diet (CM; TD.06416 Teklad Custom Diet; 10/fat) for a minimum of 5 weeks.

Approximately 45% of the total calories in the HFD is derived from fat and its fatty acid profile is 35% saturated, 40% monounsaturated, and 25% polyunsaturated. On the other hand, in the CM diet, approximately 10% of the total calories comes from fat and its fatty acid profile is 26% saturated, 33% monounsaturated, and 41% polyunsaturated. The formula composition for the standard chow diet is listed in Table 1 while the formula compositions for the HFD and CM diet are listed below in Table 2.

Table 1: Formula composition for standard chow diet.

Macronutrients:	% diet composition
Crude Protein	19.1
Fat	6.5
Carbohydrate	47.0
Crude Fiber	2.7
Neutral Detergent Fiber	12.3
Ash	5.1
Minerals, Amino Acids, Fatty Acids	7.3

Energy Density:	
In kcal/g	3.1
In kJ/g	13.0

Source of Calories:	% total calories
Calories from Protein:	**24%**
Calories from Fat:	**16%**
Calories from Carbohydrate	**60%**

Fatty Acids:	% diet composition
C16:0 Palmitic	0.6
C18:0 Stearic	0.1
C18:1ω9 Oleic	1.1
C18:2ω6 Linoleic	2.6
C18:3ω3 Linolenic	0.3
Total Saturated	0.8
Total Monounsaturated	1.1
Total Polyunsaturated	2.9

Further information on the breakdown of mineral, amino acid, and vitamin profiles of the standard chow diet which were not mentioned in Table 1 can be provided by the supplier (Envigo – Teklad) directly using the corresponding diet name (2920X Irradiated Teklad Global Soy Protein-Free Extruded Rodent Diet) and is listed in the Appendix section. The ingredients for the

standard chow diet were provided directly from the supplier (Envigo – Teklad) and are listed in descending order of inclusion:

Ground wheat, ground corn, corn gluten meal, wheat middlings, soybean oil, calcium carbonate, dicalcium phosphate, brewers dried yeast, L-lysine, iodized salt, magnesium oxide, choline chloride, DL-methionine, calcium propionate, L-tryptophan, vitamin E acetate, menadione sodium bisulfite complex (source of vitamin K activity), manganous oxide, ferrous sulfate, zinc oxide, niacin, calcium pantothenate, copper sulfate, pyridoxine hydrochloride, riboflavin, thiamin mononitrate, vitamin A acetate, calcium iodate, vitamin B12 supplement, folic acid, biotin, vitamin D3 supplement, cobalt carbonate.

Table 2: Formula compositions for high-fat and control match diets.

Ingredient (g/kg)	**TD.06415** **High-Fat Diet (HFD)**	**TD.06416** **Control Match (CM)**
Fat:	**44.8% of total kcal**	**10.2% of total kcal**
Soybean Oil	30.0	20.0
Lard	195.0	20.0
Carbohydrate:	**36.2% of total kcal**	**69.8% of total kcal**
Corn Starch	85.0	280.0
Maltodextrin	115.0	50.0
Sucrose	200.0	325.0
Protein:	**19.0% of total kcal**	**20.0% of total kcal**
Casein	245.0	210.0
L-Cystine	3.5	3.0
Other:		
Cellulose	58.0	37.15
Mineral Mix, AIN-93G-MX (94046)	43.0	35.0

Calcium Phosphate, dibasic	3.4	2.0
Vitamin Mix, AIN-93-VX (94047)	19.0	15.0
Choline Bitartrate	3.0	2.75

During the feeding period for the mice, mouse masses, food consumption, and blood glucose levels were measured on a weekly basis until day of euthanization. Food consumption was determined by calculating the difference between the amount of food added and food remaining between weekly measurement intervals. Blood glucose measurements were done using a standard blood glucometer (One Touch). First, mice were temporarily transferred from their cage to a tube, such as an open-ended 50mL conical tube or a cardboard roll, and one of their hind legs was extended, then physically restrained by applying pressure to the upper portion of their thigh. The hair on the leg was shaved using an electric razor to expose the skin and the area was sterilized using alcohol swabs. A small amount of Vaseline or petroleum jelly was applied to the surface and the saphenous vein was pricked using a thin syringe needle. A drop of blood was dabbed onto a glucometer strip and the blood glucose levels were measured by a glucometer. A small piece of gauze was placed with pressure onto the puncture site to stop the bleeding. It was ensured that all bleeding had ceased and the hind limb was unharmed prior to returning the mice to their housing units.

3.3.2 - Isolation of Liver Mitochondria

Mice were euthanized by cervical dislocation under heavy anesthesia (5% isoflurane) between 9-11 weeks of age and livers were surgically removed. The wet mass of the isolated livers were measured. The livers were then placed in an ice-cold buffer containing D-mannitol (220 mM), EGTA (1 mM), sucrose (70 mM), and HEPES (10 mM) (pH 7.4, MESH buffer). All steps for the isolation of liver mitochondria were performed on ice or at 4 ˚C. Livers were briefly washed in

MESH, then cut into small pieces and washed again in MESH to remove excess blood. The liver pieces were minced by hand on a Teflon watch glass using a small razor blade and placed in a homogenizing tube containing 25 mL of MESH with 0.5% (w/v) defatted bovine serum albumin (BSA) (MESH-B). The pieces were then homogenized on ice using the Potter-Elvejham method and a variable speed reversible homogenizer (Glas-Col) for approximately 10 - 15 passes, or until the suspension was homogenized (*128*). The homogenate solutions were transferred to centrifuge tubes and spun at 900 ×g for 9 min at 4 ˚C to pellet cellular debris and nuclei. Excess fat was skimmed from the top of the centrifuge tubes and the supernatant was collected and centrifuged again at 4000 rpm for 20 min at 4 ˚C. The supernatant was decanted, and the sides of the centrifuge tube were carefully cleaned with a Kimwipe to remove any residual fat. The pellet was then resuspended in 500 µL MESH buffer and transferred to a separate Eppendorf tube. Mitochondria were kept on ice until experimentation.

3.3.3 - Bradford Assay

The Bradford assay was used to estimate mitochondrial protein concentrations in the isolated liver mitochondria samples (*129*). One µL from the mitochondria resuspended in MESH (described above) was diluted in 999 µL of double-distilled water for a 1 in 1000 dilution. The dilutions were vortexed vigorously and then 50 µL of the diluted sample was combined with 200 µL of Bradford reagent (Sigma-Aldrich) and 750 µL of double-distilled water for a 1 in 20 000 dilution. The Bradford-diluted mitochondrial samples were carefully well by repeated pipetting and then 200 µL of each sample was plated into a clear-bottom 96-well plate (Corning) in duplicate. The absorbances at 595 nm for each well was measured by the Biotek Cytation 5 reader (Agilent) and compared against a BSA standard curve previously generated using known BSA concentrations of 0, 0.125, 0.250, 0.625, 1.250, and 1.875 µg/mL BSA. However, only the linear portion of the BSA standard curve was considered since the absorbance readings tended to saturate

at higher BSA concentrations. Therefore, an adjusted BSA standard curve was also created using the absorbances measured between 0 to 0.625 µg/mL BSA.

3.3.4 - Measuring H_2O_2 Production in Isolated Mitochondria

The production of H_2O_2 in isolated mitochondria was assessed using the AUR assay. The AUR assay relies on the conversion of a non-fluorescent AUR molecule into its fluorescent resorufin form in the presence of H_2O_2 and HRP. The degree of measured fluorescence directly and positively correlates to the amount of H_2O_2 present in a system. For example, a greater measured fluorescence, reported in relative fluorescent units (RFU), for a given sample is correlates to more H_2O_2 in that system, thus, allowing for the spectrophotometric quantification of H_2O_2 (*130*). The original resuspended mitochondrial samples with protein concentrations ranging between 10 – 25 mg/mL were used to make 1 mL working stocks of isolated mitochondria diluted in MESH to mitochondrial protein concentrations of 5 mg/mL. These mitochondrial working stocks were then used for experimentation. 80 µL of MESH buffer was pipetted in duplicate into a 96-well black clear-bottom plate, followed by 20 µL of the 5 mg/mL mitochondrial samples and 20 µL from GSNO stocks with working concentrations of 100, 500, 2000, 5000, and 10 000 µM. A control containing 100 µL of MESH buffer, 20 µL of 5 mg/mL mitochondrial samples, and no GSNO was also pipetted in duplicate. These mixtures were incubated for one hour at 25 ˚C and then 20µL of HRP, SOD, then AUR were added to each well in that order, followed by an auto-injection of 20 µL of α-ketoglutarate or pyruvate into the reaction chambers (programmed by the Biotek Cytation 5 reader). The inclusion of exogenous SOD in the reaction chamber ensured that all $O_2^{\bullet-}$ produced was accounted for in the final H_2O_2 measurements. Secondary to this, the spontaneous production of $ONOO^-$ by $O_2^{\bullet-}$ was also limited by SOD, reducing its capacity to oxidize, and consequently compromise our measured AUR signal (*131*). The working concentrations for HRP, SOD, AUR, and either α-ketoglutarate or pyruvate were 30 U/mL, 250

U/mL, 200 µM, and 100 mM, respectively. All working stocks were vortexed prior to addition to the reaction wells to ensure homogeneity in the stocks. The final volume in each well totalled to 200 µL. Therefore, the final concentration of mitochondrial protein in each well was 0.5 mg/mL and the final concentrations of GSNO were 0, 10, 50, 200, 500, and 1000 µM. The final concentrations of HRP, SOD, AUR, and either α-ketoglutarate or pyruvate were 3 U/mL, 25 U/mL, 20 µM, and 10 mM, respectively.

The reactions mixtures were mixed for 5 seconds by an automatic shake step by the Biotek Cytation 5 reader. This was followed by a read step which monitored the change in resorufin fluorescence spectrophotometrically at excitation/emission wavelengths of 565nm/610nm every 30 seconds for 10 minutes (*132*). The shake and read steps were performed at 25˚C. Sample fluorescence readings in RFU were normalized against an AUR standard curve previously generated using known H_2O_2 concentrations of 0, 20, 300, 500, 700, 1000, 1300, 1600, 1800, and 2000 nM. This allowed for the quantification of H_2O_2 produced in each reaction chamber.

The production of H_2O_2 in isolated mitochondria in the presence or absence of mitochondrial antioxidant inhibitors was also assessed using the AUR assay as described above with only slight modifications, which were as follows: 20 µL of 5 mg/mL mitochondria samples were incubated for at least 20 minutes at 25˚C with either 100 µL or 80 µL of MESH and 0 µL of CDNB or AF, or 80 µL or 60 µL of MESH and 20 µL of CDNB or AF with working concentrations of 1000 µM. Following the incubation of isolated mitochondria with or without CDNB or AF, the wells with 80 µL MESH and no CDNB or AF, and 60 µL MESH and 20 µL of CDNB or AF were supplemented with an additional 20 µL of GSNO with working concentrations of either 2500 µM or 7500 µM and incubated at 25˚C for one hour. The wells totalled to 200 µL. Therefore, the final

concentration of CDNB or AF in the wells was 100 µM while the final GSNO concentrations were 0, 250, or 750 µM.

3.3.5 - Measurements of H_2O_2 Production and Enzyme Activity for Purified KGDH and PDH

The production of H_2O_2 and enzymatic activity of purified KGDH and PDH was assessed using the AUR assay. 20 µL of MESH buffer was pipetted in duplicate into a 96-well black clear-bottom plate, followed by 20 µL of either purified KGDH or PDH, with working concentrations of 1000 mU/mL, then 20 µL of GSNO from working stocks with concentrations of 100, 500, 2000, 5000, and 10 000 µM. A control containing 40 µL of MESH, 20 µL of 1000 mU/mL purified KGDH or PDH, and no GSNO was also plated in duplicate. The reaction mixtures were incubated at 25˚C for 1 hour. Next, 20 µL of TPP, CoASH, HRP, SOD, AUR, and NAD+ were pipetted into each well in that order. The working concentrations for each of the added reagents were 3 mM, 1 mM, 30 U/mL, 250 U/mL, 200 µM, and 10 mM, respectively. Finally, 20 µL of either α-ketoglutarate or pyruvate was injected into the wells automatically by the Biotek Cytation 5 reader. The final volume of each reaction mixture was 200 µL. Therefore, the final concentration of purified KGDH or PDH in each well was 100 mU/mL, and the final concentrations of GSNO were 0, 10, 50, 200, 500, or 1000 µM. The final concentrations of TPP, CoASH, HRP, SOD, AUR, and NAD+ in each well were 0.3 mM, 0.1 mM, 3 U/mL, 25 U/mL, 20 µM, and 1 mM, respectively. Finally, the final concentration of α-ketoglutarate or pyruvate in the reaction mixtures was 10 mM. The wells were mixed automatically for 5 seconds during a shake step by the Biotek Cytation 5 reader, followed by a read step which monitored the change in resorufin fluorescence spectrophotometrically at excitation/emission wavelengths of 565nm/610nm every 30 seconds for 10 minutes (*132*). The shake and read steps were performed at 25˚C. Sample fluorescence readings in RFU were normalized against an AUR standard curve previously generated using known H_2O_2 concentrations of 0, 20, 300, 500, 700, 1000, 1300, 1600, 1800, and 2000 nM. This allowed for

the quantification of H_2O_2 produced in each reaction chamber. Sample fluorescence measurements were also obtained at excitation/emission wavelengths of 376nm/450nm at the same time intervals to describe the production of NADH, which is generated at the E3 subunits of KGDH and PDH when they consume their respective substrates (*132*). Sample readings for NADH measurements were normalized against an NADH standard curve previously generated using known NAD+ concentrations.

The production of H_2O_2 of purified KGDH and PDH in the presence of varying concentrations of mitochondrial antioxidant inhibitors, CDNB and AF, was also assessed using the AUR assay as described above with only slight modifications, which were as follows: 20 µL of MESH buffer was pipetted in duplicate into a 96-well black clear-bottom plate, followed by 20 µL of either purified KGDH or PDH, with working concentrations of 1000 mU/mL, and 20 µL of either CDNB or AF with working concentrations of 5, 10, 100, 500, and 1000 µM. Control wells containing 40 µL of MESH, 20 µL of 1000 mU/mL purified KGDH or PDH, and no CDNB or AF were also plated in duplicate. The reaction mixtures were allowed to incubate at 25˚C for at least 20 minutes. The volume of each reaction mixture totalled to 200 µL. Therefore, the final concentration of purified KGDH or PDH in each well was 100 mU/mL, and the final concentrations of CDNB or AF were 0, 0.5, 1, 10, 50, or 100 µM.

Additionally, the production of H_2O_2 by reverse electron transfer (RET) from purified KGDH and PDH in the presence of varying concentrations of GSNO was assessed by the AUR assay in accordance with the experimental protocol listed above, with some modifications, which were as follows: 20 µL of purified KGDH or PDH from 1000 mU/mL working stocks was pipetted in duplicate into a 96-well black clear-bottom plate with either 100 µL or 80 µL of MESH buffer. The wells containing 80 µL of MESH buffer were further supplemented with 20 µL of GSNO

from working stocks with concentrations of 100, 500, 1000, 2000, and 5000 µM. The reaction mixtures were incubated at 25˚C for at least 20 minutes. 20 µL of HRP, SOD, and AUR from working stocks with concentrations previously mentioned was added to each well. Finally, 20 µL of NADH from a 1000 µM working stock was added automatically to each well by the Biotek Cytation 5 reader to initiate H_2O_2 production by RET. The total volume in each well was 200 µL; therefore, the final concentration of GSNO in each well was either 0, 10, 50, 100, 200, or 500 µM, and the final concentration of NADH in each well was 100 µM.

3.4 - Statistical Analyses

All experiments were performed in duplicates with n = 4. All data was reported as mean ± standard of error (SEM). Data for all assays was analyzed by ordinary one-way ANOVA, followed by Dunnett's multiple comparison test or by ordinary two-way ANOVA, followed by Tukey's multiple comparison test using the GraphPad Prism 9 software. $p < 0.05$ was considered statistically significant. * denotes effects within the same mouse group; # denotes effects across different mouse groups.

* or #	$p \leq 0.05$
** or ##	$p \leq 0.01$
*** or ##	$p \leq 0.001$
**** or ####	$p \leq 0.0001$

4 – RESULTS

4.0 – Sample Preparation and Data Measurements

4.0.1 – Standardization of Sample Hepatic Mitochondrial Protein Content

Using the protocol listed above, the mitochondrial protein concentrations within the isolated liver samples were determined using the Bradford Assay. A sample BSA standard curve and adjusted BSA standard curve are shown below in Figure 7.

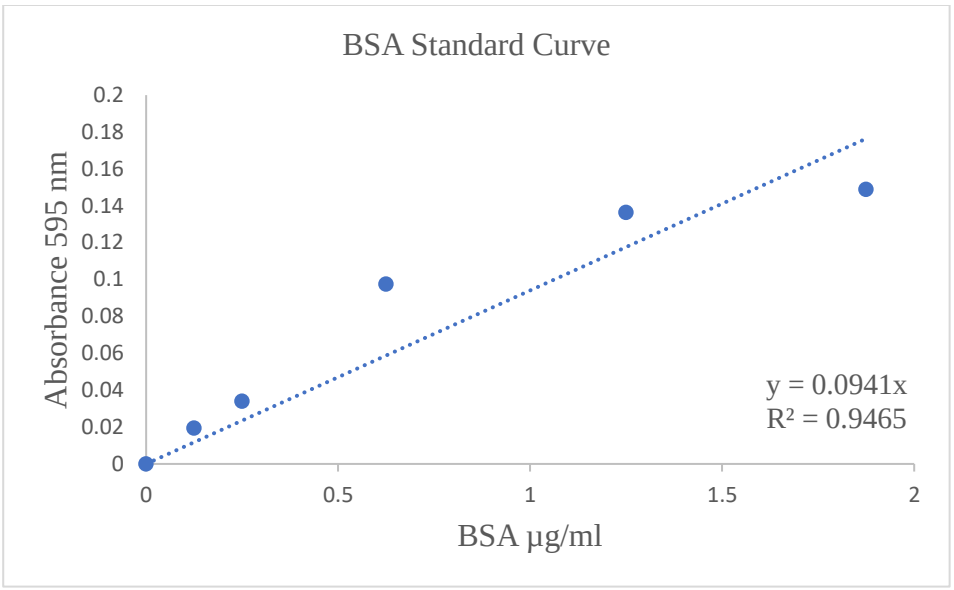

(A)

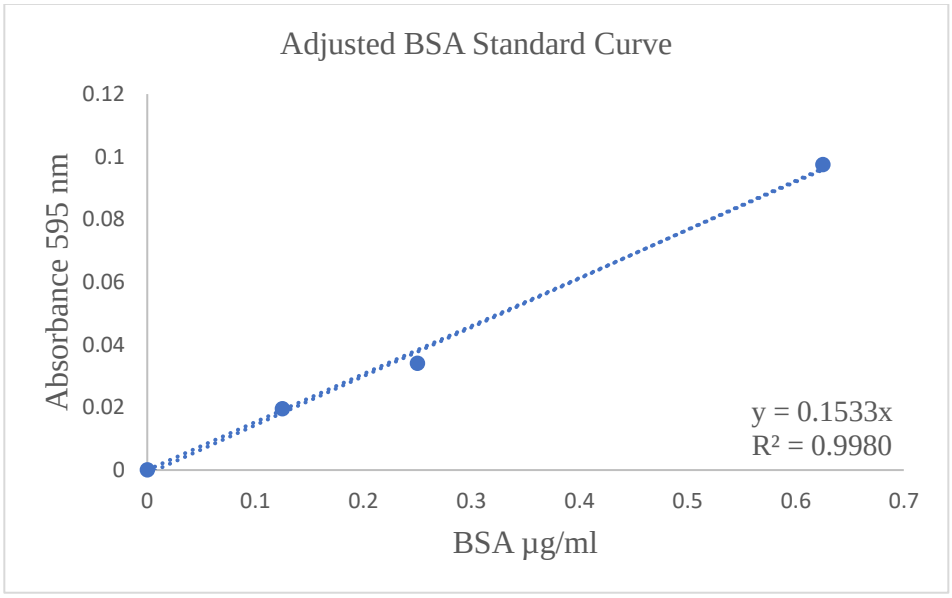

(B)

Figure 7: Sample BSA and adjusted BSA standard curves. The absorbances at 595nm of known BSA concentrations ranging from 0 to 1.875 µg/mL **(A)** were measured and plotted in Excel. The absorbances at 595nm of known BSA concentrations ranging from 0 to 0.625 µg/mL **(B)** were measured and plotted in Excel. The equation for the line of best fit and the R^2 linear correlation value for both plots were calculated in Excel and displayed on their respective graphs. An R^2 value of approximately 0.99 or greater was considered significant.

Based on the linear equation generated by Excel, the protein concentrations in the isolated mitochondria samples were calculated from their observed absorbances. In this case, the "y" variable represented the measured absorbance at 595nm, and the "x" variable represented the

concentration of mitochondrial protein in mg/mL of the Bradford-diluted mitochondrial sample. Sample calculations for determining the protein concentration of a given mitochondrial sample using the Adjusted BSA Standard Curve in Figure 7 are shown below in Equation 3.

Equation 3: Sample calculations for determining protein concentration via Bradford assay.

$$y = 0.1533x$$

y = measured absorbance at 595nm of Bradford diluted mitochondria sample
x = concentration of Bradford diluted mitochondria sample in mg/mL
Let measured absorbance (y_1) of a given sample equal 0.275.
Let measured absorbance of zero-control well containing no mitochondria or BSA (y_c) equal 0.108.

The first step is to determine the measured absorbance from the protein (y_p) by subtracting the zeroed absorbance, y_c, from the sample absorbance, y_1.

$$y_p = y_1 - y_c = 0.275 - 0.108 = 0.167$$

Therefore, the measured absorbance of the sample accounting for the zeroed control is 0.167.

The next step is to solve for x by substituting in the measured absorbance for y.

$$y = 0.1533x, \text{ where } y = 0.167$$
$$0.167 = 0.1533x$$
$$x = \frac{0.167}{0.1533} \approx 1.089$$

Therefore, the protein concentration in the Bradford-diluted mitochondrial sample was approximately 1.089.

Finally, the Bradford dilution factor is accounted for by multiplying the calculated x by 20. This number represents the final concentration of protein in the original resuspended isolated mitochondria sample.

$$[Original\ Resuspended\ Mitochondria\ Sample] = 20x = (20)(1.089) \approx 21.787\ mg/mL$$

Thus, the protein concentration of this mitochondria sample is approximately 21.787 mg/mL. Overall, the concentrations of mitochondrial protein for all experimental samples ranged between 10 to 25 mg/mL. Samples were then standardized to a 5 mg/mL dilution rather than to the number of total mitochondria within each sample.

4.0.2 – H_2O_2 Quantitation using AUR Standard Curve

The production of H_2O_2 from the mitochondrial samples were determined through the AUR assay and following the protocol listed above. A sample AUR standard curve is shown below in Figure 8.

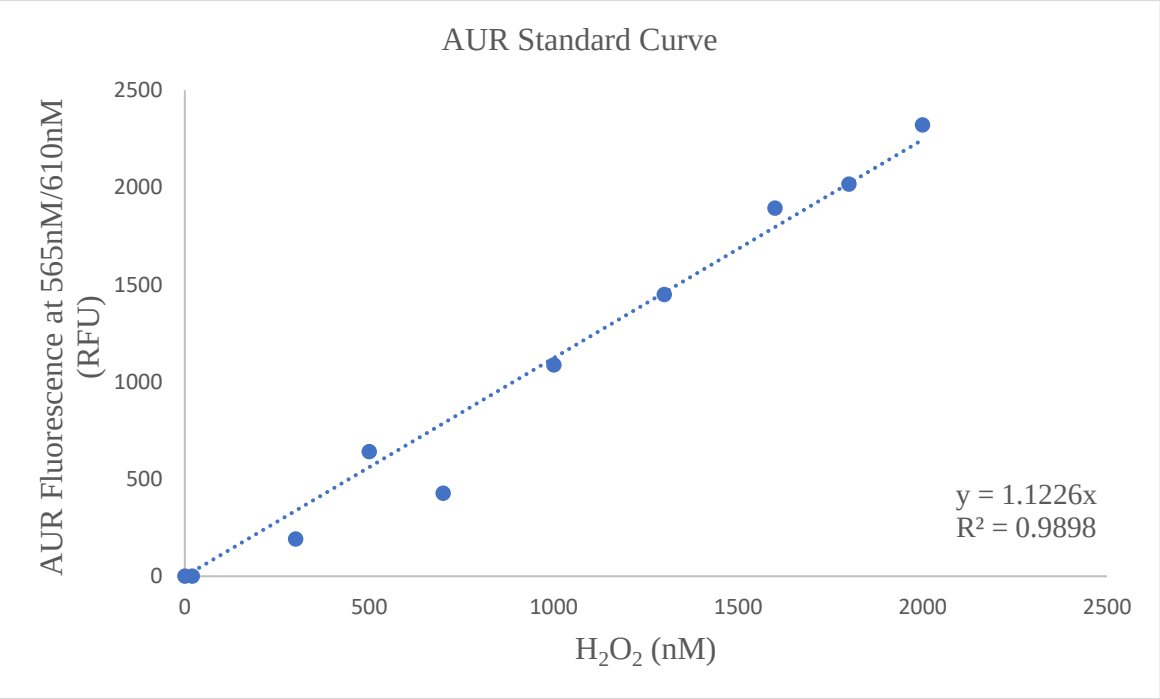

Figure 8: Sample AUR standard curve. The AUR fluorescence measured at 565nm/610nM for known H_2O_2 concentrations ranging from 0 to 2000 nM were measured and plotted in Excel. The equation for the line of best fit and the R^2 linear correlation value were calculated in Excel and displayed on the graph. R^2 values of approximately 0.99 or greater were considered significant.

Based on the linear equation generated by Excel, the amount of H_2O_2 produced in the isolated mitochondria samples were calculated from their observed fluorescence measurements. In this case, the "y" variable represented the measured fluorescence at 565nM/610nM, and the "x" variable represented the concentration of H_2O_2 in each reaction well.

4.1 - Investigation of GSNO-effect on H_2O_2 production by KGDH and PDH

4.1.1 - H_2O_2 production is decreased by GSNO in isolated male, but not female, liver mitochondria energized with α-ketoglutarate.

Figure 9 displays the effect of increasing doses of GSNO on the rate of H_2O_2 production in liver mitochondria isolated from male and female C57BL6N mice that were ~10 weeks of age. The estimation of H_2O_2 production was conducted in Figure 9 using α-ketoglutarate as a substrate. It should be noted that we had previously shown α-ketoglutarate at concentrations as low as 0.1 mM can be transported rapidly into liver mitochondria and used as a fuel for H_2O_2 genesis (*36*). Figure 9A revealed that the rate of H_2O_2 production from the male isolated liver mitochondria did not change from 0 – 200 µM GSNO, but then significantly decreased at 500 µM GSNO. This contrasted with liver mitochondria isolated from female rodents, which did not show any significant changes in the rate of H_2O_2 production regardless of GSNO concentration (Figure 9B). Sex comparisons revealed that liver mitochondria isolated from male mice generated ~ 4- to 5-fold more H_2O_2 when compared samples from females (Figure 9C). Indeed, analysis of rates in reaction mixtures devoid of GSNO revealed that the rate of H_2O_2 generation in males was ~ 0.08 pmol min^{-1} mg^{-1} whereas in samples collected from females, the rate was ~ 0.015 pmol min^{-1} mg^{-1} (Figure 9C). Incubations with GSNO (500 and 2000 µM) suppressed H_2O_2 production in male liver mitochondria while no effect was observed in samples collected from female mice (Figure 9C). Furthermore, the GSNO effect observed in males decreased H_2O_2 production to a rate that was comparable to that of the female samples (Figure 9C).

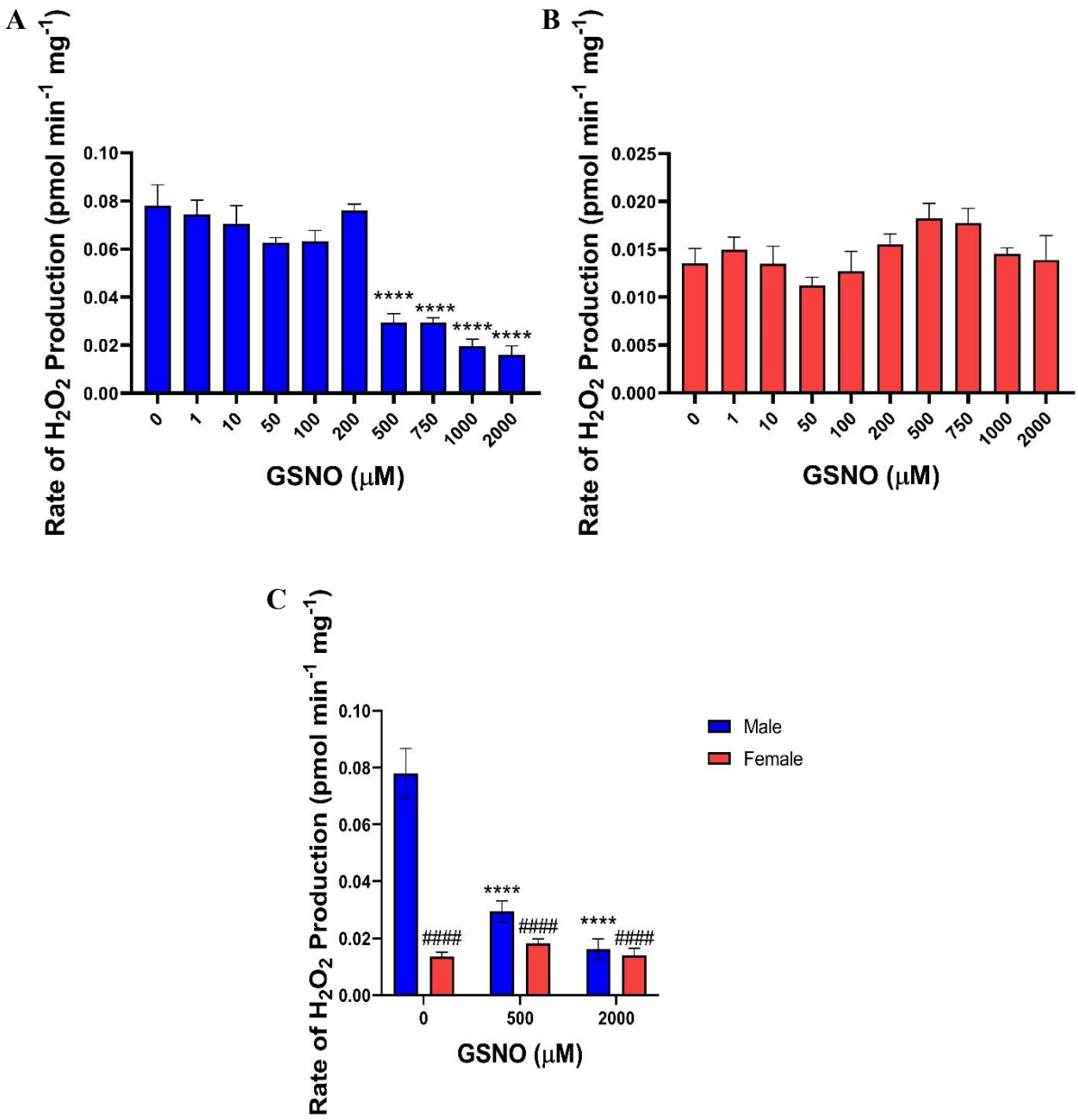

Figure 9: Rate of H_2O_2 production by male isolated liver mitochondria fed with α-ketoglutarate are higher than females and inhibited with increasing concentrations of GSNO. Liver mitochondria of 10-week (**A; Blue**) male and (**B; Red**) female C57BL6N mice were isolated by differential centrifugation and diluted to 0.5 mg/mL of protein equivalent. The rate of H_2O_2 production by isolated male and female liver mitochondria in the presence of α-ketoglutarate and increasing concentrations of GSNO, a protein S-nitrosylation catalyst, was assessed by the AUR assay. Rates are expressed as pmol of H_2O_2 produced per minute per milligram of mitochondrial protein. (**C**) The rates of H_2O_2 production by male and female isolated liver mitochondria were compared at select GSNO concentrations. n = 4, mean ± SEM, ordinary one-way ANOVA with Tukey's multiple comparisons test, or two-way ANOVA with Tukey's multiple comparisons test. **** or ####, $p \leq 0.0001$.

4.1.2 - GSNO does not affect H_2O_2 production in isolated male or female liver mitochondria energized with pyruvate.

Figure 10 shows the effects of increasing concentrations of GSNO on the rate of H_2O_2 production in isolated liver mitochondria of both 10-week male and female C57BL6N mice energized with pyruvate. Figure 10A and 10B indicated that GSNO did not change the rate of H_2O_2 production in either male or female isolated liver mitochondria, regardless of GSNO concentration. Meanwhile, Figure 10C showed that males generated H_2O_2 at significantly higher rates than females. Indeed, the rate of H_2O_2 production was found to be ~ 0.03 pmol min^{-1} mg^{-1} in samples collected from males whereas it was ~0.015 pmol min^{-1} mg^{-1} in female liver mitochondria (Figure 10C). Furthermore, GSNO at a final concentration of 500 and 2000 µM did not significantly affect these rates in male or female liver mitochondria (Figure 10C). However, the rates for H_2O_2 production remained significantly higher in the male liver mitochondria, regardless of whether GSNO was present (Figure 10C). Together, these findings demonstrate KGDH is more sensitive to the inhibition of H_2O_2 production by GSNO and that there is a sex dimorphic effect in the GSNO response and the amount of H_2O_2 generated by liver mitochondria.

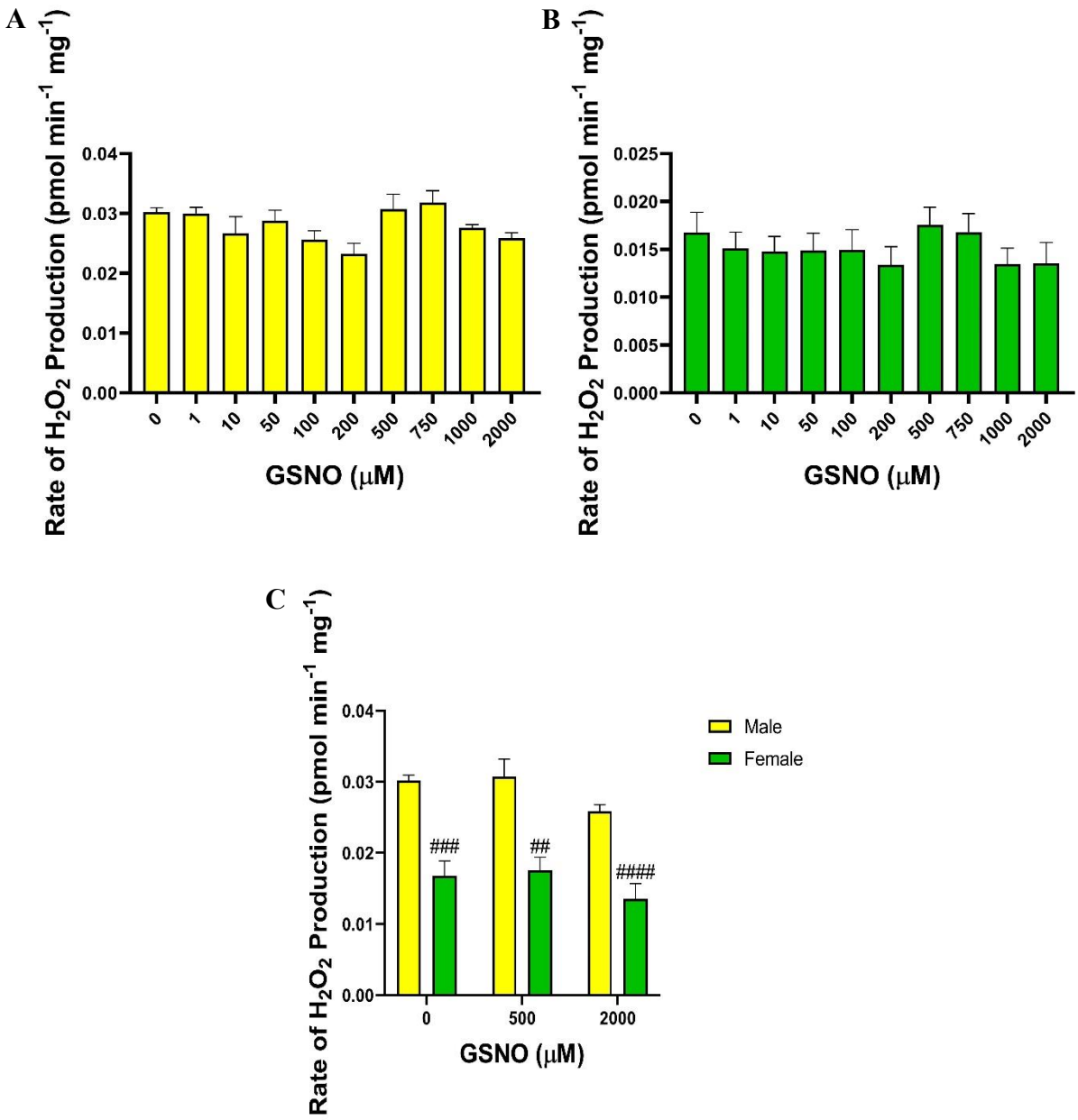

Figure 10: Rate of H_2O_2 production by male isolated liver mitochondria fed with pyruvate are higher than females, but unaffected by GSNO. Liver mitochondria of 10-week (**A; Yellow**) male and (**B; Green**) female C57BL6N mice were isolated by differential centrifugation and diluted to 0.5 mg/mL of protein equivalent. The rate of H_2O_2 production by isolated male and female liver mitochondria in the presence of pyruvate and increasing concentrations of GSNO, a protein S-nitrosylation catalyst, was assessed by the AUR assay. Rates are expressed as pmol of H_2O_2 produced per minute per milligram of mitochondrial protein. (**C**) The rates of H_2O_2 production by male and female isolated liver mitochondria were compared at select GSNO concentrations. n = 4, mean ± SEM, ordinary one-way ANOVA with Tukey's multiple comparisons test, or two-way ANOVA with Tukey's multiple comparisons test. ##, $p \leq 0.01$; ###, $p \leq 0.001$; ####, $p \leq 0.0001$.

4.1.3 - GSNO decreases enzyme activity and H_2O_2 production of purified KGDH of porcine heart origin.

Our group has previously used purified KGDH and PDH of porcine heart origin to investigate mechanisms for the redox regulation of H_2O_2 production by these enzyme complexes (*35*). Next, I examined the impact of GSNO titration to higher concentrations on the NADH and H_2O_2-generating activities of purified KGDH. For this, I employed a method previously established by our group which allows the simultaneous measurement of NADH and H_2O_2 production using the autofluorescence of nicotinamides and the conversion of AUR to resorufin by H_2O_2 (*132*). Figure 11A demonstrated a dose-dependent decrease in KGDH activity, represented by NADH production, relative to the concentration of GSNO. KGDH activity was significantly decreased at 500 µM GSNO, and had a comparable degree of inhibition to KMV, a known potent competitive inhibitor of KGDH (*36*). Figure 11B showed the effects of GSNO on H_2O_2 production by KGDH, which also demonstrated a dose-dependent decrease in the rate of H_2O_2 production relative to the concentration of GSNO. Significant decreases in the rates were observed at 200 µM and 500 µM GSNO, with 500 µM GSNO reaching comparable levels of inhibition to KMV. Figure 11C traced the amount of H_2O_2 produced over 10 minutes from purified KGDH treated with 0 GSNO, 500 µM GSNO, and 10 mM KMV, respectively, revealing an approximate 4-fold decrease in the amount of H_2O_2 produced in both the 500 µM GSNO and KMV samples.

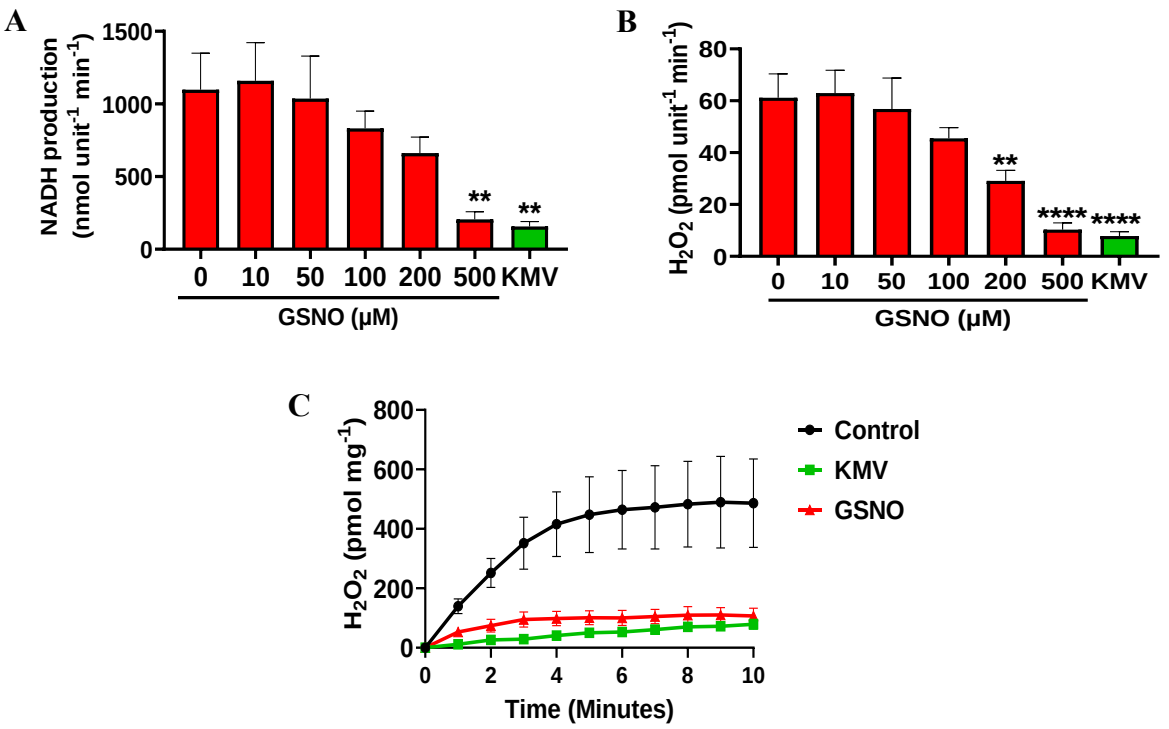

Figure 11: GSNO inhibits the activity of purified KGDH of porcine heart origin. KGDH was incubated in varying concentrations of GSNO or KMV (10 mM; Green) and its enzyme activity (**A)** and H_2O_2 production (**B)** was evaluated. KMV, a selective inhibitor for KGDH, was included to confirm its NADH and H_2O_2 producing activity. (**C)** Representative traces for H_2O_2 production in response to GSNO (500 μM) or KMV (10 mM). n = 4, mean ± SEM, ordinary one-way ANOVA with Dunnett's multiple comparisons test. **, $p \leq 0.01$; ***, $p \leq 0.001$; ****, $p \leq 0.0001$.

4.1.4 - GSNO affects enzyme activity and H_2O_2 production by purified PDH of porcine heart origin, but to a lesser extent when compared to KGDH.

Our group has previously worked with purified KGDH and PDH of porcine heart origin using a method we developed that allows for the simultaneous measurements of NADH and H_2O_2 production by accounting for the autofluorescence of nicotinamides and the conversion of AUR to its fluorescent resorufin form in the presence of H_2O_2 (*36, 132*). Figure 12A revealed that increasing concentrations of GSNO did not have a significant effect on NADH production by purified PDH, further evidenced by the significant decrease in PDH activity caused by CPI613, a known PDH inhibitor, which was not comparable to any of the GSNO treatment groups (*36*).

Figure 12B demonstrated that H_2O_2 production by purified PDH trended towards a decrease in a dose-dependent manner by GSNO. H_2O_2 production by PDH was significantly decreased with 500 µM GSNO, but not to the same degree as CPI613. Figure 12C traced H_2O_2 production over 10 minutes by purified PDH treated with 0 GSNO, 500 µM GSNO, and 10mM CPI613, respectively, further supporting the previous observation that 500 µM GSNO led to a decrease in H_2O_2, but to a lesser degree than CPI613. Collectively, Figure 12 demonstrates purified PDH is more resistant to dose-dependent inhibition by GSNO when compared to KGDH of porcine heart origin (Figure 11). .

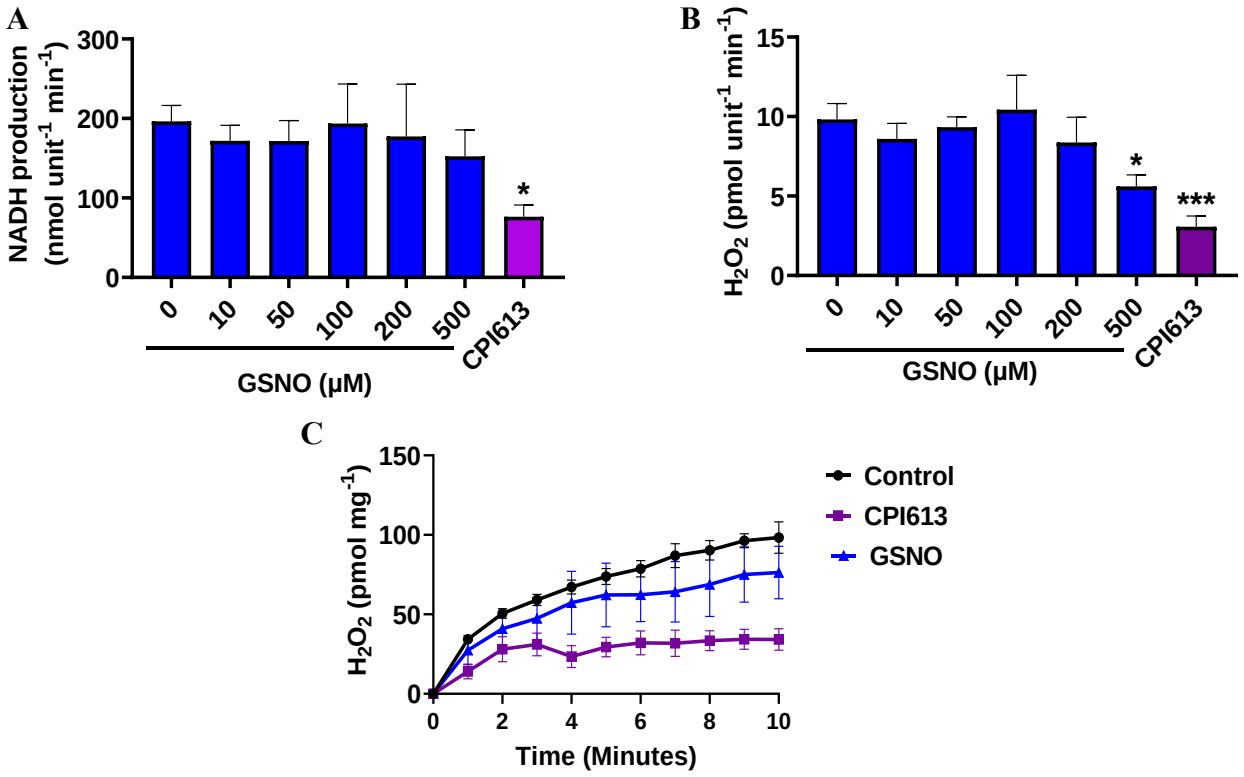

Figure 12: GSNO inhibits the activity of purified PDH of porcine heart origin but is more resistant to inhibition when compared to KDGH. PDH was incubated in varying concentrations of GSNO or CPI613 (10 µM; Purple) and then the activity **(A)** and H_2O_2 production **(B)** was evaluated. CPI613, a selective inhibitor for PDH, was included to confirm its NADH and H_2O_2 producing activity. **(C)** Representative traces for H_2O_2 production in response to GSNO (500 µM) or CPI613 (10 mM). n = 4, mean ± SEM, ordinary one-way ANOVA with Dunnett's multiple comparisons test. *, $p \leq 0.05$; **, $p \leq 0.01$; ***, $p \leq 0.001$.

4.2 - GSNO-effect on H_2O_2 production via Reverse Electron Transfer (RET) by KGDH and PDH

4.2.1 - GSNO did not affect rate of H_2O_2 production by RET through purified KGDH

KGDH and PDH can generate H_2O_2 by reverse electron transfer (RET) from NADH, which occurs at the E3 subunit of the complexes (*32*). Our group had previously shown that redox modifications like glutathionylation can augment H_2O_2 genesis by purified KGDH and PDH during RET from NADH (*78*). The results above show GSNO impedes electron fluxes through KGDH, and to a much lesser extent, PDH, prompting me to examine its effect on H_2O_2 release during RET. Figure 13A revealed that GSNO did not significantly affect the rates of H_2O_2 generated via RET, regardless of GSNO concentration, although a trend for a decrease was observed at 200 μM followed by a trend for an increase at 500 μM. However, these changes were not statistically significant. Tracing the data from Figure 13A, which is displayed in Figure 13B, revealed that GSNO at 200 μM did induce a small decline in H_2O_2 production, but this was not statistically significant when compared to control samples. Overall, these findings demonstrate GSNO does not significantly affect RET-driven H_2O_2 production by KGDH.

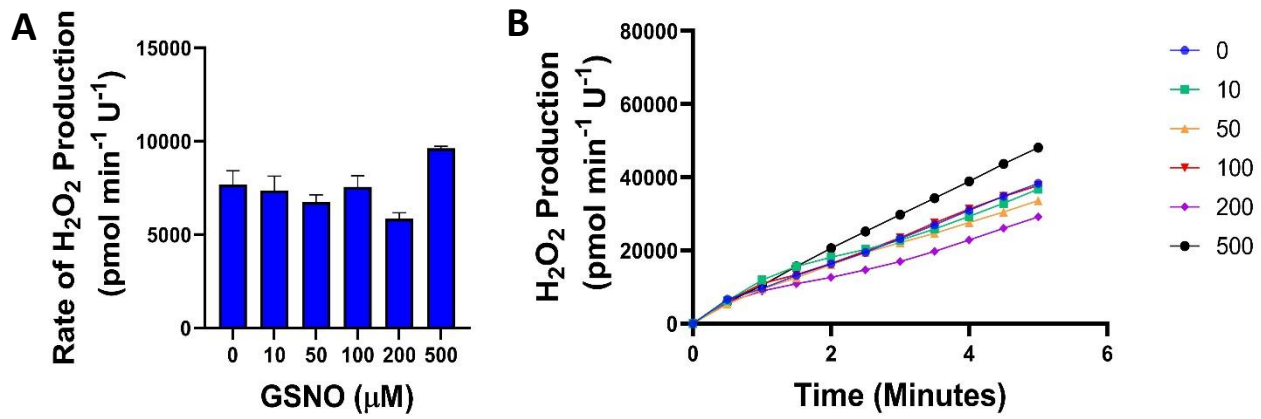

Figure 13: Rate of H_2O_2 production by purified KGDH via reverse electron transfer does not change with increasing concentrations of GSNO. (**A)** Purified KGDH was treated with increasing concentrations GSNO and the rate of H_2O_2 production by KGDH via reverse electron transfer (RET) was assessed by the AUR assay. Rates are expressed as pmol of H_2O_2 produced per minute per unit of enzyme. (**B**) Representative trace for H_2O_2 produced by KGDH via RET in the presence of increasing concentrations of GSNO measured over 5 minutes. Only the linear portion of each trace is plotted. n = 4, mean ± SEM, ordinary one-way ANOVA with Tukey's multiple comparisons test.

4.2.2 - GSNO did not affect rate of H_2O_2 production by RET through purified PDH

As mentioned before, our group has shown in the past that glutathionylation can increase RET-driven H_2O_2 production by KGDH and PDH (*78*). Moreover, the results from this study indicate that GSNO can inhibit electron flux through these two dehydrogenase complexes. Figure 14A revealed that GSNO only caused a significant decrease in the rate of RET-driven H_2O_2 production by purified PDH at 100 µM. However, rates trended back towards an increase to comparable levels to the control following 200 µM and 500 µM GSNO treatments. Figure 14B displays representative traces of the findings from Figure 14A, showing that while a decrease in H_2O_2 was observed at 100 µM GNO, this was not significantly different from the control group. Combined, these results suggest that GSNO does not significantly impact RET-driven H_2O_2 production by PDH.

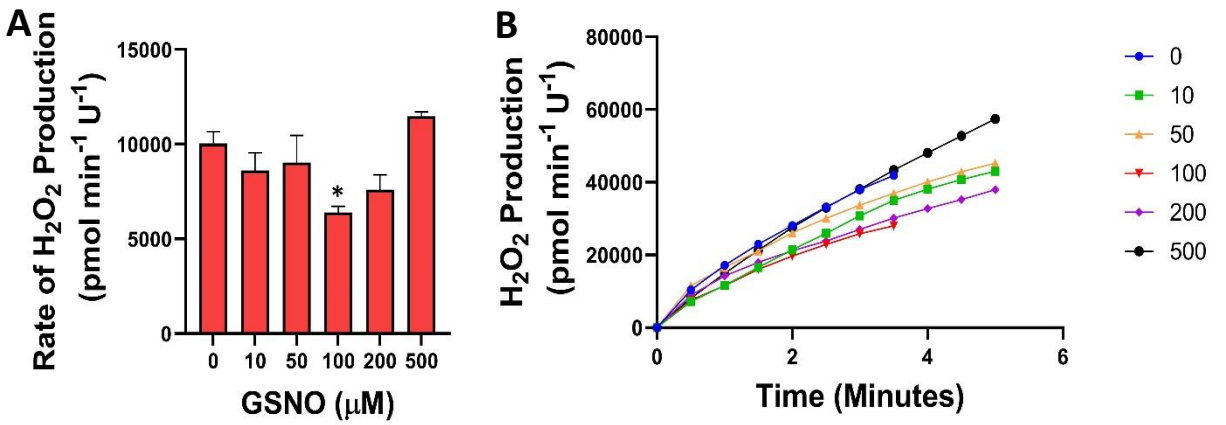

Figure 14: Rate of H_2O_2 production by purified PDH via reverse electron transfer does not change with increasing concentrations of GSNO. (**A)** Purified PDH was treated with increasing concentrations GSNO and the rate of H_2O_2 production by PDH via reverse electron transfer (RET) was assessed by the AUR assay. Rates are expressed as pmol of H_2O_2 produced per minute per unit of enzyme. (**B**) Representative trace for H_2O_2 produced by PDH via RET in the presence of increasing concentrations of GSNO measured over 5 minutes. Only the linear portion of each trace is plotted. n = 4, mean ± SEM, ordinary one-way ANOVA with Tukey's multiple comparisons test. *, $p \leq 0.05$.

4.3 - Examination of mitochondrial antioxidant inhibitors on H_2O_2 production by KGDH and PDH

4.3.1 - CDNB and AF decreased rate of H_2O_2 production by KGDH, but not PDH, in male isolated liver mitochondria.

CDNB and AF are antioxidant inhibitors that specifically target the Gpx and Prx/Trx antioxidant systems, respectively (*133*, *134*). CDNB is an electrophilic alkylating compound that depletes reduced GSH availability by targeting its cysteinyl thiol group. As a result, CDNB compromises the antioxidative capacity of GSH itself and GSH-dependent systems, such as Gpx (*133*). AF is a member of the gold (I)-based drug class with high specificity for sulfur and selenium-containing proteins, such as TrxR, and therefore, inhibits the Trx/Prx antioxidant system by preventing the regeneration of reduced Trx (*134*). The purpose of inhibiting these endogenous mitochondrial antioxidant systems with either CDNB or AF during our H_2O_2 measurements was two-fold: 1) to amplify our measurable AUR signal by decreasing the amount of H_2O_2 removed

and 2) to improve our observable GSNO effect by inhibiting their potential denitrosylase activity (*103*). Figure 15 displays the rates of H_2O_2 production by male 10-week isolated liver mitochondria fed with either α-ketoglutarate (15A) or pyruvate (15B) and treated with increasing concentrations of GSNO as well as either CDNB or AF mitochondrial antioxidant inhibitors. Figure 15A reiterated previous findings that higher concentrations of GSNO resulted in a decrease in the rate of H_2O_2 produced in male isolated liver mitochondria energized with α-ketoglutarate, as evidenced by the statistically significant decrease observed with 750 µM GSNO and no antioxidant inhibitor treatment (NI). Interestingly, the addition of either CDNB or AF led to a significant decrease in the rate of H_2O_2 generated when no GSNO was added. AF also resulted in a significant decrease when 250 µM GSNO was added. These findings contradict the initial hypothesis that CDNB or AF would lead to an increase in the measured H_2O_2 signal since less H_2O_2 would be removed by the mitochondria antioxidant systems. These observations suggest that there may be off-target interactions between CDNB and AF and KGDH in an isolated mitochondria system that were previously unaccounted for that subsequently lead to a reduction in H_2O_2 production from this source. On the other hand, Figure 15B revealed that male isolated liver mitochondria energized with pyruvate did not share these same qualities since the rate of H_2O_2 production did not alter between differing GSNO concentrations or in the presence of either CDNB or AF. Comparisons between Figure 15A and 15B showed that the α-ketoglutarate-fed mitochondria had higher rates of H_2O_2 production at control levels than pyruvate-fed mitochondria (~0.06 pmol min^{-1} mg^{-1} > ~0.04 pmol min^{-1} mg^{-1}) but was decreased to rates below or comparable to that of pyruvate-fed mitochondria following supplementation with CDNB, AF, or 750 µM GSNO (~ 0.02 - 0.03 pmol min^{-1} mg^{-1}).

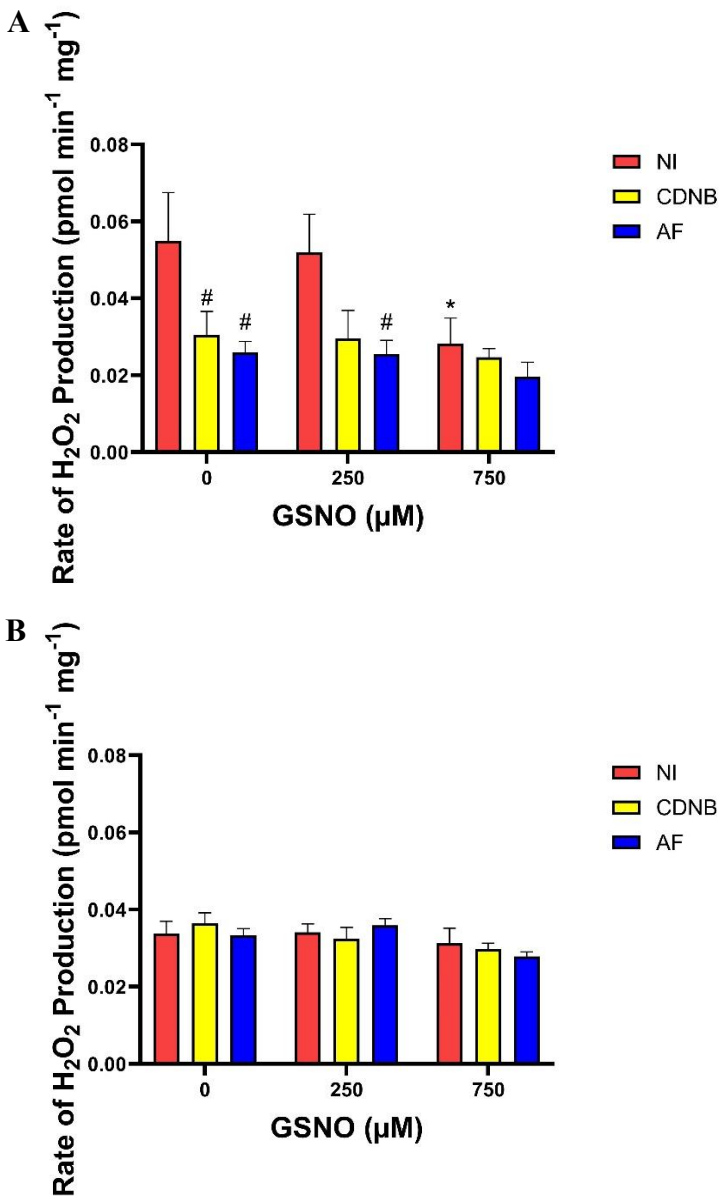

Figure 15: Rate of H_2O_2 production by male isolated liver mitochondria fed with α-ketoglutarate decreased when treated with antioxidant inhibitors and GSNO, but not mitochondria fed with pyruvate. Liver mitochondria of 10-week male C57BL6N mice were isolated by differential centrifugation and diluted to 5 mg/mL of protein equivalent. Mitochondria were treated without inhibitors (NI; Red), with 10 μM 1-chloro-2, 4-dinitrobenzene (CDNB; depletion of GSH; Yellow), or with 10 μM auranofin (AF; Trx reductase inhibitor; Blue). Samples were also supplemented with increasing concentrations of GSNO, a protein S-nitrosylation catalyst. The rate of H_2O_2 production by these mitochondrial samples when consuming (**A**) α-ketoglutarate or (**B**) pyruvate was assessed by the AUR assay. Rates are expressed as pmol of H_2O_2 produced per minute per milligram of mitochondrial protein. n = 4, mean ± SEM, ordinary two-way ANOVA with Tukey's multiple comparisons test. * or #, $p \leq 0.05$.

4.3.2 - Increasing concentrations of CDNB or AF do not significantly affect rate of H_2O_2 production by purified KGDH of porcine heart origin.

Figure 16 examined the effect of increasing concentrations of CDNB or AF on the rate of H_2O_2 production by purified KGDH of porcine heart origin. Figure 16A revealed that incubation with CDNB did not significantly increase H_2O_2 production by purified KGDH, regardless of concentration, though it seemed to trend towards an increase starting from approximately 1 – 10 µM CDNB. The rate of H_2O_2 production was approximately 250 pmol min^{-1} U^{-1} at control, then increased gradually up to around 400 pmol min^{-1} U^{-1} by the 10 µM CDNB mark. Figure 16B showed that AF did not significantly affect the rate of H_2O_2 production by purified KGDH regardless of AF concentration applied. The rate of H_2O_2 production stayed relatively consistent between 300 – 350 pmol min^{-1} U^{-1}. These findings were in contrast to the proposal that CDNB and AF were having off-target effects on KGDH that led to an inhibition of H_2O_2 production at these sites. However, the possibility still remains that these interactions may occur, perhaps through an indirect or intermediary mechanism, that inhibits H_2O_2 production by KGDH, especially if one considers the complexity of the mitochondrial environment in comparison to just a purified enzyme system.

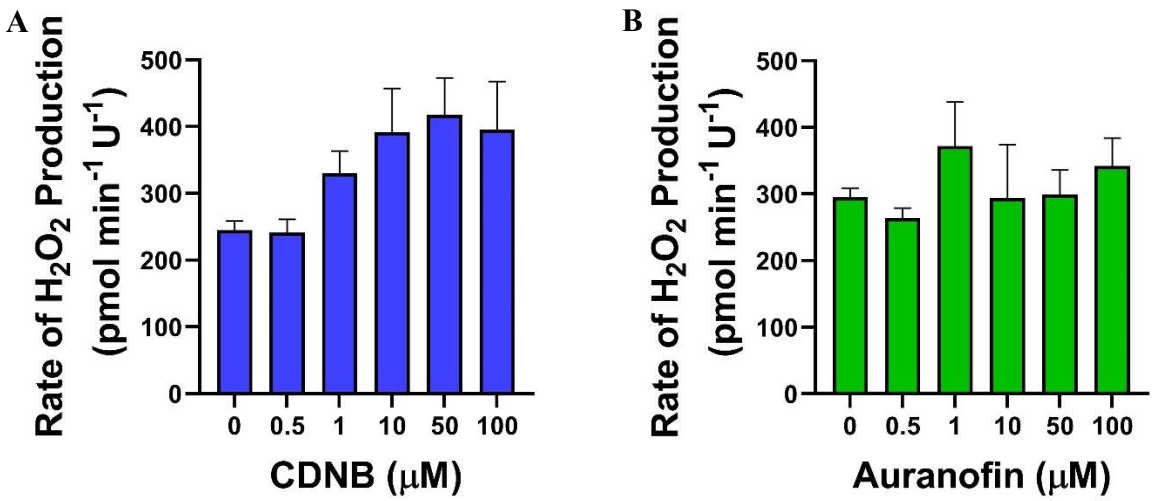

Figure 16: Rate of H_2O_2 production by purified KGDH does not change with increasing concentrations of antioxidant inhibitors. Purified KGDH was treated with increasing concentrations of (**A**) 1-chloro-2, 4-dinitrobenzene (CDNB), or (**B**) auranofin (AF). The rate of H_2O_2 production by KGDH was assessed by the AUR assay. Rates are expressed as pmol of H_2O_2 produced per minute per unit of enzyme. n = 4, mean ± SEM, ordinary one-way ANOVA with Tukey's multiple comparisons test.

4.3.3 - Increasing concentrations of CDNB or AF do not significantly affect rate of H_2O_2 production by purified PDH of porcine heart origin.

Figure 17 showed the effects of increasing concentrations of CDNB or AF on the rate of H_2O_2 production by purified PDH of porcine heart origin. Figure 17A indicated that while there were no statistically significant differences in the rates of H_2O_2 production between treatments, it seemed to trend towards an increase with higher CDNB concentrations. The rate of H_2O_2 generated by purified KGDH begun at around 200 pmol min^{-1} U^{-1} but increased to approximately 300 pmol min^{-1} U^{-1} in the presence of 50 μM and 100 μM CDNB. Figure 17B showed that there was no effect by AF on PDH-mediated H_2O_2 generation for any of the AF concentrations used and the rates were consistent at around 200 pmol min^{-1} U^{-1}.

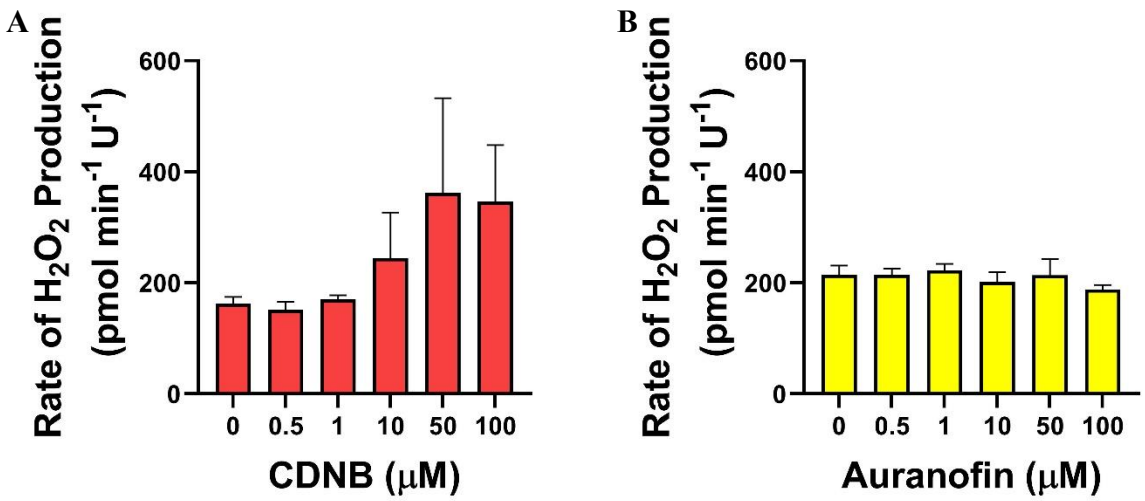

Figure 17: Rate of H_2O_2 production by purified PDH does not change with increasing concentrations of antioxidant inhibitors. Purified PDH was treated with increasing concentrations of (**A**) 1-chloro-2, 4-dinitrobenzene (CDNB), or (**B**) auranofin (AF). The rate of H_2O_2 production by PDH was assessed by the AUR assay. Rates are expressed as pmol of H_2O_2 produced per minute per unit of enzyme. n = 4, mean ± SEM, ordinary one-way ANOVA with Tukey's multiple comparisons test.

4.4 - Effects of GSNO on H_2O_2 production by isolated liver mitochondria challenged with a HFD

4.4.1 - Male, but not female, HFD mouse mass increased with age, food consumption increased for both HFD mice sexes, and blood glucose levels did not change.

Figure 18 examined the average mouse weight, food consumption, and blood glucose levels for male and female mice placed on either the HFD or the CM diet. Figure 18A shows that the average mouse mass for male HFD mice was significantly greater between the ages of 7 – 9 weeks in comparison to male CM mice (~ 30 g vs. ~23 g at week 9), while there were no significant differences in average mouse masses between the female HFD and CM mice, which ranged between 20 – 22 g. Figure 18B revealed that the average weekly food consumption for the first 3 weeks of feeding were comparable between male and female CM mice (~60 g), and male and female HFD mice (~40 g). However, by weeks 4 and 5, both male and female HFD mice had increased average weekly food consumption to comparable levels measured with the CM mice.

Figure 18C tracked the average blood glucose levels on a weekly basis, revealing no significant changes occurred between weekly measurements among any of the mouse groups. In general, the male CM and HFD mice had slightly more elevated blood glucose levels in comparison to the female CM and HFD mice. The blood glucose levels for both sexes and diet groups ranged between ~ 7 – 12 mmol/L, where male mice stayed generally consistent within the upper range (~ 10 – 12 mmol/L) and female mice were consistent within the lower range (~7 – 10 mmol/L). There were no noticeable differences between the HFD and CM group.

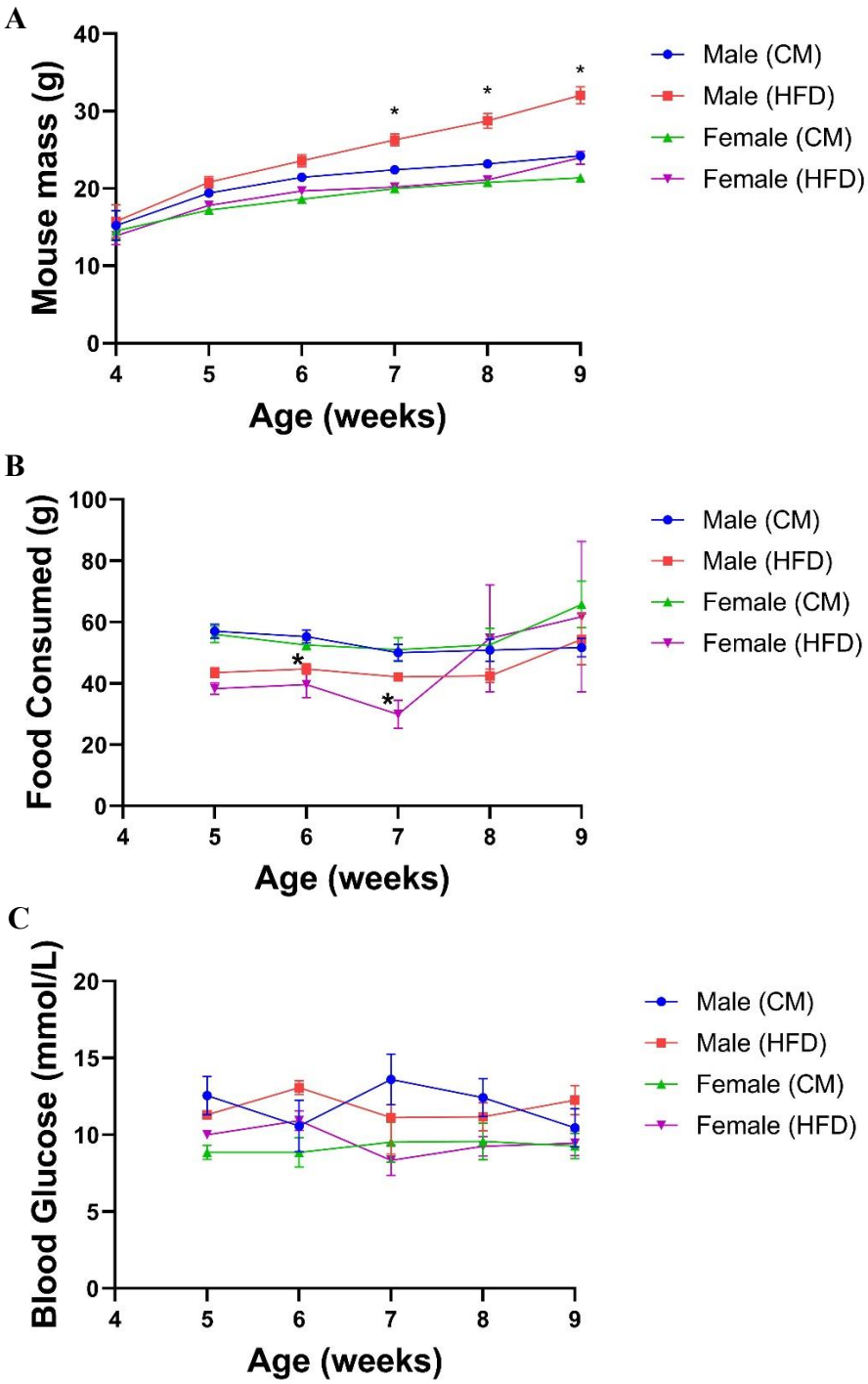

Figure 18: Male high-fat diet mouse mass and food consumption increased while blood glucose remained consistent. Male and female C57BL6N mice were placed on high fat (HFD) or control match (CM) specialty diets at 4 weeks for at least 5 weeks. (**A**) Mouse mases, (**B**) diet food consumption, and (**C**) blood glucose levels were monitored every week until liver mitochondria isolation. n = 4, mean ± SEM, two-way ANOVA with Dunnett's multiple comparisons test. * or #, $p \leq 0.05$

4.4.2 - Isolated liver masses were comparable between groups and sex.

Figure 19 displays the average wet masses of the isolated livers between the diet groups and sexes. The livers from each sex and diet group were surgically removed and their wet masses were immediately measured. The average wet masses of the isolated livers are plotted in Figure 19, revealing no significant differences between sexes or diets. Overall, the average wet mass for the isolated livers ranged between approximately 1.3 – 1.5 g.

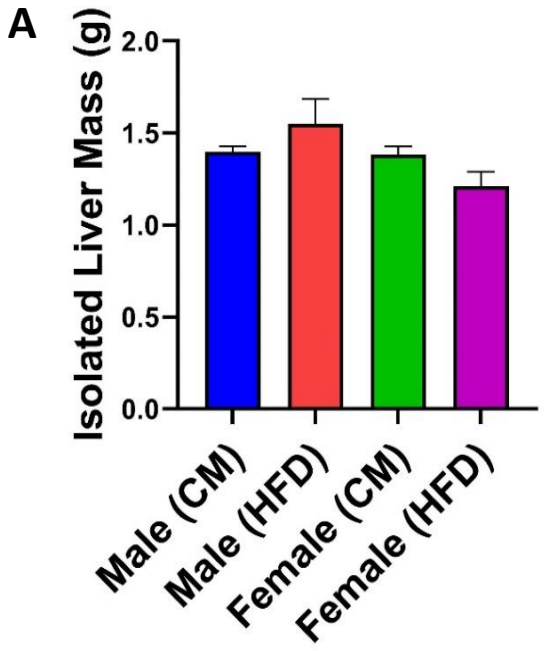

Figure 19: Isolated liver wet masses were comparable between diet mice groups. Male and female C57BL6N mice were placed on high fat (HFD) or control match (CM) specialty diets at 4 weeks of age for at least 5 weeks. Isolated liver wet masses were determined immediately after isolation. n = 4, mean ± SEM, two-way ANOVA with Dunnett's multiple comparisons test.

4.4.3 - Rate of H_2O_2 production by KGDH from male, but not female, HFD-challenged isolated liver mitochondria decreased with increasing GSNO.

Figure 20 displayed the effects of increasing concentrations of GSNO on H_2O_2 production by HFD and CM male and female isolated liver mitochondria energized with α-ketoglutarate. Figure 20A demonstrated that increasing concentrations of GSNO did not significantly affect the

rates of H_2O_2 production from male isolated liver mitochondria that were fed with the control-match diet. However, a decrease was observed at higher GSNO concentrations for the male liver mitochondria from the HFD-fed mice. There was a significant decrease in the rate of H_2O_2 production at 500 µM GSNO between HFD mitochondria and CM mitochondria and a significant decrease at 1000 µM GSNO between HFD mitochondria and CM mitochondria, and from the 0 GSNO HFD control samples. Figure 20B showed that GSNO did not significantly affect the rate of H_2O_2 production of female HFD and CM isolated liver mitochondria energized with α-ketoglutarate, regardless of GSNO concentration. Male CM mitochondria had rates of approximately 0.008 – 0.010 pmol min^{-1} mg^{-1} H_2O_2 produced across GSNO treatments, while male HFD mitochondria had similar rates at lower concentrations of GSNO (0-50 µM GSNO), which gradually dropped to approximately 0.005 pmol min^{-1} mg^{-1} H_2O_2 produced by the 500 µM GSNO and 1000 µM GSNO mark. On the other hand, both female CM and HFD mitochondria had rates of H_2O_2 production between approximately 0.005 – 0.006 pmol min^{-1} mg^{-1} for all GSNO concentrations.

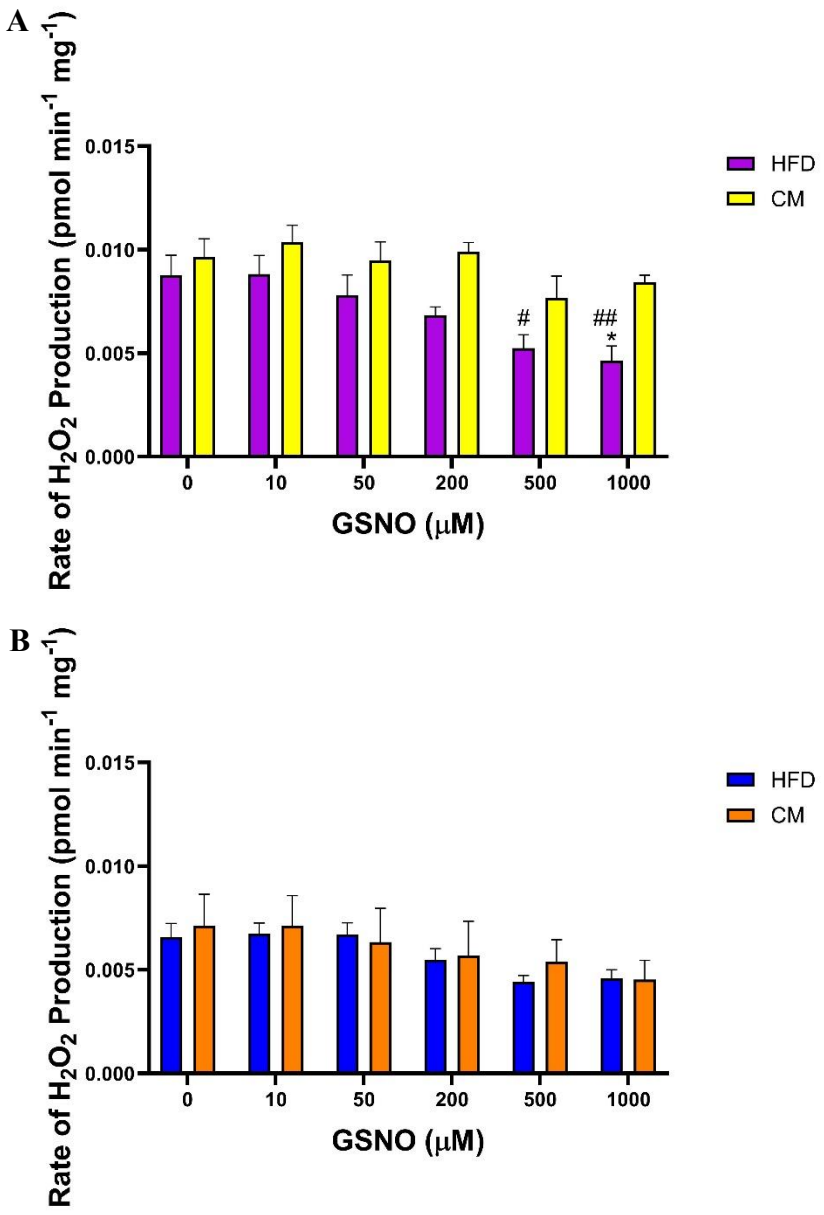

Figure 20: Rate of H_2O_2 production by male high-fat isolated liver mitochondria fed with α-ketoglutarate decreased with increasing GSNO concentrations compared to male control-match while females had no change. (**A**) Male and (**B**) female C57BL6N mice were placed on high fat (HFD) or control match (CM) specialty diets at 4 weeks for at least 5 weeks. Liver mitochondria were isolated by differential centrifugation and samples were diluted down to 5 mg/mL of protein. The rate of H_2O_2 production by isolated male and female liver mitochondria in the presence of α-ketoglutarate and increasing concentrations of GSNO, an S-nitrosylation catalyst, was assessed by the AUR assay. Rates are expressed as pmol of H_2O_2 produced per minute per milligram of mitochondrial protein. n = 4, mean ± SEM, two-way ANOVA with Tukey's multiple comparisons test. * or #, $p \leq 0.05$; ** or ##, $p \leq 0.01$

4.4.4 - Rate of H_2O_2 production by PDH from male, but not female, HFD-challenged and control isolated liver mitochondria decreased with increasing GSNO.

Figure 21 indicated the effects of increasing concentrations of GSNO on the rates of H_2O_2 production of HFD and CM male and female isolated liver mitochondria energized with pyruvate. Figure 21A showed that the CM male mitochondria experienced significant decreases in their rates of H_2O_2 production compared to the CM control group (0 GSNO) when treated with 500 µM and 1000 µM GSNO. These rates were also significantly decreased when compared to the HFD control group. Furthermore, the rates of H_2O_2 generation for HFD male mitochondria showed significant decreased at the 200 µM, 500 µM, and 1000 µM GSNO marks when compared to both CM and HFD male control groups. In contrast, Figure 21B revealed that neither female CM nor female HFD isolated liver mitochondria experienced significant changes in their rates of H_2O_2 generation by GSNO, regardless of concentration. Overall, male CM rates declined from approximately 0.010 to 0.007 pmol min^{-1} mg^{-1} by GSNO in a dose-dependent manner, male HFD rates decreased from 0.010 to 0.005 pmol min^{-1} mg^{-1}, and rates of H_2O_2 synthesis for both female CM and HFD remained relatively consistent between 0.005 – 0.007 pmol min^{-1} mg^{-1} for all GSNO treatments.

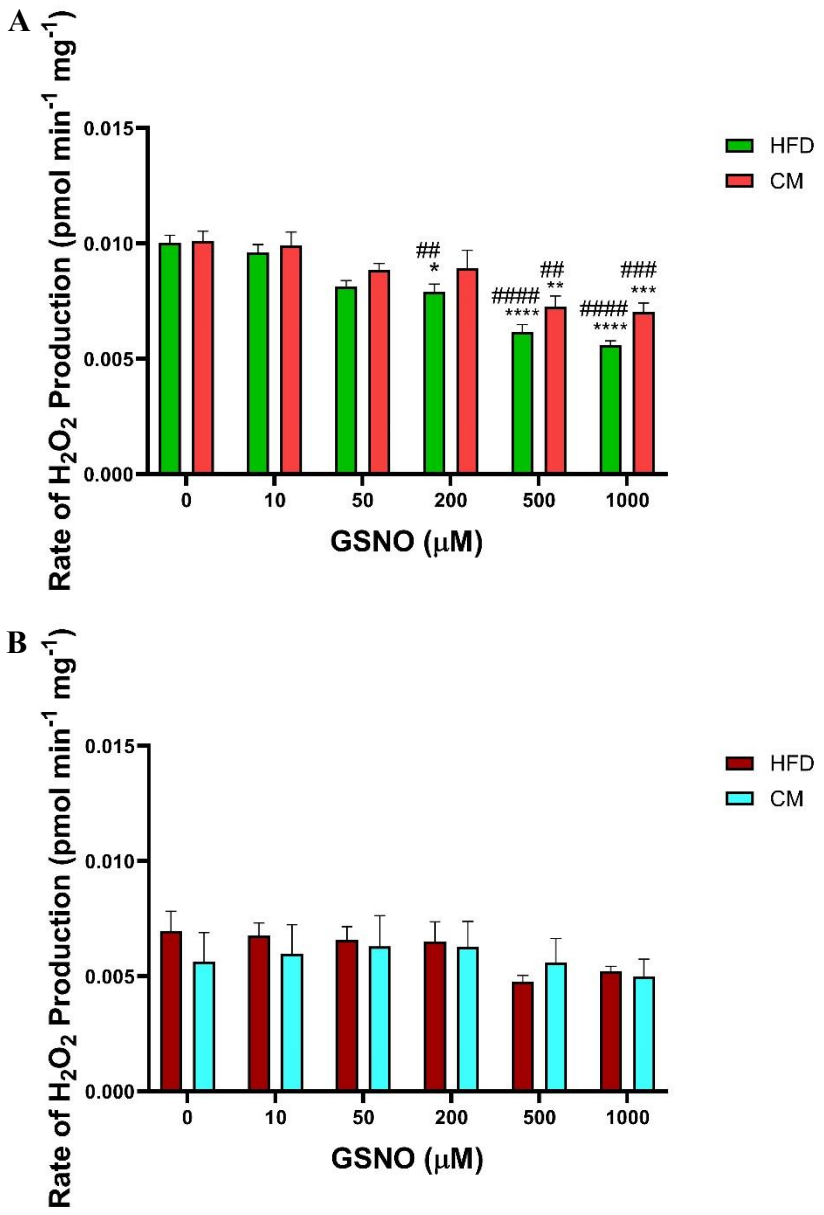

Figure 21: Rate of H_2O_2 production by male high-fat and control-match isolated liver mitochondria fed with pyruvate decreased with increasing GSNO concentrations, but females did not. (**A**) Male and (**B**) female C57BL6N mice were placed on high fat (HFD) or control match (CM) specialty diets at 4 weeks for at least 5 weeks. Liver mitochondria were isolated by differential centrifugation and samples were diluted down to 5 mg/mL of protein. The rate of H_2O_2 production by isolated male and female liver mitochondria in the presence of pyruvate and increasing concentrations of GSNO, an S-nitrosylation catalyst, was assessed by the AUR assay. Rates are expressed as pmol of H_2O_2 produced per minute per milligram of mitochondrial protein. n = 4, mean ± SEM, two-way ANOVA with Tukey's multiple comparisons test. * or #, $p \leq 0.05$; ** or ##, $p \leq 0.01$; *** or ###, $p \leq 0.001$; **** or ####, $p \leq 0.0001$.

5 - DISCUSSION

5.1 - Regulation of mitochondrial H_2O_2 production

5.1.1 - KGDH is more sensitive to SNO-mediated inhibition of H_2O_2 production compared to PDH

This study is one of the first of its kind in identifying and evaluating protein S-nitrosylation as a regulatory redox modification for H_2O_2 production at the site-specific level, with a particular focus on the hepatic mitochondrial metabolic enzymes, KGDH and PDH. Our work in male isolated liver mitochondria demonstrated significant decreases in H_2O_2 production by KGDH in a dose-dependent manner relative to increasing concentrations of GSNO, an established NO-donor and protein S-nitrosylation catalyst (*114*). Moreover, the results obtained from our purified enzyme system supported these observations, demonstrating a significant decrease in KGDH-driven H_2O_2 relative to the concentration of GSNO. Intriguingly, it was observed in this thesis that PDH is less susceptible to inhibition by GSNO. Indeed, experiments conducted with isolated liver mitochondria demonstrated pyruvate supported H_2O_2 genesis was unaffected by GSNO, even at a concentration 2000 µM. Assays carried out with the purified PDH of porcine heart origin confirmed these findings, although some inhibition was observed in these assays. Notably though the activity of the purified PDH was not affected, even though a small but significant decrease in its H_2O_2 generating capacity was observed. Overall, these findings show for the first time that S-nitrosylation can be a negative feedback loop for the inhibition of mitochondrial H_2O_2 production.

As noted in the introduction, tight spatiotemporal control over H_2O_2 production and availability elicits eustress signals, which are targeted reversible redox modification of specific proteins required to elicit changes in cell behavior. Mitochondria are documented to be an important cell platform eustress communication, using H_2O_2 as a second messenger for the activation of many signaling pathways (*47*). However, several contemporary issues in the field

still remain in understanding cell H_2O_2 communication, and these are 1) the source(s) of this mitochondrial H_2O_2 and 2) the mechanisms used to activate or inhibit its production for the regulation of redox signals. In the section below, I will first discuss challenges related to delineating the source(s) of this H_2O_2, focusing on evidence collected by our group using liver and cardiac tissue, but also findings made with other mammalian systems such as muscle mitochondria and tissues and cell culture models. Discussing the source(s) of this H_2O_2 is integral to this thesis since it is focused on protein S-nitrosylation and the inhibition of KGDH and PDH. This is significant because both of these α-keto acid dehydrogenases are documented to be vital H_2O_2 sources and have been postulated to be redox signaling platforms. Therefore, a mechanism like S-nitrosylation may be of significant importance for regulating H_2O_2 production by a major source for signaling.

To date, there are 16 known sites of mitochondrial H_2O_2, 12 of which are associated with nutrient metabolism and the respiratory chain. These 12 sources can be categorized based on the two isopotential groups required for H_2O_2 production: $NADH/NAD^+$ and $CoQH_2/CoQ$ (*17*). KGDH and PDH are part of the $NADH/NAD^+$ isopotential group and have been established to be important H_2O_2 sources in several mammalian tissues (*17*). KGDH and PDH generate 8x and 4x more H_2O_2 than complex I in muscle and both complexes account for ~40% of the total H_2O_2 generated in the liver (*34*). Moreover, it has been documented KGDH generates more H_2O_2 than PDH in liver tissue (*35*). KGDH was also found to be a vital source of H_2O_2 in synaptosome preparations (*32*). Recent use of mouse models heterozygous for the E2 and E3 subunits of KGDH further established its important in H_2O_2 and was found to be the major source in mitochondrial preparations (*135*). Finally, Fisher-Wellman et al. found in two separate studies PDH was a high capacity site for H_2O_2 genesis in mouse, rat, and human muscle tissue (*33*). In this thesis, I found

that KGDH was a higher capacity site when compared to PDH. I did not examine the relative rate of H_2O_2 genesis by these sites in comparison to other prominent sources like complex III. Indeed, our previous studies have shown complex III can account for ~45% of the H_2O_2 genesis during the oxidation of Krebs cycle-linked (or NADH/NAD^+ isopotential group) metabolites (*36*). However, based on my findings here, I can conclude that my results are consistent with these previous studies where it was found that KGDH and, to a lesser extent, PDH are critical H_2O_2 sources in mitochondria. KGDH and PDH are mitochondrial redox sensors and it has been hypothesized that both enzymes are involved in mitochondrial H_2O_2 signaling. The findings I collected here further support this notion that both KGDH and, to a lesser extent, PDH are vital for mitochondrial H_2O_2 signaling.

The central aim of this thesis was to determine if S-nitrosylation could deactivate H_2O_2 genesis by KGDH and PDH. Given that both enzymes are major H_2O_2 contributors in the mitochondria, it stands to reason there are mechanisms required to feedback on KGDH and PDH to deactivate its production. In this thesis, I observed for the first time that S-nitrosylation deactivates H_2O_2 production by KGDH in 1) liver mitochondria collected from male mice and 2) purified enzyme of porcine heart origin. The first important point to raise with this novel finding is that our group has already documented that KGDH and PDH are inhibited by a similar redox signaling mechanism: S-glutathionylation. Glutathionylation involves the formation of a disulfide bridge between a vicinal proteinaceous thiol and GSH (*64*). It has been found that glutathionylation occurs on the vicinal thiols of the lipoic acid in the E2 subunit of KGDH (*136*). This occurs in response to the H_2O_2-mediated oxidation of the GSH pool and although it lowers KGDH activity, it is required to protect the enzyme complex from irreversible oxidative deactivation by electrophiles, such as lipid peroxidation end products (*136*). Moreover, in 2015, Dr. Mailloux's

group hypothesized that it served a second function: to directly mitigate H_2O_2 genesis by KGDH and PDH to protect cells from oxidative distress but also simultaneously modulate cell redox signaling pathways (*137*). Since then, his group has conducted extensive research on this regulatory mechanism. One reproducible observation is that protein S-glutathionylation serves as a negative feedback loop to mediate H_2O_2 production by KGDH and PDH. Mailloux et al. observed this in 2016 when they demonstrated for the first time that glutathione can indeed significantly alter mitochondrial H_2O_2 genesis from KGDH via its glutathionylation in both a purified enzyme and isolated liver mitochondria system (*138*). In 2017, O'Brien et al. extended these findings using a similar experimental design (*78*). They saw that NADH-driven H_2O_2 production by RET in purified PDH was increased with GSSG, but decreased for FET-driven H_2O_2 synthesis, and both reversed by Grx2, indicating that PDH is targeted for protein S-glutathionylation. Moreover, immunoblot analysis for protein glutathione mixed disulfides (PSSG) using exogenous protein S-glutathionylation catalysts, such as diamide or disulfiram, confirmed that purified PDH is indeed able to be S-glutathionylated. These findings were similarly observed in mouse liver mitochondria and with KGDH. In 2018, Chalker et al. continued this investigation using the liver and cardiac mitochondria of mice partly or completely deficient in the Grx2 gene (*77*). In the isolated liver mitochondria of Grx2-deleted heterozygote ($Grx2^{+/-}$) and homozygote ($Grx2^{-/-}$) mice, the rates of H_2O_2 production were significantly lower compared to the controls for both pyruvate and α-ketoglutarate substrates. In contrast, the rates of H_2O_2 production in cardiac mitochondria of $Grx2^{+/-}$ and $Grx2^{-/-}$ mice were significantly increased when consuming either pyruvate or α-ketoglutarate. Further analysis revealed that the deletion of the Grx2 gene was associated with an increase in protein expression for PDH, but not KGDH, in liver mitochondria and a decrease in protein levels for PDH and KGDH in cardiac mitochondria. Combined, these results provide

accumulating evidence that protein S-glutathionylation intimately modulates H_2O_2 production by KGDH and PDH, but also shed light on the possible differential tissue-dependency for regulating H_2O_2. These collective studies on protein S-glutathionylation and H_2O_2 production piqued our interest in studying protein S-nitrosylation to determine if this redox modification shares a similar role in regulating sites of mitochondrial H_2O_2.

The finding that glutathionylation serves as a feedback loop for the inhibition of H_2O_2 genesis by KGDH and PDH is highly novel and suggests it is a system required to desensitize mitochondria-to-cell eustress signals. Here, I have discovered S-nitrosylation may fulfill a similar role. The first thing to acknowledge is that the modulation of mitochondrial redox and bioenergetics by S-nitrosylation is not a new concept. Indeed, in 2011, Cheng et al. discovered that the enzymes, mitochondrial permeability transition pore (mPTP) and voltage-dependent anion channel (VDAC), were targeted and regulated by protein S-nitrosylation in the mitochondria (*122*). Exogenous NO• inhibits VDAC and proteomic studies have demonstrated several mitochondrial enzymes required for fatty acid oxidation, Krebs cycle flux, and OXPHOS are targeted for S-nitrosylation (*118*). KGDH and PDH have very recently been identified as targets for S-nitrosylation, resulting in the decrease in the NADH producing activity of both complexes (*127*). Nitric oxide donor, DETA NONOate, inhibits the mitochondrial bioenergetics in primary aortic endothelial cells through KGDH nitrosylation, which can be reversed by lipoic acid supplementation (*127*). It has also been observed that KGDH and PDH can be inactivated through nitrosylation of the E2 lipoic acid arm following the activation of macrophages by lipopolysaccharide (LPS) and interferon-γ (IFN-γ), which was suggested to be required for the metabolic reprogramming of immune cells for pathogen elimination (*127*). Here, we have extended on these observations by showing S-nitrosylation also inhibits H_2O_2 genesis by KGDH.

The novelty here lies with the fact that mitochondrial H_2O_2 is also known to activate cells required for both the adaptive and innate immune systems. This would suggest S-nitrosylation may be used as a mechanism to deactivate H_2O_2 genesis by KGDH, which would aid in governing its availability for secondary signaling. This could also be the case for cells located in tissues like the liver where H_2O_2 is used to stimulate organ regeneration by activating hepatocyte proliferation (*139*). The deactivation of H_2O_2 genesis would also aid in the prevention of potential oxidative distress. For example, NO• can induce nitrosative stress through interactions with proximal ROS like $O_2^{\bullet-}$ and H_2O_2. Therefore, deactivation of H_2O_2 may serve as an additional mechanism for the prevention of oxidative/nitrosative stress. Another important finding here is that the purified KGDH displayed a high sensitivity to GSNO. Only 55 µM was required to induce 50% inhibition of its H_2O_2 producing activity, which was mirrored by a corresponding decrease in NADH production. Mitochondrial levels of GSNO vary in the mid-µM range, getting as high as 500 µM in physiological conditions. Additionally, KGDH in liver mitochondria could be inhibited by ~70-80% at 500 µM GSNO. Overall, this would suggest KGDH is highly sensitive to GSNO inhibition, validating the importance of GSNO clearance by its corresponding reductase. Interesting, PDH exhibited much less sensitivity towards GSNO, which is discussed further below. The ability of S-nitrosylation to function as a means for preventing oxidative/nitrosative stress is highlighted by its role in complex I modification. Cys39 in the ND3 subunit of complex I is targeted for S-nitrosylation, which has been shown to prevent oxidative distress through the inhibition of H_2O_2 genesis (*140*). This mechanism also prevents the oxidative deactivation of complex I, which curtails myocardial damage during ischemia-reperfusion injury (*140*). Taken together, I have identified S-nitrosylation as a new mechanism for the direct inhibition of H_2O_2 genesis by KGDH, a major H_2O_2 generator in mitochondria. This has strong implications for understanding the use of

redox signals in the modulation of H_2O_2 signaling in mitochondria. Coupled with this, S-nitrosylation is also likely required to preventing oxidative/nitrosative stress (*114*).

Also novel to this study was the finding I made regarding PDH: unlike KGDH, it is less, or not at all, sensitive to GSNO inhibition. This is unique considering our group previously found KGDH and PDH to be equally sensitive to inhibition by glutathionylation through the modification of the vicinal thiols of the E2 subunit. This difference in sensitivity to GSNO inhibition was observed in isolated mitochondria and then highlighted with the purified enzyme. Indeed, in liver mitochondria from male mice, GSNO had little to no effect on PDH. Similarly, its impact on the purified enzyme was limited, with an IC_{50} of 52 μM but with 48% of its activity retained. PDH and KGDH share the same basic structure, being composed of decarboxylase, acyltransferase, and dehydrogenase subunits. However, the difference in their regulation by S-nitrosylation may be related to several factors that set these isozymes apart from one another. The first is redox properties: KGDH is a superior H_2O_2 source when compared to PDH (discussed above). In addition, although both complexes are equally sensitive to glutathionylation, KGDH can be more easily modified with electrophiles like 4-hydroxy-2-nonenal (*141*). This would imply KGDH may display enzymatic characteristics that increase its likelihood for the formation of Michael adducts with redox active electrophiles. This increased sensitivity to modification to S-nitrosylation in KGDH could be related to redox differences in the vicinal thiol in the E2 subunit. These differences may be related to the overall structure of the multimer form of the enzymes. For example, PDH forms a ~9.5 MDa multi-subunit holoenzyme comprised of an E1:E2:E3 stoichiometry of 40:40:20 (*9*). By contrast, KGDH is predicted to by composed of 12 E1 and 12 E3 subunits surrounding a 24-mer E2 complex, which is ~3.2 MDa in size (*10*). This could supply the requisite protein microenvironment required to change redox states of the vicinal E2 thiols making KGDH more

amenable to S-nitrosylation. Finally, PDH and KGDH are subjected to different means of overall regulation. For example, PDH, unlike KGDH, is actively regulated by a kinase and phosphatase system that inhibits and activates the enzyme in response to changes in energy and nutritional demands (*7, 142*). Taken together, I demonstrate here that KGDH, but not PDH, is modulated by S-nitrosylation and this may be related to differences in the role that both enzymes play during mitochondrial redox sensing and signaling.

5.1.2 - Protein S-nitrosylation does not affect RET-induced H_2O_2 production by KGDH/PDH

We also examined the role of protein S-nitrosylation on H_2O_2 production by KGDH and PDH through NADH-stimulated RET. Our results showed that with purified KGDH and PDH, the rate of NADH-driven H_2O_2 production by RET was not significantly different between GSNO concentrations. While the data trended towards a reduction in the rate of H_2O_2 synthesis between 100 – 200 µM GSNO, followed by an increase at 500 µM GSNO for both KGDH and PDH, overall, GSNO did not appear to have a major impact on RET-driven H_2O_2 generation by either enzyme. To our knowledge, this is the first time protein S-nitrosylation has been investigated within the context of RET by KGDH and PDH. These preliminary findings suggest that protein S-nitrosylation, unlike protein S-glutathionylation, is not a major regulatory mechanism for NADH-driven H_2O_2 production during RET for KGDH or PDH. This is in contrast to previous findings that demonstrated a potent regulatory effect for protein S-glutathionylation on H_2O_2 production by KGDH and PDH via NADH-driven RET. Tretter and Adam-Vizi saw that KGDH and PDH can generate H_2O_2 by RET through their E3 subunits in the presence of NADH (*32*). More recently, Mailloux et al. demonstrated that the rate of H_2O_2 production by KGDH under RET conditions is approximately 3 – 3.5 times higher than PDH and can be stimulated with lower concentrations of NADH that are representative of its physiological concentration (*35*). These findings contradict those by Quinlan et al., as they did not observe high rates of H_2O_2 production during the reverse

reaction from NADH (*34*). Furthermore, O'Brien et al. in 2017 demonstrated that protein S-glutathionylation plays a regulatory role on RET-driven H_2O_2 production by KGDH and PDH (*78*). While this redox modification reduced H_2O_2 production during the forward reaction, the opposite was true for RET as both purified KGDH and PDH demonstrated an increase in RET-driven H_2O_2 generation following their S-glutathionylation. Collectively, these observations reveal intriguing differences in the regulation of H_2O_2 production by FET and RET by S-glutathionylation, while re-enforcing previous findings that identify KGDH as being the superior H_2O_2 producer compared to PDH. Our preliminary results with S-nitrosylation are interesting to consider when compared with the previous work on S-glutathionylation. Though there were no statistically significant changes, the rate of RET-driven H_2O_2 synthesis for both purified KGDH and PDH trended towards a decrease between 100 – 200 µM GSNO, followed by a trend towards an increase at 500 µM GSNO. Notably, a recent study by Seim et al. demonstrated that the incubation of purified PDH with GSNO resulted in a near-complete inhibition of forward PDH enzyme activity through the NO-modification of their lipoic arm at the E2 subunit (*127*). This presents a possible explanation for an increase in RET-driven H_2O_2 by GSNO; the NO-modifications on the lipoic moieties could prevent their reduction during reverse electron transfer reactions by E3 driven by NADH, thereby increasing the likelihood of electron leakage and H_2O_2 formation at this site. While additional research must be continued, collectively, these observations show potential for a novel regulatory mechanism in RET-driven H_2O_2 production by KGDH and PDH.

5.2 - Sex dimorphisms in regulation of mitochondrial H_2O_2 production

In addition to determining if protein S-nitrosylation by GSNO serves as a shut-off mechanism for H_2O_2 production by KGDH and PDH, our aim was also to explore whether sex

influences GSNO signaling within mitochondria. To our knowledge, our study demonstrates for the first time sex dimorphic differences in the regulation of mitochondrial H_2O_2 production by protein S-nitrosylation in the liver at the site-specific level for KGDH and PDH. In 10-week female isolated liver mitochondria energized with either α-ketoglutarate or pyruvate, we discovered that GSNO did not significantly affect the rate of H_2O_2 production for either substrate regardless of GSNO concentration. Moreover, quantitative analysis revealed that the 10-week female liver mitochondria had significantly lower rates across the board in comparison to their male counterparts.

These findings are comparable to what our group has previously observed regarding sex differences in protein S-glutathionylation and H_2O_2 production by KGDH and PDH. First, Mallay et al. demonstrated that KGDH and PDH from male liver mitochondria possessed rates of H_2O_2 production that were approximately 5- and 3.5-fold higher than females (*79*). Furthermore, using the isolated liver mitochondria of Grx2-deleted heterozygote ($Grx2^{+/-}$) and homozygote ($Grx2^{-/-}$) mice, they revealed that for the males, Grx2 gene deletion resulted in an increase in glutathionylation of KGDH and PDH which led to the inhibition of H_2O_2 production from these two enzymes. On the other hand, the liver mitochondria from female mice did not share these properties and the deletion of the Grx2 gene did not alter the rates of H_2O_2 synthesis by KGDH or PDH. Mallay et al. also examined male and female muscle mitochondria and showed that the opposite occurred; female muscle mitochondria displayed greater rates of H_2O_2 production by PDH and KGDH than males (*79*). However, like in liver mitochondria, KGDH and PDH-driven H_2O_2 production in female muscle mitochondria did not appear to be affected by alterations in protein S-glutathionylation status. Taken together, these observations suggested that female mitochondria were less reliant on glutathionylation to negatively modulate H_2O_2 generation by

KGDH and PDH and showed for the first time the significance of sex in regulating H_2O_2 production at the enzymatic, site-specific level. Given this, it is not surprising that in our present study, we observed a similar insensitivity to GSNO modification for KGDH and PDH in female mitochondria, but not the male mitochondria.

These sex differences are largely attributed to the greater redox buffering capacity that exists in female mitochondria. Indeed, there have been many studies indicating that females possess numerous mitochondrial features and mechanisms that allow them to maintain cellular and mitochondrial redox homeostasis more effectively. For example, Justo et al. observed in 2005 that female rat liver mitochondria possessed significantly higher mitochondrial protein content, cardiolipin content and greater respiratory capacities than males (*143*). More specifically, they saw that the protein levels for mitochondrial transcription factor A (TFAM), a critical regulator for both the replication and expression of mitochondrial DNA (mtDNA), were nearly 4-times higher in female mitochondria compared to males (*144*). Thus, Justo et al. suggested that these sex-dependent differences in oxidative capacity were likely related to improved mitochondrial machinery in females and in association with greater mitochondrial differentiation (*143*). Furthermore, there is significant evidence indicating that female mitochondria possess higher amounts of antioxidants and H_2O_2-regulating enzymes, thus giving them a greater ability to maintain cellular redox status. For example, Rikans et al. demonstrated that the concentration of hepatic Vitamin E, a chain-breaking antioxidant compound, was lower in young adult male rats compared to females (*145*). Borrás et al. examined the sex-differences in oxidative capacity between male and female rat liver mitochondria, revealing that the concentration of total peroxides in females was about half of that found in their male counterparts (*146*). They attributed this to the higher expression levels and enzymatic activities of SOD2 and Gpx in female liver mitochondria.

Research conducted by Viña et al. also supported these previous findings (*147*). Combined, these findings present a likely explanation for our observations in this study where females in general produced H_2O_2 at lower measurable rates than their male counterparts, regardless of GSNO treatment. Their increased antioxidant capacity likely led to less H_2O_2 available to be measured since more of it was being removed or quenched.

In addition, sex hormone signaling, namely estrogen-driven signaling, has been heavily implicated as playing a major role in providing an improved redox buffering capacity in female mitochondria. In 2003, Borrás et al. employed an ovariectomy rat model to assess the effects of estrogen replacement therapy with 17β-estradiol (*146*). First, they demonstrated that hepatic mitochondrial GSH levels were initially higher in female rates compared to male rats. When females were subjected to ovariectomy surgery, these GSH levels fell to comparable levels as the males. However, estrogen replacement via 17β-estradiol supplementation fully recovered GSH levels in females. Combined, these results reveal that 1) females inherently possess a greater GSH pool and 2) the higher GSH levels are attributable to the availability of estrogen. Adding to this, McConnachie et al. demonstrated that the activity levels of glutamate cysteine ligase (GCL), which catalyzes the first rate-limiting step in GSH biosynthesis, were significantly higher in female liver mitochondria compared to males (*148*). Borrás et al. continued investigating the role of estradiol in protecting mitochondria from oxidative distress and noticed that it was capable of upregulating the expressions SOD and Gpx genes (*149*). Bellanti et al. explored the effects of surgical estrogen deprivation and replacement (ERT) in fertile women (*150*). They noticed that following estrogen depletion by surgery, patients had depleted levels of circulating GSH, a decreased GSH:GSSG ratio, and marked reductions in SOD and Gpx expression levels, all indicative of increased

oxidative distress. However, treatment with estrogen attenuated all of these effects, returning the GSH:GSSG ratio and SOD and Gpx expressions back to physiological levels.

Taken all together, these previous findings present a reasonable explanation for our observations regarding the effects of GSNO on H_2O_2 production by KGDH and PDH in the female isolated liver mitochondria. It is well-established that females possess a greater redox buffering capacity due to a number of factors, such as higher antioxidant activity and a larger reduced GSH pool due to estrogen availability. This is certainly a probable cause for our observed lower rates of H_2O_2 production in female mitochondria compared to male as it is likely that more H_2O_2 was scavenged within female mitochondria, thereby reducing our measured AUR signal. However, we also saw that the female liver mitochondria, unlike the males, were resistant to any changes in H_2O_2 production induced by GSNO treatment. Perhaps females are less reliant on S-nitrosylation, like S-glutathionylation, to protect reactive protein cysteine thiols from nitrosative or oxidative stress and for the governance of H_2O_2 by KGDH and PDH due to their inherently greater antioxidant capacity, which may be sufficient enough to maintain redox homeostasis. This would also explain why H_2O_2 genesis by KGDH and PDH in male mitochondria was observably more sensitive to these redox modifications given that male mitochondria do not possess the same tools that the females have to maintain the integrity of its redox status and would therefore need to rely on other mechanisms, such as S-nitrosylation or S-glutathionylation, to protect enzymes from nitrosative stress and to inhibit H_2O_2 genesis.

Another potential mechanism for the insensitivity to GSNO in females may be related to their greater GSH availability. While mitochondrial proteins can be S-nitrosylated with GSNO, likewise, mitochondria also possess denitrosylation systems in order to mediate NO-signaling, including GSNO reductase (GSNOR). GSNOR is endogenously found within mitochondria and

mediates GSNO metabolism in a NADH-dependent manner (*104*). In the presence of GSH and NADH, GSNOR first catalyzes the enzymatic degradation of GSNO into an unstable glutathione-*N*-hydroxysulfinamide (GSNHOH) intermediate, which subsequently gets resolved by reduced GSH to generate GSSG and nitrogen by-products that are excreted (*151*). As previously stated, female hepatic mitochondria are known to possess higher levels of GSH compared to males. Therefore, it is possible that the increased GSH availability results in female liver mitochondria having increased GSNOR enzymatic activity levels. This serves as potential mechanism for our observed lack of GSNO effect in females: they posses a greater capacity to degrade GSNO via GSNOR, thus, preventing the GSNO-mediated modification on target proteins, such as KGDH and PDH. Indeed, several groups, such as Brown-Steinke et al. in 2010 and Casin et al. in 2018, have already observed higher GSNOR activities in female mouse lung and heart mitochondria compared to males (*152, 153*). Therefore, it would not be unexpected to see a similar trend in female mouse hepatic mitochondria. It would be intriguing to continue to explore the effects of S-nitrosylation on H_2O_2 production by hepatic KGDH and PDH, but also keeping endogenous GSNOR activity in consideration. Nonetheless, I have demonstrated for the first time that there are sex dimorphisms regarding the effects of GSNO on KGDH and PDH-driven H_2O_2 genesis in liver mitochondria, likely related to the inherent differences that exist between the male and female mitochondrial environment and redox buffering capacities.

5.3 - Impact of HFD on mitochondrial H_2O_2 production

In this study, we examined the effects of HFD-feeding on mitochondrial H_2O_2 production by KGDH and PDH and its regulation by protein S-nitrosylation. To our knowledge, this is the first study that examined this at the site-specific enzymatic level. 4-week old male and female C57BL6N mice were placed on either a Teklad HFD or Teklad CM diet for a minimum of 5 weeks.

During this feeding period, the average mouse weight for males increased significantly with HFD feeding in comparison to the male CM mice while there were no significant differences in weight for the females. The HFD mice also consumed more food in comparison to their CM counterparts for both sexes, though this was only apparent at weeks 4 and 5. Furthermore, weekly blood glucose levels stayed relatively consistent between the HFD and CM pairs for both sexes. The isolated livers between the HFD and CM pairs were also comparable in dry weight for both sexes, with only the male HFD isolated livers showing some visual signs of hepatic lipid accumulation. Overall, these findings are not surprising and agree with several previous studies that have used similar HFD mouse models, including from our own group (*154*, *155*).

Our investigation into the effects of HFD-feeding on hepatic mitochondrial H_2O_2 production revealed that, in male mice, the rate of H_2O_2 genesis in HFD liver mitochondria energized with α-ketoglutarate trended towards a decrease with GSNO in a dose-dependent manner with a significant decrease observed at the highest GSNO concentration (1000 μM). On the other hand, the rate of H_2O_2 production from CM liver mitochondria energized with α-ketoglutarate did not display any obvious trends regardless of GSNO concentration. Interestingly, when comparing between the two diet types, their zero-control samples (0 GSNO) displayed similar rates of H_2O_2 production while the 500 μM and 1000 μM GSNO HFD samples had significantly reduced rates from their CM counterparts. For the females, both HFD and CM liver mitochondria energized with α-ketoglutarate did not have any significant differences, nor trended towards any changes, in their rates of H_2O_2 production between the GSNO treatments or the diets. When pyruvate was used as the primary substrate, the male HFD liver mitochondria, again, displayed significantly reduced rates of H_2O_2 production in a GSNO concentration-dependent manner, comparable rates at the zero-control samples to the male CM liver mitochondria, and

significantly decreased rates at higher concentrations of GSNO compared their respective CM counterparts. For the females, the rates of H_2O_2 production in HFD and CM liver mitochondria consuming pyruvate were similarly unaffected by GSNO or diet type as previously observed with α-ketoglutarate. Combined, these results highlight intriguing interactions and sex-dimorphic effects between HFD-feeding and the regulation of H_2O_2 production by KGDH and PDH via protein S-nitrosylation.

Notably, HFD-feeding allowed for a greater decrease in H_2O_2 production with GSNO in both α-ketoglutarate- and pyruvate-consuming male liver mitochondria in comparison to their CM partners. Perhaps changes in the hepatic mitochondrial redox environment following extended HFD-feeding rendered KGDH and PDH more amenable to S-nitrosylation by GSNO, thus resulting in the observed inhibition of H_2O_2 synthesis. It has previously been established that while KGDH and PDH share the same basic E1, E2, and E3 enzymatic structure, they differ in their stoichiometric subunit composition and possess unique regulators, such as PDK/PDP for PDH (*7, 9, 10, 142*). It is possible that these distinct enzymatic properties are one of the determining factors that make KGDH a greater H_2O_2 producer compared to PDH, as well as the reason why we observed that KGDH-driven H_2O_2 genesis was affected to a higher degree by GSNO than PDH (mentioned above). However, in our HFD models, KGDH and PDH were both susceptible to GSNO modification to a high degree, suggesting a more universal change in mitochondrial redox buffering capacity rather than a site-specific one. It is likely that hepatic lipid accumulation resulted in oxidative or nitrosative distress, which resulted in the diminishment of redox buffering capacity in the males, such as a decrease in reduced GSH availability. This in turn could perpetuate into a greater reduction in redox buffering capabilities as well as a decrease in GSNOR activity, thus, rendering KGDH an PDH more sensitive to GSNO modification. This increased amenability

to S-nitrosylation may indeed be a natural response to the HFD-induced rise in oxidative and nitrosative distress. First, the S-nitrosylation of KGDH and PDH could potentially serve to protect their reactive cysteine thiol groups from oxidation in order to retain proper enzymatic function. Therefore, the increased GSNO sensitivity for KGDH and PDH during HFD-feeding may be a preventative measure in response to the more oxidized environment in order to effectively protect these key enzymes from damage. Next, I have previously demonstrated that GSNO is capable of inhibiting the H_2O_2 production from these two enzymes. This could imply that their increased amenability to S-nitrosylation during HFD-feeding, which subsequently inhibits H_2O_2 production in the mitochondria, may also be part of an overall response by the cell to manage the HFD-driven increase in oxidative and nitrosative distress.

Understanding the nature in which HFD-feeding affects hepatic mitochondrial redox homeostasis is highly relevant in a disease setting. Indeed, there has been a concerted effort towards researching how HFDs affect the modulation of H_2O_2 and induce oxidative distress, which has been intimately linked with the development of insulin resistance, NAFLD, and other metabolic diseases. A major roadblock in this collective effort is the high degree of variability and lack of standardization between the different experimental conditions, such as the compositions of the high-fat and control diets, the duration of feeding, and the strain and species of rodent. Despite this, some key observations have been reproducible thus far, one of which is the promotion of oxidative imbalance by HFDs. Nadal-Casellas et al. saw that male and female Wister rat liver mitochondria energized with succinate produced significantly higher H_2O_2 in response to HFD-feeding compared to their control mice (*156*). Lionetti et al. also observed a significant increase in H_2O_2 genesis from isolated liver mitochondria of HFD-fed Wistar rats with succinate as the substrate (*157*). In this case, their HFD was primarily lard-based with 40% of its total caloric

energy derived from fat, as opposed to the homemade cafeteria diet composition (cookies, pork liver paté, fresh bacon, chocolate, ensaïmada, pelleted standard diet) and 55% fat-derived energy of the HFD used by Nadal-Casellas et al. (*156, 157*). Interestingly, when Lionetti et al. used an HFD that was fish-based instead of lard, there were no statistically significant changes in H_2O_2 production. Vial et al. assessed other substrates besides succinate, revealing increases in H_2O_2 production by HFD-fed Wistar rat liver mitochondria stimulated with palmitoyl-CoA, but not malate/glutamate (*158*). Cardoso et al. investigated the effects of an 8-week HFD feeding period on H_2O_2 in a female Swiss mouse model, demonstrating that the isolated liver mitochondria of HFD-mice displayed greater H_2O_2 synthesis with palmitoyl-CoA, succinate, or malate/glutamate as substrates (*159*). A later study by Cardoso et al. examined the effects of a 1-week HFD feeding period, revealing a significant increase in H_2O_2 with palmitoyl-CoA, but no significant changes with succinate, malate/glutamate, or α-ketoglutarate (*160*). Eccleston et al. assessed the effects of a corn oil-based HFD (71% energy from fat) on H_2O_2 production over an 8-week and 16-week period using a male C57BL/6J mouse model (*161*). They saw an increase in H_2O_2 generation from liver mitochondria of the 8-week group in the presence of succinate, but a decrease from the 16-week group, raising intriguing questions regarding the differential regulation of H_2O_2 arising from prolonged exposure to HFDs. Even though these studies employed different rodent strains, diet types, and treatment protocols, in general, they collectively observed significant increases in mitochondrial H_2O_2 synthesis in response to HFD feeding.

Interestingly, in our present study, unlike these previous findings, we did not observe marked differences in the rates of H_2O_2 production between the control samples from the HFD and CM groups for both KGDH and PDH. One potential explanation for this observation is based on the standard chow diets that our mice were placed on prior to their delivery to our facility. Since

we did not raise our own mice from birth and instead acquired them from Charles River Laboratories at 4-weeks of age, we were not able to control for the standard chow diet they were placed on during that growth period. Even though we know the composition of the standard chow diet, it contains such a wide range of different ingredients and it is possible that one or more of its components had unintended effects on their hepatic liver mitochondria. This is certainly more pronounced when comparing the results from our 10-week male mice, who would have been consuming the standard chow diet for at least 9 weeks prior to their delivery, and the 4-week CM-fed male mice. For example, in the 10-week male mitochondria, we observed a higher degree of GSNO-mediated inhibition on H_2O_2 production by KGDH than in the CM male mice, suggesting that some aspect of the standard chow diet altered their hepatic mitochondrial environment which rendered them more sensitive to GSNO modification. Thus, it is possible that feeding on the standard chow diet could have not only affected our observed HFD-effect on H_2O_2 production by hepatic KGDH and PDH, but also changed the manner in which GSNO modifies H_2O_2 genesis from these sources. Another possible reason may be related to the duration in which our mice were placed on the HFD. Our protocol, which has previously been shown to be effective in causing oxidative imbalance, stipulates an approximate 5-6 week feeding period for the mice from 4-weeks to 9-weeks of age (*154, 155*). However, some studies contrast these findings, stating that a longer feeding duration is required in order to observe the HFD-induced changes within hepatic mitochondria. Indeed, in the case of Chan et al., they only noticed HFD-related alterations of the mitochondrial proteome after 10 weeks of feeding, and not at 2- and 4-weeks, suggesting that the HFD mice may have been utilizing compensatory mechanisms to maintain homeostasis during the early stages of feeding, but prolonged feeding eventually resulted in observed disruptions within the mitochondria (*162*). Therefore, it certainly plausible that a similar situation occurred in our

study where either 1) our HFD mice developed compensatory mechanisms in response to HFD-feeding in order to maintain redox homeostasis, or 2) the mice had not been placed on the HFD long enough to reach the point of an observable disruption in H_2O_2 regulation. In the future, it would certainly be interesting to assess different feeding duration periods and diet compositions to see how these factors influence the overall effect of HFDs on hepatic mitochondrial redox buffering capacity.

Our group has also recently looked more closely at the impact of HFDs on regulatory mechanisms of H_2O_2 production, namely protein S-glutathionylation. Young et al. investigated the relationship between protein S-glutathionylation and diet-induced obesity using a Grx2 knockout mouse model (*154*). Grx2 plays a crucial role in mediating reversible protein S-glutathionylation reactions in the mitochondria and has previously been shown to regulate key metabolic enzymes such as complex I, UCP3, KGDH and PDH (*25*). First, they observed a significant increase in body mass, white adipose tissue hypertrophy, hepatic lipid accumulation, and blood insulin and triglyceride levels in wild-type mice placed on the HFD compared to their control diet counterparts. However, intriguingly, their Grx2 heterozygote ($Grx2^{+/-}$) mice fed with the HFD displayed similar body mass, white adipose tissue weight, hepatic lipid content, and blood insulin and triglyceride levels to their control diet counterparts. Upon closer examination of the muscle mitochondria, their analysis revealed that the attenuation of the HFD-induced weight gain in Grx2 heterozygotes was attributed to increases in fuel combustion, mitochondrial respiration, and mitochondrial H_2O_2 production, primarily from complexes I and II. While it may seem counterintuitive for an increase in H_2O_2 to be associated with improved health, it is possible that its upregulated production in the HFD state resulted in the improved capacity for H_2O_2-mediated signal transduction, which subsequently promoted physiologically beneficial pathways that

prevented diet-induced weight gain. It is well-known that H_2O_2 serves as a critical secondary messenger in redox signaling pathways and governs a wide range of cellular growth and metabolic processes (*163*). Indeed, mitochondrial H_2O_2 plays a significant physiological role in muscle tissue during exercise, including the promotion of antioxidant defense systems, the induction of myokine production, and during the repair of damaged myofibers (*164,165*). Young et al. stipulate that in the $Grx2^{+/-}$ model, the partial deletion of Grx2 gene likely led to the deglutathionylation of complexes I and II, thus, freeing them from the inhibitory effects of protein S-glutathionylation and subsequently increasing H_2O_2 production from these sources (*154*). These novel findings demonstrated for the first time that alterations in mitochondrial redox signaling, namely protein S-glutathionylation, can serve as an "exercise mimetic" in muscle tissue to attenuate HFD-induced weight-gain and other symptoms.

In addition to glutathionylation, there has been growing interest surrounding NO and its implication in HFD-induced diseases such as NAFLD. Mantena et al. investigated whether the hepatic mitochondrial impairments brought on by HFD-feeding were associated with alterations in the mitochondrial proteome by RNS (*166*). They showed that with 16 weeks of HFD-feeding, liver mitochondria from C57BL/6 mice possessed elevated triglyceride levels, iNOS protein levels, and greater sensitivity to NO-dependent inhibition of respiration compared to controls. Furthermore, they observed significant increases in hypoxia within the pericentral region of the HFD livers that was proportional to the measured 3-tyrosine (3-NT) levels, a marker for RNS-modified proteins (*166, 167*). Combined, these results suggested that chronic HFD-feeding altered the hepatic mitochondrial proteome through NO-dependent modifications driven by RNS. Eccleston et al. examined the NO-metabolism proteins, arginase-1 and eNOS (NOS3) (*161*). Using a male C57BL/6 mouse model and an 8-week and 16-week HFD duration, their proteomic analysis

revealed that HFD-feeding led to increases in arginase-1 and decreases in eNOS activation and serum and liver nitrate + nitrite levels. Altogether, these results reveal several ways in which HFD exposure alters NO metabolism and highlights the potential role for NO in the development of NAFLD symptoms. Adding to this, numerous studies have further implicated the importance of NO metabolism and NO-mediated processes in HFD-settings through their studies on dietary nitrate supplementation. Cordero et al. studied the therapeutic effects of dietary nitrate on liver steatosis (*168*). Remarkably, supplementation with dietary nitrate was shown to effectively attenuate HFD-driven liver steatosis and other key features of NAFLD. The benefits of dietary nitrate were attributed to its contribution to a nitrate-nitrite-NO signaling pathway, which was shown to inhibit H_2O_2 production by NADPH oxidase (NOX) and activate AMP-activated protein kinase (AMPK), a master regulator of signaling pathways involved in fatty acid oxidation, lipogenesis, and glucose metabolism (*168*). More recently, DesOrmeaux et al. examined the effectiveness of dietary nitrate in attenuating HFD-induced complications using a male C57BL/6J mouse model (*169*). They confirmed that HFD exposure resulted in whole body glucose intolerance, increased hepatic lipid accumulation, elevated liver mitochondrial H_2O_2 and markers of oxidative distress. However, all of the pathological responses to HFD-feeding were attenuated with dietary nitrate. DesOrmeaux et al. also concluded that the salutary effects of dietary nitrate were independent of changes in AMPK signaling, mitochondrial content or respiratory capacity, or sensitivity to lipid-driven respiration (*169*). Altogether, these findings highlight the therapeutic potential of dietary nitrate supplementation in preventing the progression of NAFLD, but more research must be conducted in order to properly define its mechanisms of attenuation. In our present study, we demonstrated that GSNO induced an inhibition of H_2O_2 production by KGDH and PDH. Taken together, one potential mechanism in which dietary nitrate prevents the

development of NAFLD-symptoms may be through regulating H_2O_2 production directly at their enzymatic sources. Perhaps the increased NO supply with dietary nitrate supplementation allowed for greater S-nitrosylation of H_2O_2-producing enzymes, such as KGDH and PDH, resulting in the inhibition of H_2O_2 genesis and preventing oxidative distress. It would be interesting to explore this further to determine how dietary nitrate attenuates HFD-induced alterations of the mitochondrial environment, but with a particular focus on the major H_2O_2 contributors within hepatic mitochondria.

Furthermore, studies have also examined the role of estrogen in the attenuation of insulin resistance and diabetes-related symptoms, which are known to be caused by the dysregulation of H_2O_2 production. For example, Bryzgalova et al. showed that when female C57BL/6 mice placed on a HFD were supplemented with 17β-estradiol, they displayed remarkable improvements in glucose tolerance, insulin sensitivity and decreases in overall body weight (*170*). They attributed these effects to a reduction in lipogenic gene expression in white adipose tissue and the inhibition of hepatic glucose-6-phosphatase activity. Riant et al. performed a similar study with estradiol supplementation using ovariectomized mice exposed to either a normal chow diet or a HFD and also noticed a significant amelioration in glucose tolerance and insulin sensitivity following estradiol treatment within the HFD mice (*171*). Diaz et al. extended this research further, investigating the therapeutic effects of estrogen treatment in combating increases in oxidative stress by T2D (*172*). Using Wistar and Goto-Kazizaki (GK) rats, they first demonstrated that female diabetic rats had lower glycaemia levels and enhanced insulin sensitivity compared to males due to the actions of estrogen. Next, they observed that the diabetic female liver mitochondria had reduced H_2O_2 production, decreased xanthine oxidase activity, lower levels of lipid oxidation, and a more reduced mitochondrial GSH pool compared to the diabetic males. The

liver mitochondria from female diabetic ovariectomy rats displayed similar increases in oxidative stress as the diabetic males, which was subsequently attenuated with estrogen replacement therapy. Collectively, these results implicate estrogen as a key metabolite in maintaining redox homeostasis within female mitochondria under HFD-induced conditions. The findings by Torres et al. further supported this notion (*173*). Using a female C57BL/6N ovariectomy mouse model, they saw that the depletion of estradiol following surgical ovariectomy induced a pro-diabetic state and increased insulin resistance in the mice. Moreover, there were considerable alterations in the mitochondrial redox environment, such as marked reductions in the GSH/GSSG ratio and a 2-fold increase in PDH-driven H_2O_2 production, as well as a significant decrease in mitochondrial respiratory function. However, as previously observed, supplementation with exogenous estradiol attenuated all of these effects, showing improvements in glucose tolerance, insulin sensitivity, and the restoration of redox homeostasis in the mitochondria. Torres et al. attributed some of these improvements by estradiol to the upregulation of respiratory complex activities and the localization and incorporation of estradiol into mitochondrial membranes, thereby improving their microviscosity (*173*).

However, there is still much to discover regarding sex-dependent differences in the regulation of H_2O_2 production as it pertains to the development of NAFLD and metabolic syndrome. In this study, we demonstrate a sex-dimorphic difference in the regulation of H_2O_2 production by KGDH and PDH by protein S-nitrosylation in response to HFD-feeding. To our knowledge, this study is the first of its kind to report on these effects on H_2O_2 production at the site-specific level. Overall, we saw that the isolated liver mitochondria of female HFD mice, when compared to female CM mice, did not display any significant changes in the rates of H_2O_2 production for both α-ketoglutarate and pyruvate substrates and regardless of GSNO

concentration. This is contrast to male liver mitochondria, who displayed higher levels of inhibition by GSNO following HFD-feeding. In addition, the rates of H_2O_2 production for the female mitochondria were lower than the males until higher GSNO concentrations were applied, at which point, the rates of H_2O_2 generation in male HFD mitochondria were inhibited to comparable levels observed in the females. Altogether, our results highlight the significance of sex differences in the handling of H_2O_2 and the maintenance of mitochondrial redox homeostasis.

The lack of response to HFD-feeding in the females is likely due to similar reasons as their insensitivity to GSNO that we had previously observed. It is probable that the greater redox buffering capacity in females allowed them to mitigate the deleterious effects of hepatic lipid accumulation more effectively. For example, we saw that HFD-feeding led to an increase in sensitivity to GSNO modification by both KGDH and PDH in the males, but not the females. A potential mechanism for this observation is that the HFD-feeding induced a decrease in reduced mitochondrial GSH content in males, which subsequently led to an inhibition of GSNOR activity. Consequently, this reduction in GSNOR resulted in less GSNO being degraded, thereby, increasing its availability and capacity to modify its targets, such as KGDH and PDH. However, given that female hepatic mitochondria possess a larger GSH pool, it is likely that HFD-feeding was unable to deplete enough GSH to compromise their GSNOR activities, thus, keeping KGDH and PDH in female mitochondria unmodified by GSNO. Future studies should aim to elucidate this potential mechanism in determining if GSNOR plays a significant role in mediating GSNO modifications within HFD-compromised hepatic mitochondria. Additionally, the interaction between estrogen-signaling pathways and the S-nitrosylation of mitochondrial targets is unclear. While there is significant evidence pointing towards estrogen as being a key factor for greater

redox control in female mitochondria, future research should aim to elucidate whether its function extends to mediating NO signals on major mitochondrial H_2O_2 producers.

5.4 - Antioxidant inhibitor interactions with KGDH and PDH

Our experiments with the antioxidant inhibitors CDNB and AF yielded intriguing results that were in contrast to our initial hypotheses. In 10-week male isolated liver mitochondria consuming α-ketoglutarate, we observed a decrease in the measured H_2O_2 signal with CDNB or AF incubation regardless of GSNO incubation and no change when pyruvate was used as the substrate. Typically, one would expect to see an increase in the measurable H_2O_2 signal with the inclusion of inhibitors for H_2O_2-scavenging systems since less of the generated H_2O_2 would be removed. Thus, this observation suggested that perhaps CDNB and AF were having off-target interactions with KGDH and PDH directly, resulting in decreased H_2O_2 production from these sources. To determine if this were the case, we conducted CDNB and AF titration experiments in both purified KGDH and PDH. Interestingly, both CDNB and AF did not significantly affect the rate of H_2O_2 production by purified KGDH or PDH. However, in the case of CDNB, there was a noticeable trend towards an increase by the 10 μM mark. AF on the other hand remained relatively stagnant across all concentrations.

CDNB and AF have been widely used as antioxidant inhibitors in experiments largely for their supposed specificity towards their respective targets and minimal off-target effects. CDNB is a potent inhibitor for the Gpx antioxidant system by depleting GSH directly by targeting its cysteinyl thiol group, while AF targets selenocysteine-containing proteins, such as TrxR, thereby impairing the Prx/Trx antioxidant system (*133, 134*). The mechanisms in which CDNB and AF can target sulfur and sulfur-containing moieties raises concerns as to whether they could also modify reactive cysteinyl thiols, such as the catalytic cysteine residues within the lipoic arm of the

E2 subunit of KGDH. Indeed, Aon et al. observed decreases in the rates of H_2O_2 production by CDNB and AF in mouse, rat, and guinea pig heart mitochondria consuming NADH-linked substrates (*174*). Munro et al. supported these findings when they also demonstrated decreases in H_2O_2 production in intact mitochondria consuming NADH-linked substrates, such as glutamate and malate (*130*). Munro et al. extended this further by investigating the effects of direct CDNB addition to permeabilized mitochondria, demonstrating that H_2O_2 production at NADH-linked sites began to increase at even low concentrations of CDNB (5 μM). They concluded that instances of undetectable alterations in the rate of H_2O_2 production for substrates such as malate should not necessarily be interpreted as an absence of change as it is possible that CDNB may be eliciting off-target effects on the enzymatic site (*130*). This indeed may have been the case in this present study as well given our observations regarding CDNB and PDH in isolated mitochondria. Thus, with my present findings, there is now accumulating evidence pointing towards the undesired targeting of NADH-linked sites of H_2O_2 production by CDNB.

Nonetheless, it is intriguing that our observed inhibition on H_2O_2 production by KGDH following CDNB and AF treatment in the male isolated liver mitochondria system was not reproduced with the purified enzymes. It is possible that KGDH, which seemed more susceptible to alteration by CDNB and AF compared to PDH, is preferentially targeted by these antioxidant inhibitors due to its differential subunit composition. Previous evidence has revealed that the full enzymatic structure of KGDH is comprised of more E2 subunits than PDH (*9, 10*). Since KGDH has more E2 subunits, therefore, it also possesses more reactive cysteine thiols, which are located in the lipoic arms within the E2 subunits (*8*). Considering the mechanism in which CDNB depletes GSH (directly targeting its cysteine thiol), it is reasonable to speculate that CDNB had a more pronounced off-target effect on KGDH due to it containing a higher availability of cysteine thiols,

making it a more susceptible target for CDNB (*133*). Additional research investigating these potential non-specific antioxidant inhibitor interactions would certainly be beneficial in preventing the underestimation of data and other confounding variables in future HRP-based H_2O_2 evaluation assays.

6 - CONCLUSION

Redox signals have emerged as a vital means for the control of many cellular and physiological programs. Here, I have demonstrated for the first time that KGDH, a major H_2O_2 source in liver tissue, is inhibited by GSNO-mediated S-nitrosylation. It was found that physiologically relevant concentrations of GSNO could induce this effect, but only with KGDH. GSNO, on the other hand, had little to no effect on H_2O_2 genesis by PDH in liver mitochondria and was less effective as an inhibitor of the purified enzyme of porcine heart origin. The observations I have presented here also suggest the modification occurs on the E2 subunit of KGDH. Overall, these findings not only expand on the current knowledge surrounding the importance of S-nitrosylation in regulating mitochondrial bioenergetics, but also reveal a new mechanism for the inhibition of mitochondria-to-cell signaling. Indeed, I saw that KGDH was an important H_2O_2 generator that could be inhibited by S-nitrosylation, further validating the importance of this enzyme in redox signaling. Moreover, I discovered that biological/physiological factors such as sex and diet are crucail determinants for dictating the impact of GSNO on KGDH and PDH. First, female mice were more resistant to the GSNO-mediated inhibition of KGDH, demonstrating that there are fundamental sex dimorphic differences in cell redox signaling. Secondly, exposure to a high fat diet augmented the sensitivity of KGDH and even PDH towards inhibition by GSNO. Overall, the insights provided here demonstrate that S-nitrosylation overlaps with S-glutathionylation to modulate H_2O_2 production by KGDH. Additionally, physiological factors affect this redox signaling.

7 - REFERENCES

1. Nelson, Kristin K., et al. "Elevated sod2 activity augments matrix metalloproteinase expression: evidence for the involvement of endogenous hydrogen peroxide in regulating metastasis." *Clinical Cancer Research* 9.1 (2003): 424-432.
2. Li, Xue-bing, Jun-dong Gu, and Qing-hua Zhou. "Review of aerobic glycolysis and its key enzymes–new targets for lung cancer therapy." *Thoracic cancer* 6.1 (2015): 17-24.
3. Ediriweera, Meran Keshawa, and Sharmila Jayasena. "The Role of Reprogrammed Glucose Metabolism in Cancer." *Metabolites* 13.3 (2023): 345.
4. Ruiz-Iglesias, Ainhoa, and Santos Mañes. "The importance of mitochondrial pyruvate carrier in cancer cell metabolism and tumorigenesis." *Cancers* 13.7 (2021): 1488.
5. Korla, Kalyani, and Chanchal K. Mitra. "Modelling the Krebs cycle and oxidative phosphorylation." *Journal of Biomolecular Structure and Dynamics* 32.2 (2014): 242-256.
6. Tretter, Laszlo, and Vera Adam-Vizi. "Alpha-ketoglutarate dehydrogenase: a target and generator of oxidative stress." *Philosophical Transactions of the Royal Society B: Biological Sciences* 360.1464 (2005): 2335-2345.
7. Patel, Mulchand S., et al. "The pyruvate dehydrogenase complexes: structure-based function and regulation." *Journal of Biological Chemistry* 289.24 (2014): 16615-16623.
8. Solmonson, Ashley, and Ralph J. DeBerardinis. "Lipoic acid metabolism and mitochondrial redox regulation." *Journal of Biological Chemistry* 293.20 (2018): 7522-7530.
9. Brautigam, Chad A., et al. "Subunit and catalytic component stoichiometries of an in vitro reconstituted human pyruvate dehydrogenase complex." *Journal of Biological Chemistry* 284.19 (2009): 13086-13098.
10. Wagenknecht, Terence, Noreen Francis, and David J. DeRosier. "α-Ketoglutarate dehydrogenase complex may be heterogeneous in quaternary structure." *Journal of Molecular Biology* 165.3 (1983): 523-539.
11. Johnson, James D., et al. "Genetic evidence for the expression of ATP-and GTP-specific succinyl-CoA synthetases in multicellular eucaryotes." *Journal of Biological Chemistry* 273.42 (1998): 27580-27586.
12. Cecchini, Gary. "Function and structure of complex II of the respiratory chain." *Annual review of biochemistry* 72 (2003): 77-103.
13. Sazanov, Leonid A. "A giant molecular proton pump: structure and mechanism of respiratory complex I." *Nature reviews Molecular cell biology* 16.6 (2015): 375-388.
14. Guo, Runyu, et al. "Structure and mechanism of mitochondrial electron transport chain." *Biomedical journal* 41.1 (2018): 9-20.
15. Bezawork-Geleta, Ayenachew, et al. "Mitochondrial complex II: at the crossroads." *Trends in biochemical sciences* 42.4 (2017): 312-325.
16. Wittig, Ilka, et al. "Supercomplexes and subcomplexes of mitochondrial oxidative phosphorylation." *Biochimica et Biophysica Acta (BBA)-Bioenergetics* 1757.9-10 (2006): 1066-1072.
17. Brand, Martin D. "Mitochondrial generation of superoxide and hydrogen peroxide as the source of mitochondrial redox signaling." *Free Radical Biology and Medicine* 100 (2016): 14-31.
18. Iwata, So, et al. "Complete structure of the 11-subunit bovine mitochondrial cytochrome bc1 complex." *Science* 281.5373 (1998): 64-71.

19. Ghezzi, Daniele, and Massimo Zeviani. "Assembly factors of human mitochondrial respiratory chain complexes: physiology and pathophysiology." *Mitochondrial Oxidative Phosphorylation: Nuclear-Encoded Genes, Enzyme Regulation, and Pathophysiology* (2012): 65-106.
20. Hinkle, Peter C. "P/O ratios of mitochondrial oxidative phosphorylation." *Biochimica et Biophysica Acta (BBA)-Bioenergetics* 1706.1-2 (2005): 1-11.
21. Saier Jr, Milton H. "Eukaryotic transmembrane solute transport systems." *International review of cytology* 190 (1999): 61-136.
22. Chouchani, Edward T., et al. "Mitochondrial ROS regulate thermogenic energy expenditure and sulfenylation of UCP1." *Nature* 532.7597 (2016): 112-116.
23. Sies, Helmut, Carsten Berndt, and Dean P. Jones. "Oxidative stress." *Annual review of biochemistry* 86 (2017): 715-748.
24. Mailloux, Ryan J., Skye L. McBride, and Mary-Ellen Harper. "Unearthing the secrets of mitochondrial ROS and glutathione in bioenergetics." *Trends in biochemical sciences* 38.12 (2013): 592-602.
25. Young, Adrian, Robert Gill, and Ryan J. Mailloux. "Protein S-glutathionylation: The linchpin for the transmission of regulatory information on redox buffering capacity in mitochondria." *Chemico-Biological Interactions* 299 (2019): 151-162.
26. Pacher, Pal, et al. "Nitrosative stress and pharmacological modulation of heart failure." *Trends in pharmacological sciences* 26.6 (2005): 302-310.
27. Catalá, Angel, and Mario Díaz. "Impact of lipid peroxidation on the physiology and pathophysiology of cell membranes." *Frontiers in physiology* 7 (2016): 423.
28. Freese, Elisabeth Bautz, et al. "Inactivating DNA alterations induced by peroxides and peroxide-producing agents." *Mutation Research/Fundamental and Molecular Mechanisms of Mutagenesis* 4.5 (1967): 517-531.
29. Kehrer, James P. "The Haber–Weiss reaction and mechanisms of toxicity." *Toxicology* 149.1 (2000): 43-50.
30. Flint, Dennis H., J. F. Tuminello, and M. H. Emptage. "The inactivation of Fe-S cluster containing hydro-lyases by superoxide." *Journal of Biological Chemistry* 268.30 (1993): 22369-22376.
31. Starkov, Anatoly A., et al. "Mitochondrial α-ketoglutarate dehydrogenase complex generates reactive oxygen species." *Journal of Neuroscience* 24.36 (2004): 7779-7788.
32. Tretter, Laszlo, and Vera Adam-Vizi. "Generation of reactive oxygen species in the reaction catalyzed by α-ketoglutarate dehydrogenase." *Journal of Neuroscience* 24.36 (2004): 7771-7778.
33. Fisher-Wellman, Kelsey H., et al. "Mitochondrial glutathione depletion reveals a novel role for the pyruvate dehydrogenase complex as a key H2O2-emitting source under conditions of nutrient overload." *Free Radical Biology and Medicine* 65 (2013): 1201-1208.
34. Quinlan, Casey L., et al. "The 2-oxoacid dehydrogenase complexes in mitochondria can produce superoxide/hydrogen peroxide at much higher rates than complex I." *Journal of Biological Chemistry* 289.12 (2014): 8312-8325.
35. Mailloux, Ryan J., Danielle Gardiner, and Marisa O'Brien. "2-Oxoglutarate dehydrogenase is a more significant source of O2·−/H2O2 than pyruvate dehydrogenase in cardiac and liver tissue." *Free Radical Biology and Medicine* 97 (2016): 501-512.

36. Slade, Liam, et al. "Examination of the superoxide/hydrogen peroxide forming and quenching potential of mouse liver mitochondria." *Biochimica et Biophysica Acta (BBA)-General Subjects* 1861.8 (2017): 1960-1969.
37. Fukui, Masayuki, and Bao Ting Zhu. "Mitochondrial superoxide dismutase SOD2, but not cytosolic SOD1, plays a critical role in protection against glutamate-induced oxidative stress and cell death in HT22 neuronal cells." *Free Radical Biology and Medicine* 48.6 (2010): 821-830.
38. Heck, Diane E., et al. "Mechanisms of oxidant generation by catalase." *Annals of the New York Academy of Sciences* 1203.1 (2010): 120-125.
39. Dogar, Ibrahim, et al. "C57BL/6J mice upregulate catalase to maintain the hydrogen peroxide buffering capacity of liver mitochondria." *Free Radical Biology and Medicine* 146 (2020): 59-69.
40. Janaky, R., et al. "Glutathione and signal transduction in the mammalian CNS." *Journal of neurochemistry* 73.3 (1999): 889-902.
41. Mailloux, Ryan J. "Teaching the fundamentals of electron transfer reactions in mitochondria and the production and detection of reactive oxygen species." *Redox biology* 4 (2015): 381-398.
42. Nelson, Kimberly J., et al. "Analysis of the peroxiredoxin family: using active-site structure and sequence information for global classification and residue analysis." *Proteins: Structure, Function, and Bioinformatics* 79.3 (2011): 947-964.
43. Spadaro, Davide, et al. "The redox switch: dynamic regulation of protein function by cysteine modifications." *Physiologia plantarum* 138.4 (2010): 360-371.
44. Netto, Luis ES, and Fernando Antunes. "The roles of peroxiredoxin and thioredoxin in hydrogen peroxide sensing and in signal transduction." *Molecules and cells* 39.1 (2016): 65.
45. Sobotta, Mirko C., et al. "Peroxiredoxin-2 and STAT3 form a redox relay for H2O2 signaling." *Nature chemical biology* 11.1 (2015): 64-70.
46. Grillo, Michela, et al. "Stat3 oxidation-dependent regulation of gene expression impacts on developmental processes and involves cooperation with Hif-1α." *Plos one* 15.12 (2020): e0244255.
47. Stöcker, Sarah, et al. "The conundrum of hydrogen peroxide signaling and the emerging role of peroxiredoxins as redox relay hubs." *Antioxidants & redox signaling* 28.7 (2018): 558-573.
48. Wood, Zachary A., Leslie B. Poole, and P. Andrew Karplus. "Peroxiredoxin evolution and the regulation of hydrogen peroxide signaling." *Science* 300.5619 (2003): 650-653.
49. Jeong, Woojin, et al. "Role of sulfiredoxin as a regulator of peroxiredoxin function and regulation of its expression." *Free Radical Biology and Medicine* 53.3 (2012): 447-456.
50. Zambrano, Samuel, et al. "NF-κB oscillations translate into functionally related patterns of gene expression." *Elife* 5 (2016): e09100.
51. Divakaruni, Ajit S., and Martin D. Brand. "The regulation and physiology of mitochondrial proton leak." *Physiology* 26.3 (2011): 192-205.
52. Kuksal, Nidhi, Julia Chalker, and Ryan J. Mailloux. "Progress in understanding the molecular oxygen paradox–function of mitochondrial reactive oxygen species in cell signaling." *Biological chemistry* 398.11 (2017): 1209-1227.
53. Brown, Guy C., et al. "Mitochondrial proton and electron leaks." *Essays in biochemistry* 47 (2010): 53-67.

54. Ricquier, Daniel. "Uncoupling protein 1 of brown adipocytes, the only uncoupler: a historical perspective." *Frontiers in endocrinology* 2 (2011): 85.
55. Azzu, Vian, and Martin D. Brand. "The on-off switches of the mitochondrial uncoupling proteins." *Trends in biochemical sciences* 35.5 (2010): 298-307.
56. Ramsden, David B., et al. "Human neuronal uncoupling proteins 4 and 5 (UCP4 and UCP5): structural properties, regulation, and physiological role in protection against oxidative stress and mitochondrial dysfunction." *Brain and behavior* 2.4 (2012): 468-478.
57. Mailloux, Ryan J., et al. "Crucial yet divergent roles of mitochondrial redox state in skeletal muscle vs. brown adipose tissue energetics." *The FASEB Journal* 26.1 (2012): 363-375.
58. Shabalina, Irina G., et al. "ROS production in brown adipose tissue mitochondria: the question of UCP1-dependence." *Biochimica et Biophysica Acta (BBA)-Bioenergetics* 1837.12 (2014): 2017-2030.
59. Nègre-Salvayre, Anne, et al. "A role for uncoupling protein-2 as a regulator of mitochondrial hydrogen peroxide generation." *The FASEB Journal* 11.10 (1997): 809-815.
60. Echtay, Karim S., et al. "Superoxide activates mitochondrial uncoupling proteins." *Nature* 415.6867 (2002): 96-99.
61. Hirschenson, Jonathan, Emiliano Melgar-Bermudez, and Ryan J. Mailloux. "The uncoupling proteins: a systematic review on the mechanism used in the prevention of oxidative stress." *Antioxidants* 11.2 (2022): 322.
62. Nulton-Persson, Amy C., and Luke I. Szweda. "Modulation of mitochondrial function by hydrogen peroxide." *Journal of Biological Chemistry* 276.26 (2001): 23357-23361.
63. Nulton-Persson, Amy C., et al. "Reversible inactivation of α-ketoglutarate dehydrogenase in response to alterations in the mitochondrial glutathione status." *Biochemistry* 42.14 (2003): 4235-4242.
64. Mailloux, Ryan J. "Protein S-glutathionylation reactions as a global inhibitor of cell metabolism for the desensitization of hydrogen peroxide signals." *Redox biology* 32 (2020): 101472.
65. Gallogly, Molly M., and John J. Mieyal. "Mechanisms of reversible protein glutathionylation in redox signaling and oxidative stress." *Current opinion in pharmacology* 7.4 (2007): 381-391.
66. Klatt, Peter, et al. "Redox regulation of c-Jun DNA binding by reversible S-glutathiolation." *The FASEB Journal* 13.12 (1999): 1481-1490.
67. Chen, Yeong-Renn, et al. "Mitochondrial complex II in the post-ischemic heart: oxidative injury and the role of protein S-glutathionylation." *Journal of Biological Chemistry* 282.45 (2007): 32640-32654.
68. Mailloux, Ryan J., and Mary-Ellen Harper. "Uncoupling proteins and the control of mitochondrial reactive oxygen species production." *Free Radical Biology and Medicine* 51.6 (2011): 1106-1115.
69. Stroeher, Elke, and A. Harvey Millar. "The biological roles of glutaredoxins." *Biochemical Journal* 446.3 (2012): 333-348.
70. Gallogly, Molly M., et al. "Kinetic and mechanistic characterization and versatile catalytic properties of mammalian glutaredoxin 2: implications for intracellular roles." *Biochemistry* 47.42 (2008): 11144-11157.
71. Cooper, Arthur JL, John T. Pinto, and Patrick S. Callery. "Reversible and irreversible protein glutathionylation: biological and clinical aspects." *Expert opinion on drug metabolism & toxicology* 7.7 (2011): 891-910.

72. Beer, Samantha M., et al. "Glutaredoxin 2 catalyzes the reversible oxidation and glutathionylation of mitochondrial membrane thiol proteins: implications for mitochondrial redox regulation and antioxidant DEFENSE." *Journal of Biological Chemistry* 279.46 (2004): 47939-47951.

73. Gallogly, Molly M., and John J. Mieyal. "Mechanisms of reversible protein glutathionylation in redox signaling and oxidative stress." *Current opinion in pharmacology* 7.4 (2007): 381-391.

74. Mailloux, Ryan J., Cathryn Grayson, and Olivia Koufos. "Regulation of Mitochondrial Hydrogen Peroxide Availability by Protein S-glutathionylation." *Cells* 12.1 (2022): 107.

75. Zhang, Huihui, et al. "Glutaredoxin 2 reduces both thioredoxin 2 and thioredoxin 1 and protects cells from apoptosis induced by auranofin and 4-hydroxynonenal." *Antioxidants & Redox Signaling* 21.5 (2014): 669-681.

76. Lönn, Maria Elisabet, et al. "Expression pattern of human glutaredoxin 2 isoforms: identification and characterization of two testis/cancer cell-specific isoforms." *Antioxidants & redox signaling* 10.3 (2008): 547-558.

77. Chalker, Julia, et al. "Characterization of the impact of glutaredoxin-2 (GRX2) deficiency on superoxide/hydrogen peroxide release from cardiac and liver mitochondria." *Redox biology* 15 (2018): 216-227.

78. O'Brien, Marisa, et al. "Protein S-glutathionylation alters superoxide/hydrogen peroxide emission from pyruvate dehydrogenase complex." *Free Radical Biology and Medicine* 106 (2017): 302-314.

79. Mallay, Sarah, et al. "Sex-dependent differences in the bioenergetics of liver and muscle mitochondria from mice containing a deletion for glutaredoxin-2." *Antioxidants* 8.8 (2019): 245.

80. Ventura-Clapier, Renée, et al. "Mitochondria: a central target for sex differences in pathologies." *Clinical science* 131.9 (2017): 803-822.

81. Koufos, Olivia, and Ryan J. Mailloux. "Protein S-glutathionylation and sex dimorphic effects on hydrogen peroxide production by dihydroorotate dehydrogenase in liver mitochondria." *Free Radical Biology and Medicine* 194 (2023): 123-130.

82. Mailloux, Ryan J., et al. "Glutaredoxin-2 is required to control proton leak through uncoupling protein-3." *Journal of Biological Chemistry* 288.12 (2013): 8365-8379.

83. Hess, Douglas T., et al. "Protein S-nitrosylation: purview and parameters." *Nature reviews Molecular cell biology* 6.2 (2005): 150-166.

84. Furchgott, Robert F. "Introduction to EDRF research." *Journal of Cardiovascular Pharmacology* 22 (1993): S1-2.

85. Howlett, Rory. "Nobel award stirs up debate on nitric oxide breakthrough." *Nature* 395.6703 (1998): 625-626.

86. Inserte, Javier, and David Garcia-Dorado. "The cGMP/PKG pathway as a common mediator of cardioprotection: translatability and mechanism." *British Journal of Pharmacology* 172.8 (2015): 1996-2009.

87. Wink, David A., et al. "Mechanisms of the antioxidant effects of nitric oxide." *Antioxidants and redox signaling* 3.2 (2001): 203-213.

88. Thomas, Douglas D., et al. "The biological lifetime of nitric oxide: implications for the perivascular dynamics of NO and O2." *Proceedings of the National Academy of Sciences* 98.1 (2001): 355-360.

89. Fernando, Veani, et al. "S-nitrosylation: an emerging paradigm of redox signaling." *Antioxidants* 8.9 (2019): 404.
90. Förstermann, Ulrich, and William C. Sessa. "Nitric oxide synthases: regulation and function." *European heart journal* 33.7 (2012): 829-837.
91. Prolo, Carolina, María Noel Álvarez, and Rafael Radi. "Peroxynitrite, a potent macrophage-derived oxidizing cytotoxin to combat invading pathogens." *Biofactors* 40.2 (2014): 215-225.
92. Broniowska, Katarzyna A., et al. "Cytochrome c-mediated formation of S-nitrosothiol in cells." *Biochemical Journal* 442.1 (2012): 191-197.
93. Kalinina, Elena, and Maria Novichkova. "Glutathione in protein redox modulation through S-glutathionylation and S-nitrosylation." *Molecules* 26.2 (2021): 435.
94. Lancaster Jr, Jack R. "Nitric oxide: a brief overview of chemical and physical properties relevant to therapeutic applications." *Future Science OA* 1.1 (2015).
95. Chang, Allen HK, et al. "Respiratory substrates regulate S-nitrosylation of mitochondrial proteins through a thiol-dependent pathway." *Chemical research in toxicology* 27.5 (2014): 794-804.
96. Ravi, Kandasam, et al. "S-nitrosylation of endothelial nitric oxide synthase is associated with monomerization and decreased enzyme activity." *Proceedings of the National Academy of Sciences* 101.8 (2004): 2619-2624.
97. Jia, Jie, et al. "Target-selective protein S-nitrosylation by sequence motif recognition." *Cell* 159.3 (2014): 623-634.
98. Doulias, Paschalis-Thomas, et al. "Structural profiling of endogenous S-nitrosocysteine residues reveals unique features that accommodate diverse mechanisms for protein S-nitrosylation." *Proceedings of the National Academy of Sciences* 107.39 (2010): 16958-16963
99. Broniowska, Katarzyna A., and Neil Hogg. "The chemical biology of S-nitrosothiols." *Antioxidants & redox signaling* 17.7 (2012): 969-980.
100. Möller, Matias N., et al. "Membrane "Lens" effect: focusing the formation of reactive nitrogen oxides from the• NO/O2 reaction." *Chemical research in toxicology* 20.4 (2007): 709-714.
101. Cheng, Shangli, et al. "Features of S-nitrosylation based on statistical analysis and molecular dynamics simulation: cysteine acidity, surrounding basicity, steric hindrance and local flexibility." *Molecular BioSystems* 10.10 (2014): 2597-2606.
102. Whiteman, Matthew, et al. "Nitric oxide protects against mitochondrial permeabilization induced by glutathione depletion: role of S-nitrosylation?" *Biochemical and Biophysical Research Communications* 339.1 (2006): 255-262.
103. Stomberski, Colin T., Douglas T. Hess, and Jonathan S. Stamler. "Protein S-nitrosylation: determinants of specificity and enzymatic regulation of S-nitrosothiol-based signaling." *Antioxidants & redox signaling* 30.10 (2019): 1331-1351.
104. Foster, Matthew W., Douglas T. Hess, and Jonathan S. Stamler. "Protein S-nitrosylation in health and disease: a current perspective." *Trends in molecular medicine* 15.9 (2009): 391-404.
105. Nikitovic, Dragana, and Arne Holmgren. "S-nitrosoglutathione is cleaved by the thioredoxin system with liberation of glutathione and redox regulating nitric oxide." *Journal of Biological Chemistry* 271.32 (1996): 19180-19185.

106. Stoyanovsky, Detcho A., et al. "Thioredoxin and lipoic acid catalyze the denitrosation of low molecular weight and protein S-nitrosothiols." *Journal of the American Chemical Society* 127.45 (2005): 15815-15823

107. Caplin, Ben, and James Leiper. "Endogenous nitric oxide synthase inhibitors in the biology of disease: markers, mediators, and regulators?" *Arteriosclerosis, thrombosis, and vascular biology* 32.6 (2012): 1343-1353.

108. Fan, Jing-Song, et al. "Protein inhibitor of neuronal nitric-oxide synthase, PIN, binds to a 17-amino acid residue fragment of the enzyme." *Journal of Biological Chemistry* 273.50 (1998): 33472-33481.

109. Nakamura, Tomohiro, and Stuart A. Lipton. "Emerging role of protein-protein transnitrosylation in cell signaling pathways." *Antioxidants & redox signaling* 18.3 (2013): 239-249.

110. Hara, Makoto R., et al. "S-nitrosylated GAPDH initiates apoptotic cell death by nuclear translocation following Siah1 binding." *Nature cell biology* 7.7 (2005): 665-674.

111. Kornberg, Michael D., et al. "GAPDH mediates nitrosylation of nuclear proteins." *Nature cell biology* 12.11 (2010): 1094-1100.

112. Kohr, Mark J., Elizabeth Murphy, and Charles Steenbergen. "Glyceraldehyde-3-phosphate dehydrogenase acts as a mitochondrial trans-S-nitrosylase in the heart." *PLoS One* 9.10 (2014): e111448.

113. Piantadosi, Claude A. "Regulation of mitochondrial processes by protein S-nitrosylation." *Biochimica et Biophysica Acta (BBA)-General Subjects* 1820.6 (2012): 712-721.

114. Chouchani, Edward T., et al. "Cardioprotection by S-nitrosation of a cysteine switch on mitochondrial complex I." *Nature medicine* 19.6 (2013): 753-759.

115. Ghasemi, Mehdi, et al. "Nitric oxide and mitochondrial function in neurological diseases." *Neuroscience* 376 (2018): 48-71.

116. Basu, Swati, et al. "A novel role for cytochrome c: Efficient catalysis of S-nitrosothiol formation." *Free Radical Biology and Medicine* 48.2 (2010): 255-263.

117. Brown, Guy C., and Vilmante Borutaite. "Inhibition of mitochondrial respiratory complex I by nitric oxide, peroxynitrite and S-nitrosothiols." *Biochimica et Biophysica Acta (BBA)-Bioenergetics* 1658.1-2 (2004): 44-49.

118. Chouchani, Edward T., et al. "Identification of S-nitrosated mitochondrial proteins by S-nitrosothiol difference in gel electrophoresis (SNO-DIGE): implications for the regulation of mitochondrial function by reversible S-nitrosation." *Biochemical Journal* 430.1 (2010): 49-59.

119. Sun, Junhui, et al. "Preconditioning results in S-nitrosylation of proteins involved in regulation of mitochondrial energetics and calcium transport." *Circulation research* 101.11 (2007): 1155-1163.

120. Doulias, Paschalis-Thomas, et al. "Nitric oxide regulates mitochondrial fatty acid metabolism through reversible protein S-nitrosylation." *Science signaling* 6.256 (2013): rs1-rs1.

121. Nguyen, Tiffany Tuyen Minh, et al. "S-nitrosylation of cyclophilin D alters mitochondrial permeability transition pore." (2011): 1031-1033.

122. Cheng, Qunli, et al. "Biphasic effect of nitric oxide on the cardiac voltage-dependent anion channel." *FEBS letters* 585.2 (2011): 328-334.

123. Carvalho-Filho, Marco A., et al. "S-nitrosation of the insulin receptor, insulin receptor substrate 1, and protein kinase B/Akt: a novel mechanism of insulin resistance." *Diabetes* 54.4 (2005): 959-967.
124. Perreault, Mylène, and André Marette. "Targeted disruption of inducible nitric oxide synthase protects against obesity-linked insulin resistance in muscle." *Nature medicine* 7.10 (2001): 1138-1143.
125. Montagna, Costanza, et al. "When S-nitrosylation gets to mitochondria: From signaling to age-related diseases." *Antioxidants & Redox Signaling* 32.12 (2020): 884-905.
126. Rizza, Salvatore, et al. "S-nitrosylation drives cell senescence and aging in mammals by controlling mitochondrial dynamics and mitophagy." *Proceedings of the National Academy of Sciences* 115.15 (2018): E3388-E3397.
127. Seim, Gretchen L., et al. "Nitric oxide-driven modifications of lipoic arm inhibit α-ketoacid dehydrogenases." *Nature Chemical Biology* 19.3 (2023): 265-274.
128. Wieckowski, Mariusz R., et al. "Isolation of mitochondria-associated membranes and mitochondria from animal tissues and cells." *Nature protocols* 4.11 (2009): 1582-1590.
129. Bradford, Marion M. "A rapid and sensitive method for the quantitation of microgram quantities of protein utilizing the principle of protein-dye binding." *Analytical biochemistry* 72.1-2 (1976): 248-254.
130. Munro, Daniel, et al. "The thioredoxin and glutathione-dependent H2O2 consumption pathways in muscle mitochondria: involvement in H2O2 metabolism and consequence to H2O2 efflux assays." *Free Radical Biology and Medicine* 96 (2016): 334-346.
131. Macmillan-Crow, Lee Ann, and Danielle L. Cruthirds. "Manganese superoxide dismutase in disease." *Free radical research* 34.4 (2001): 325-336.
132. Mailloux, Ryan J., et al. "Simultaneous measurement of superoxide/hydrogen peroxide and NADH production by flavin-containing mitochondrial dehydrogenases." *JoVE (Journal of Visualized Experiments)* 132 (2018): e56975.
133. Treberg, Jason R., Casey L. Quinlan, and Martin D. Brand. "Hydrogen peroxide efflux from muscle mitochondria underestimates matrix superoxide production–a correction using glutathione depletion." *The FEBS journal* 277.13 (2010): 2766-2778.
134. Zhang, Xiaonan, et al. "Repurposing of auranofin: Thioredoxin reductase remains a primary target of the drug." *Biochimie* 162 (2019): 46-54.
135. Horváth, Gergő, et al. "Reverse and Forward Electron Flow-Induced H2O2 Formation Is Decreased in α-Ketoglutarate Dehydrogenase (α-KGDH) Subunit (E2 or E3) Heterozygote Knock Out Animals." *Antioxidants* 11.8 (2022): 1487.
136. Applegate, Milana AB, Kenneth M. Humphries, and Luke I. Szweda. "Reversible inhibition of α-ketoglutarate dehydrogenase by hydrogen peroxide: glutathionylation and protection of lipoic acid." *Biochemistry* 47.1 (2008): 473-478.
137. Mailloux, Ryan J. "Teaching the fundamentals of electron transfer reactions in mitochondria and the production and detection of reactive oxygen species." *Redox biology* 4 (2015): 381-398.
138. Mailloux, Ryan J., D. Craig Ayre, and Sherri L. Christian. "Induction of mitochondrial reactive oxygen species production by GSH mediated S-glutathionylation of 2-oxoglutarate dehydrogenase." *Redox biology* 8 (2016): 285-297.
139. Bai, Hua, et al. "Mitochondria-derived H2O2 triggers liver regeneration via FoxO3a signaling pathway after partial hepatectomy in mice." *Cell Death & Disease* 14.3 (2023): 216.

140. Shi, Xiaomeng, and Hongyu Qiu. "Post-translational S-nitrosylation of proteins in regulating cardiac oxidative stress." *Antioxidants* 9.11 (2020): 1051.
141. Humphries, Kenneth M., and Luke I. Szweda. "Selective inactivation of α-ketoglutarate dehydrogenase and pyruvate dehydrogenase: reaction of lipoic acid with 4-hydroxy-2-nonenal." *Biochemistry* 37.45 (1998): 15835-15841.
142. Roche, TE and, and Y. Hiromasa. "Pyruvate dehydrogenase kinase regulatory mechanisms and inhibition in treating diabetes, heart ischemia, and cancer." *Cellular and molecular life sciences* 64 (2007): 830-849.
143. Justo, Roberto, et al. "Gender dimorphism in rat liver mitochondrial oxidative metabolism and biogenesis." *American Journal of Physiology-Cell Physiology* 289.2 (2005): C372-C378.
144. Fernández-Silva, Patricio, José A. Enriquez, and Julio Montoya. "Replication and transcription of mammalian mitochondrial DNA." *Experimental physiology* 88.1 (2003): 41-56.
145. Rikans, Lora E., Danny R. Moore, and Cynthia D. Snowden. "Sex-dependent differences in the effects of aging on antioxidant defense mechanisms of rat liver." *Biochimica et Biophysica Acta (BBA)-General Subjects* 1074.1 (1991): 195-200.
146. Borrás, Consuelo, et al. "Mitochondria from females exhibit higher antioxidant gene expression and lower oxidative damage than males." *Free radical biology and medicine* 34.5 (2003): 546-552.
147. Viña, Jose, et al. "Why females live longer than males? Importance of the upregulation of longevity-associated genes by oestrogenic compounds." *FEBS letters* 579.12 (2005): 2541-2545.
148. McConnachie, Lisa A., et al. "Glutamate cysteine ligase modifier subunit deficiency and gender as determinants of acetaminophen-induced hepatotoxicity in mice." *Toxicological Sciences* 99.2 (2007): 628-636.
149. Borrás, Consuelo, et al. "Direct antioxidant and protective effect of estradiol on isolated mitochondria." *Biochimica et Biophysica Acta (BBA)-Molecular Basis of Disease* 1802.1 (2010): 205-211.
150. Bellanti, Francesco, et al. "Sex hormones modulate circulating antioxidant enzymes: impact of estrogen therapy." *Redox biology* 1.1 (2013): 340-346.
151. Barnett, Scott D., and Iain LO Buxton. "The role of S-nitrosoglutathione reductase (GSNOR) in human disease and therapy." *Critical reviews in biochemistry and molecular biology* 52.3 (2017): 340-354.
152. Brown-Steinke, Kathleen, et al. "Gender differences in S-nitrosoglutathione reductase activity in the lung." *PLoS One* 5.11 (2010): e14007.
153. Casin, Kevin M., et al. "S-nitrosoglutathione reductase is essential for protecting the female heart from ischemia-reperfusion injury." *Circulation research* 123.11 (2018): 1232-1243.
154. Young, Adrian, et al. "Deletion of the glutaredoxin-2 gene protects mice from diet-induced weight gain, which correlates with increased mitochondrial respiration and proton leaks in skeletal muscle." *Antioxidants & Redox Signaling* 31.17 (2019): 1272-1288.
155. Gill, Robert, et al. "An investigation into the impact of deleting one copy of the glutaredoxin-2 gene on diet-induced weight gain and the bioenergetics of muscle mitochondria in female mice fed a high fat diet." *Redox Report* 25.1 (2020): 87-94.

156. Nadal-Casellas, Antònia, et al. "Long-term high-fat-diet feeding impairs mitochondrial biogenesis in liver of male and female rats." *Cellular Physiology and Biochemistry* 26.3 (2010): 291-302.
157. Lionetti, Lillà, et al. "High-lard and high-fish-oil diets differ in their effects on function and dynamic behaviour of rat hepatic mitochondria." *PloS one* 9.3 (2014): e92753.
158. Vial, Guillaume, et al. "Effects of a high-fat diet on energy metabolism and ROS production in rat liver." *Journal of hepatology* 54.2 (2011): 348-356.
159. Cardoso, Ariel R., João Victor Cabral-Costa, and Alicia J. Kowaltowski. "Effects of a high fat diet on liver mitochondria: increased ATP-sensitive K+ channel activity and reactive oxygen species generation." *Journal of bioenergetics and biomembranes* 42.3 (2010): 245.
160. Cardoso, Ariel R., Pâmela AHB Kakimoto, and Alicia J. Kowaltowski. "Diet-sensitive sources of reactive oxygen species in liver mitochondria: role of very long chain acyl-CoA dehydrogenases." *PLoS One* 8.10 (2013): e77088.
161. Eccleston, Heather B., et al. "Chronic exposure to a high-fat diet induces hepatic steatosis, impairs nitric oxide bioavailability, and modifies the mitochondrial proteome in mice." *Antioxidants & redox signaling* 15.2 (2011): 447-459.
162. Chan, Mei-Yen, Yulan Zhao, and Chew-Kiat Heng. "Sequential responses to high-fat and high-calorie feeding in an obese mouse model." *Obesity* 16.5 (2008): 972-978.
163. Sies, Helmut. "Hydrogen peroxide as a central redox signaling molecule in physiological oxidative stress: Oxidative eustress." *Redox biology* 11 (2017): 613-619.
164. Kramer, Philip A., et al. "The measurement of reversible redox dependent post-translational modifications and their regulation of mitochondrial and skeletal muscle function." *Frontiers in physiology* 6 (2015): 347.
165. Horn, Adam, et al. "Mitochondrial redox signaling enables repair of injured skeletal muscle cells." *Science signaling* 10.495 (2017): eaaj1978.
166. Mantena, Sudheer K., et al. "High fat diet induces dysregulation of hepatic oxygen gradients and mitochondrial function in vivo." *Biochemical Journal* 417.1 (2009): 183-193.
167. Venkatraman, Aparna, et al. "The role of iNOS in alcohol-dependent hepatotoxicity and mitochondrial dysfunction in mice." *Hepatology* 40.3 (2004): 565-573.
168. Cordero-Herrera, Isabel, et al. "AMP-activated protein kinase activation and NADPH oxidase inhibition by inorganic nitrate and nitrite prevent liver steatosis." *Proceedings of the National Academy of Sciences* 116.1 (2019): 217-226.
169. DesOrmeaux, Geneviève J., et al. "Independent of mitochondrial respiratory function, dietary nitrate attenuates HFD-induced lipid accumulation and mitochondrial ROS emission within the liver." *American Journal of Physiology-Endocrinology and Metabolism* 321.2 (2021): E217-E228.
170. Bryzgalova, Galyna, et al. "Mechanisms of antidiabetogenic and body weight-lowering effects of estrogen in high-fat diet-fed mice." *American Journal of Physiology-Endocrinology and Metabolism* 295.4 (2008): E904-E912.
171. Riant, Elodie, et al. "Estrogens protect against high-fat diet-induced insulin resistance and glucose intolerance in mice." *Endocrinology* 150.5 (2009): 2109-2117.
172. Díaz, Ana, et al. "Sex differences in age-associated type 2 diabetes in rats—Role of estrogens and oxidative stress." *Oxidative medicine and cellular longevity* 2019 (2019).
173. Torres, Maria J., et al. "17β-Estradiol directly lowers mitochondrial membrane microviscosity and improves bioenergetic function in skeletal muscle." *Cell metabolism* 27.1 (2018): 167-179.

174. Aon, Miguel Antonio, et al. "Glutathione/thioredoxin systems modulate mitochondrial H2O2 emission: an experimental-computational study." *Journal of General Physiology* 139.6 (2012): 479-491.
175. Simões, Inês CM, et al. "Mitochondria in non-alcoholic fatty liver disease." *The international journal of biochemistry & cell biology* 95 (2018): 93-99.
176. Palfey, Bruce A., David P. Ballou, and Vincent Massey. "Oxygen activation by flavins and pterins." *Active oxygen in biochemistry* (1995): 37-83.
177. Adapted from "Glycolysis and Glycolytic Enzymes", by BioRender.com (2023). Retrieved from https://app.biorender.com/biorender-templates
178. Adapted from "Cellular Respiration" and "Krebs Cycle", by BioRender.com (2023). Retrieved from https://app.biorender.com/biorender-templates
179. Adapted from "Electron Transport Chain", by BioRender.com (2023). Retrieved from https://app.biorender.com/biorender-templates
180. Adapted from "Cell with Mitochondria", by BioRender.com (2023). Retrieved from https://app.biorender.com/biorender-templates

APPENDIX

Minerals		
Calcium	%	0.9
Phosphorus	%	0.7
Non-Phytate Phosphorus	%	0.4
Sodium	%	0.1
Potassium	%	0.4
Chloride	%	0.4
Magnesium	%	0.2
Zinc	mg/kg	60
Manganese	mg/kg	80
Copper	mg/kg	15
Iodine	mg/kg	6
Iron	mg/kg	200
Selenium	mg/kg	0.23
Amino Acids		
Aspartic Acid	%	1.1
Glutamic Acid	%	3.5
Alanine	%	1.2
Glycine	%	0.7
Threonine	%	0.6
Proline	%	1.9
Serine	%	0.9
Leucine	%	2.3
Isoleucine	%	0.7
Valine	%	0.9
Phenylalanine	%	1.0
Tyrosine	%	0.5
Methionine	%	0.5
Cysteine	%	0.3
Lysine	%	0.9
Histidine	%	0.4
Arginine	%	0.8
Tryptophan	%	0.2
Vitamins		
Vitamin A	IU/g	15.0
Vitamin D_3	IU/g	1.5
Vitamin E	IU/kg	110
Vitamin K_3 (menadione)	mg/kg	50
Vitamin B_1 (thiamin)	mg/kg	17
Vitamin B_2 (riboflavin)	mg/kg	15
Niacin (nicotinic acid)	mg/kg	75

Vitamin B_6 (pyridoxine)	mg/kg	18
Pantothenic Acid	mg/kg	33
Vitamin B_{12} (cyanocobalamin)	mg/kg	0.08
Biotin	mg/kg	0.40
Folate	mg/kg	4
Choline	mg/kg	1200

Mineral, amino acid, and vitamin profiles of Standard Chow Diet. Information taken directly from supplier (Envigo – Teklad; 2920X Irradiated Teklad Global Soy Protein-Free Extruded Rodent Diet).